The University of Maine
DigitalCommons@UMaine

Electronic Theses and Dissertations | Fogler Library

Fall 12-16-2016

Experimental Methods and Practices for The Study of Toroidal Inflated, Braided Fabric Members

Daniel J. Whitney
University of Maine, daniel.whitney@maine.edu

Follow this and additional works at: http://digitalcommons.library.umaine.edu/etd

 Part of the Electro-Mechanical Systems Commons, and the Structural Materials Commons

Recommended Citation
Whitney, Daniel J., "Experimental Methods and Practices for The Study of Toroidal Inflated, Braided Fabric Members" (2016). *Electronic Theses and Dissertations*. 2596.
http://digitalcommons.library.umaine.edu/etd/2596

This Open-Access Thesis is brought to you for free and open access by DigitalCommons@UMaine. It has been accepted for inclusion in Electronic Theses and Dissertations by an authorized administrator of DigitalCommons@UMaine.

EXPERIMENTAL METHODS AND PRACTICES FOR THE STUDY OF TOROIDAL INFLATED, BRAIDED FABRIC MEMBERS

By

Daniel Josiah Whitney

B.S. University of Maine, 2013

A THESIS

Submitted in Partial Fulfillment of the

Requirements for the Degree of

Master of Science

(in Mechanical Engineering)

The Graduate School

The University of Maine

December 2016

Advisory Committee:

William G. Davids, John C Bridge Professor of Civil and Environmental Engineering, Advisor

Andrew J. Goupee, Libra Assistant Professor of Mechanical Engineering

Senthil S Vel, Arthur O. Willey Professor of Mechanical Engineering

EXPERIMENTAL METHODS AND PRACTICES FOR THE STUDY OF TOROIDAL INFLATED, BRAIDED FABRIC MEMBERS

By Daniel Josiah Whitney

Thesis Advisor: Dr. William G. Davids, P.E.

An Abstract of the Thesis Presented
in Partial Fulfillment of the Requirements of the
Degree of Master of Science
(in Mechanical Engineering)
December 2016

Inflatable structures have become a very important area of interest for many differing applications where lightweight packable structures are required. NASA is developing Hypersonic Inflatable Aerodynamic Decelerator (HIAD) technology that takes advantage of stacked, inflated fabric tori to form a decelerating spacecraft nose cone. The tori consist of a bladder, braided fabric shell, and reinforcing in the form of integral cords or externally bonded straps. The focus of this thesis is on the development of methods for the structural testing of inflated fabric tori and developing an enhanced understanding of their behavior. This is essential for providing insight into the mechanical behavior of the HIAD and improving simulation-based models of HIADs.

Experimentally testing braided inflated fabric tori is complex, and the University of Maine has improved on the setup originally developed by NASA for testing these articles. Further improvement of the test setup accomplished as part of this research included enhancing the control system used for torus testing to work in displacement control. This produced results that could be more easily used to validate simulation tools

being independently developed by others. Testing of these torus articles was accomplished by applying discrete, multiple point loads in the radial direction, inducing compression and bending of a single torus. Torus testing was conducted using up to sixteen actuators attached to eight straps on the article allowing for many differing testing profiles and loading protocols to be performed. Testing was also be performed at a variety of different pressures and for a large range of sizes of tori allowing for a better understanding of how these properties affect the response of the structure. Strict pressure regulation and test timing was used to ensure that the articles exhibited as little hysteretic effect as was feasible to avoid. Additionally, tori with different reinforcing schemes were tested to experimentally determine advantages and disadvantages of these reinforcing schemes.

ACKNOWLEDGMENTS

I would like to gratefully acknowledge the many individuals that have assisted me through my time here at the University of Maine as well as Maine Space Grant for funding the research associated with this thesis.

I am especially grateful to my advisor, Bill Davids, for his continual guidance throughout the course this project. I also appreciate Bill's academic and professional advice and encouragement.

I am grateful to Andrew Goupee and Senthil Vel for being a part of my thesis committee and for providing valuable insight over the course of the research work.

I am thankful for the advice of Joshua Clapp, whose experience and engineering knowledge was invaluable throughout this project.

I would like to thank all of the Undergraduates that helped conduct and monitor experimental testing efforts.

Finally, I would like to thank my family for listening to all my engineering stories over the years, putting up with my many projects and supporting me throughout my academic career.

TABLE OF CONTENTS

LIST OF TABLES

LIST OF FIGURES

Chapter 1

INTRODUCTION

1.1. Problem Description

NASA is developing a technology called the Hypersonic Inflatable Aerodynamic Decelerator (HIAD). This technology makes use of a highly robust fabric structure that allows for a blunt decelerator of large diameter to be packed into a much smaller diameter payload. Decelerators are critical in allowing for large payloads to decelerate during atmospheric reentry. Currently inflatable decelerators are critical to the prospect of placing objects larger than approximately one metric ton on the surface of mars without using wasteful retro-propulsion. The largest rigid decelerator that has been used had a diameter of 4.5m which allowed the Mars Science Laboratory, an approximately one metric ton payload to be placed at a low altitude on Mars. The HIAD would allow for the payload sizes essential for a manned mission to Mars to be landed on the surface. A manned mission to Mars will require a decelerator with a diameter of ~20 m to land ~40-80 metric tons of payload (Braun and Manning 2007). A decelerator of this size would only be possible if the decelerator can be placed in a rocket shroud much smaller than its deployed size.

The HIAD is constructed as shown in Figure 1. The diameter of the structure can be designed to suit the specific application and payload size. The HIAD is constructed using concentric tori of increasing diameter such that the desired cone angle is achieved for the specific application. Each torus is connected to its neighbor with pairing straps allowing the device to act as a single structure. There are also radial straps that connect between

the center body and specific tori adding a direct connection to the rigid center for tori located on the outer section of the HIAD.

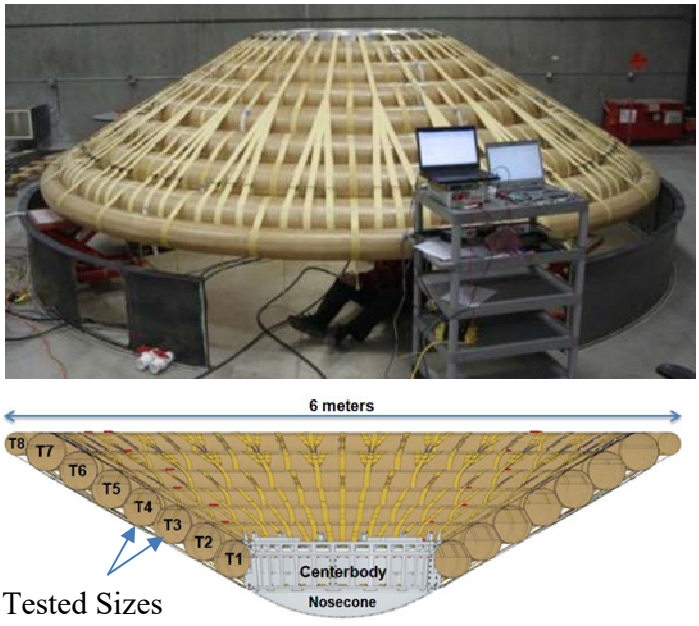

Figure 1: HIAD Construction (Swanson, 2012)

Tori used for the HIAD built to-date have used a Technora braid, which is a high strength aramid that is axially reinforced to provide a great deal of strength when the article is pressurized. Each torus has a shell consisting of synthetic fibers braided at a particular angle, two axial cords integrated within the braid, and an internal gas bladder. Axial reinforcement consisting of four axial cords as well as an external "ladder" have also been proposed instead of the current two axial cord configuration. Generally the tori used in constructing the HIAD are designed as shown in Figure 2. The two-cords that are shown carry the force of inflation and give the structure strength and stiffness since the

cords would need to be fully unloaded to remove their effective compressive strength. The three components of the torus work together to form a sufficiently strong and lightweight structure. The gas bladder allows pressurized air to be constrained inside the highly porous braid. The braid provides two very useful features: first, it has a great deal of strength in the hoop direction allowing the torus to be inflated to the required pressure, and second, the properties of the braid allow for it to be easily form to a circular shape since the braid angle of the fabric will adjust to accommodate the desired radius of curvature. This property makes it ideal for toroidal applications.

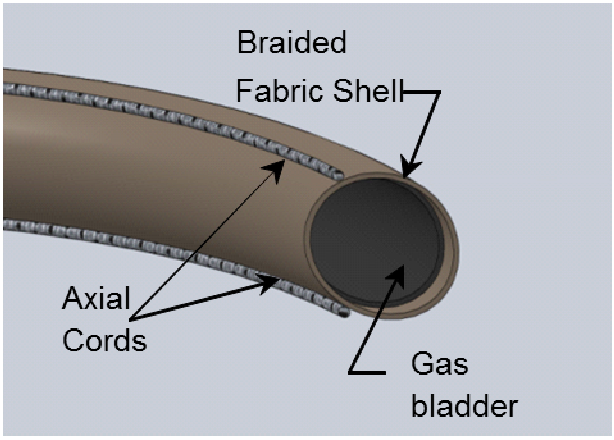

Figure 2: Torus Construction

Despite its positive attributes, an inflated torus does not exhibit linear or easily calculated responses to loads. As such, better testing and numerical modeling practices are required to understand its structural behavior for different inflation pressures and reinforcement schemes. The University of Maine (UMaine) is assisting NASA in the testing and modeling of these structural members in order to help deepen the current understanding of their properties. Torus testing presents a number of challenges that are

somewhat unique to the structure because of its compliance, the sensitivity of its response to inflation pressure, and the challenges with applying realistic load cases to a circular fabric structure.

Inflatable torus structures have the potential to provide a great possibilities for constructing decelerators for vehicles reentering the atmosphere; however, there are still a large number of unanswered questions regarding the response of the HIAD to loading that it will encounter during descent. There is currently a need for the structure to be carefully tested at a component level to obtain data for creating and validating a complete model that accurately predicts the response of the structure.

1.2. Thesis Description

This thesis focuses on the testing methods used in characterizing the response of the torus under differing loading scenarios as well as for obtaining the load-displacement response of many differing articles. The objective of the torus testing effort is to provide data that will help verify numerical modeling codes currently being constructed at UMaine in addition to providing a better understanding of the structural behavior of slender, braided, inflatable members with discrete axial reinforcing cords.

Applying load to the torus during testing required a control system to be designed and assembled. The design considerations and the methods used to build the system are covered in this thesis along with the methods used to automate the torus testing. Automation was required because of the very large number of tests that was desired as well as the need to minimize hysteretic effects by mandating strict rest times between tests to allow the fabric structure to recover for subsequent test.

The articles tested for the purpose of this thesis were T3 (3 m diameter) and T4 (3.5 m diameter) from the 6m HIAD size as shown in Figure 1. There were two pristine (not previously tested by NASA) T4 tori that were tested along with five pristine T3 tori that were tested in a variety of different ways. It was important to develop a robust understanding of the repeatability of the test so each torus was tested multiple times with the same loading configuration and a range of pressures. The four pressures that were used to demonstrate the pressure dependency of the articles were 34kPa, 69kPa, 103kPa and 138kPa. These pressures cover the potential operating range of the inflatable decelerators.

Torus testing also included two tori with non-standard reinforcing schemes. One reinforcing method that was tested in detail was a 4-cord reinforcing design shown in Figure 3. The 4-cord design has four-cords incorporated into the braid on the inner curvature of the torus. The second non-standard scheme was a ladder reinforced construction built by using an adhesive to bond straps on the outer surface of the torus as shown in Figure 3. There are also straps oriented along the minor radius that run between the two horizontal straps and prevent them from being pushed apart and separating from the braid.

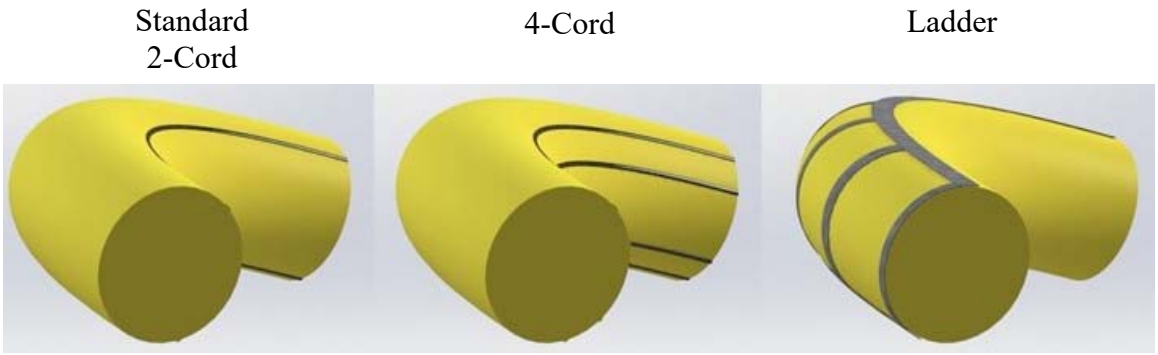

Figure 3: Multiple Reinforcing Methods Tested for T3

Along with the non-standard reinforcing scheme shown in Figure 3 two regular T3 tori with two reinforcing cords and a T3 with two-cords of different lengths were tested. These tests provided valuable information on the effects of differing reinforcing methods as well as the sensitivity of the torus to minor manufacturing defects imposed by mis-sized reinforcing cords.

1.3. Contributions

As a part of this research work significant strides were taken to develop a consistent and well-constructed test program for experimentally investigating the response of inflated, braided, toroidal articles. Methods used to test thesis articles could be used for further testing and will allow for torus testing to be conducted with a methodical manor. Great effort was devoted to ensure that the test setup that was developed for this testing was ideally constructed and the controller was ideally tuned for the testing application. Development of methods for both testing and instrumentation were developed in detail allowing for many of the properties of these articles to be

determined. Further this work allowed for a better understanding of the reinforcing used on the toroidal articles

1.4. Organization of Thesis

This thesis is organized into seven chapters. Chapter 2 is a literature review which covers previous braided, inflatable member research, modeling efforts, and current design approaches relevant to the work in this thesis.

Chapter 3 discusses the development of the testing methods and practices used for torus testing at the University of Maine. The design for HIAD testing uses the test frame acquired from NASA and used previously by NASA for torus testing. This chapter covers the modifications to the testing device and methods by which the torus was tested to determine repeatability and robustness of the structures.

Chapter 4 covers the control system design and considerations specifically imposed by testing inflated fabric tori. Designing a control system that allows for realistic loads to be applied to the torus requires a large number of independently controlled actuators as well as a well-tuned response for reacting to the nonlinear response of the tori.

Chapter 5 addresses the results from torus testing on several T4 tori subjected to a wide range of load cases and testing history of the specimens. This chapter explains the differences between all the testing load cases as well as the benefits and drawbacks of both the load and displacement control testing methods.

Chapter 6 covers the results from using differing reinforcing methods on the response of the torus to differing testing scenarios. The method by which the torus is reinforced can have large effects on the performance of the article; in addition, there are

manufacturing as well as weight considerations that impact the practicality of each method.

Finally, Chapter 7 provides a summary of the work completed for this thesis, conclusions based on the important discoveries, and recommendations for future research. Important aspects of the research are detailed and summarized to provide an over view of the work conducted.

.

Chapter 2

LITERATURE REVIEW

This Chapter presents the results and conclusions of previously reported studies that formed the foundation for this thesis. Inflatable technology has been used in tested in a number of different configurations and in numerous applications. This chapter summarizes the work that has been accomplished particularly in furthering the development of inflatable decelerators and the concepts behind inflatable mechanics. Using inflatables for space applications is not a new concept, however there is renewed interest in the application of inflatables to construct lightweight, robust and packable decelerators to reduce the launch costs (Veldman and Vermeeren 2000). With renewed interest in inflatables for space application, a great deal of work is needed to better understand the properties and load characteristics of these structures to ensure their success when in service.

2.1. Inflatable Decelerators

Previous work on inflatable technology for space application has included work on habitats, inflatable antennas, solar collectors and most recently decelerators (Veldman and Vermeeren 2000). Inflatable aerodynamic decelerator work was first developed in the 1960's when the NASA Langley Research Center proposed such devices for manned space applications (Lenard et al. 1960). Further development of inflatable decelerators continued throughout the sixties and seventies where many concepts and applications were proposed. Robinson (1965), Ryan (1966), Deveikis (1970), Jonson (1971), Bohon

(1974) proposed studies and concepts for inflatable decelerators. Further development of these structures however was not accomplished until decades later when these systems became important due to the lightweight design considerations resulting in lower fuel costs (Cheatwood 2010).

Inflatable decelerators are very applicable for Mars exploration due to the very thin atmosphere that makes entry decent and landing very difficult. Currently the largest payload delivered to the surface of Mars was the Mars Science Laboratory which had a landed mass of 850kg. This payload was delivered using a rigid decelerator 4.5m in diameter as discussed in Way et. al. (2006). This decelerator was the largest ever constructed and could not have been any larger due to the size of the rocket used. A rigid decelerator could not have be packed into a smaller diameter faring. This means that if larger pay loads are to be delivered to the surface of Mars another approach to deceleration is required. As discussed by Calomino (2011), inflatable decelerators could be used to deliver a payload of around 40Mt to the surface of mars without being prohibitively heavy or too wide in its stowed form.

2.2. Air beams

Air beams consist of fabric tubes with continuously braided or woven high strength fabrics which surround an internal bladder to allow for pressurization. These members can be manufactured to create a variety of differing curvatures or desired geometry. Once these structures are inflated they become highly rigid, and when properly incorporated into a structure, they are capable of supporting significant loads. Some of the recent work on these structures has been accomplished by Davids (2007), Davids & Zhang (2008), Malm et al. (2008), Kabche et al (2010), Nguyen et al. (2015), Clapp et al.

(2015), Guo et al. (2016) and Clapp et al. (2016). These authors discuss methods of predicting the behavior for both woven and braided pressurized airbeam structures.

Air beam structures are comprised of fibers that have a high tensile strength albeit no appreciable compressive strength. Inflatable air beams take advantage of this because using inflation pressure the fiber can be pretensied allowing for the beam to carry compressive loads up to the point that the fibers lose the pretension. This is the reason why air beams are capable of carrying significant loads and what makes these fabric structures a very interesting area of study.

It is important to understand the distinction between braided and woven inflatable fabric structures. The majority of work conducted on inflatable structures focuses on woven fabrics; however braided structures offer many benefits over woven structures most notably being a natural ability to adjust to a desired curvature. The major distinction between the two is that woven members are constructed using separate interlaced fibers at 0° and 90°. Generally the inflation pressure of woven members is less than that of braided members due to inherent weakness of the woven articles often because of a longitudinal seam or end cap. However methods have recently been developed to construct these article continuously without a longitudinal seam allowing for higher inflation pressures as discussed in Brayley (2011). Braided members are constructed using two sets of continuous fibers that wrap the circular cross-section symmetrically from the longitudinal axis as can be seen in Figure 4.

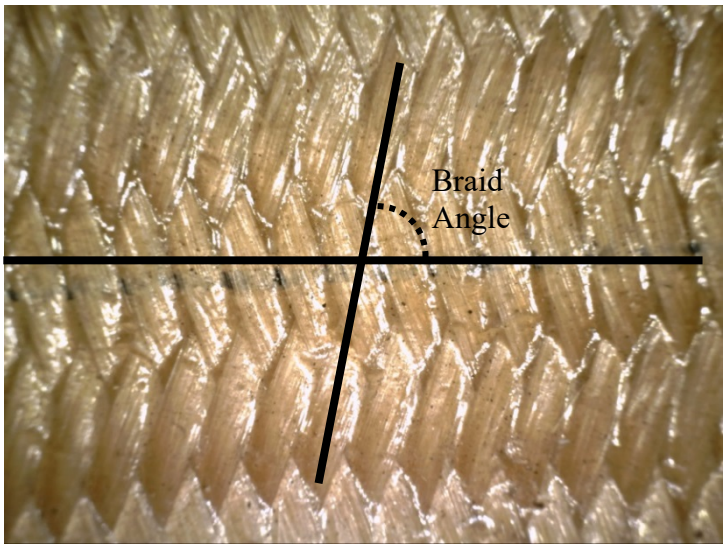

Figure 4: Braded Inflatable Braid Angle

The braid acts as a mechanism, freely adjusting to balance axial and hoop stress. This means that when a braided fabric air beam is inflated there will be a braid angle that the article will naturally go to if unrestrained. This braid angle can be shown to be 54.7° as seen in (Veldman et al. 2005). This mechanism than requires the use of axial reinforcing cords to set the air beam to the desired braid angle for the specific application. Reinforcing cords preload can be adjusted based on the braid angle chosen and internal inflation pressure allowing the article to be designed for the specific application.

2.3. HIAD Testing

Significant effort has be committed to testing HIAD structures in both ground and flight environments. Studies conducted by NASA have included single torus articles as well as full HIAD systems tested in the lab as well as flight testing as discussed in Litton, et al. (2011). Testing conducted on single torus articles was conducted by NASA with same loading fixture that was used in this testing program. Single torus testing was

conducted using a 64 load point system desiged to allow for evely distributed loading on the articles. Similar testing has also be conducted on arch structures comprised of inflated braided arch structes with externally boned renforcing straps to on the inside and outside of the articles. Details of testing conducted on thes arch structures is detailed in Davids (2009).

Chapter 3

TORUS TESTING SETUP

Testing of toroidal structures presents many interesting challenges due to the complex nature of the loading and inherent instability of the structure. This chapter discusses the test setup, testing methods and hardware used to perform testing of the HIAD single torus structures.

3.1. Fixture Setup and Physical Design

Torus testing requites complex loading cases since in-use tori will be loaded in many differing ways, and testing data is critical for developing numerical models that can accurately predict the system response. This requires that the data be very repeatable and that the initial state of the toroidal structure be very well defined so as many parameters as can be feasibly modeled are done so correctly. Torus testing conducted at UMaine improved methods that were developed by NASA for their internal testing of the toroidal structures.

The fixture that was used by both UMaine and NASA was a self-reacting frame that allowed for the torus to be radially loaded by up to 32 points on the top and 32 points on the bottom. In order to develop the best possible data from torus testing some of the loading methods and fixture setup were modified as discussed in the following section. In order to construct a cost-effective testing program, electric actuators and electronic controls were used, including electronically controlled air pressure regulation.

3.1.1. Fixture Setup

The fixture used for torus testing was constructed so that the actuators can be placed vertically and transfer the load through cables that act horizontally; this was necessary because of the space requirements imposed by the internal dimensions of the torus as well as the complication in constructing a radial load frame. Instrumentation of the torus was placed on the cable downstream of the pulley so that the pulleys did not result in inaccurate load or displacement values being either recorded as output or used by the control algorithms.

The actual design of the setup is detailed in Figure 5, which shows the layout of the cables and instrumentation that were used for the majority of the testing at UMaine. The center body shown in Figure 5 is the same fixture that was previously used by NASA for torus testing.

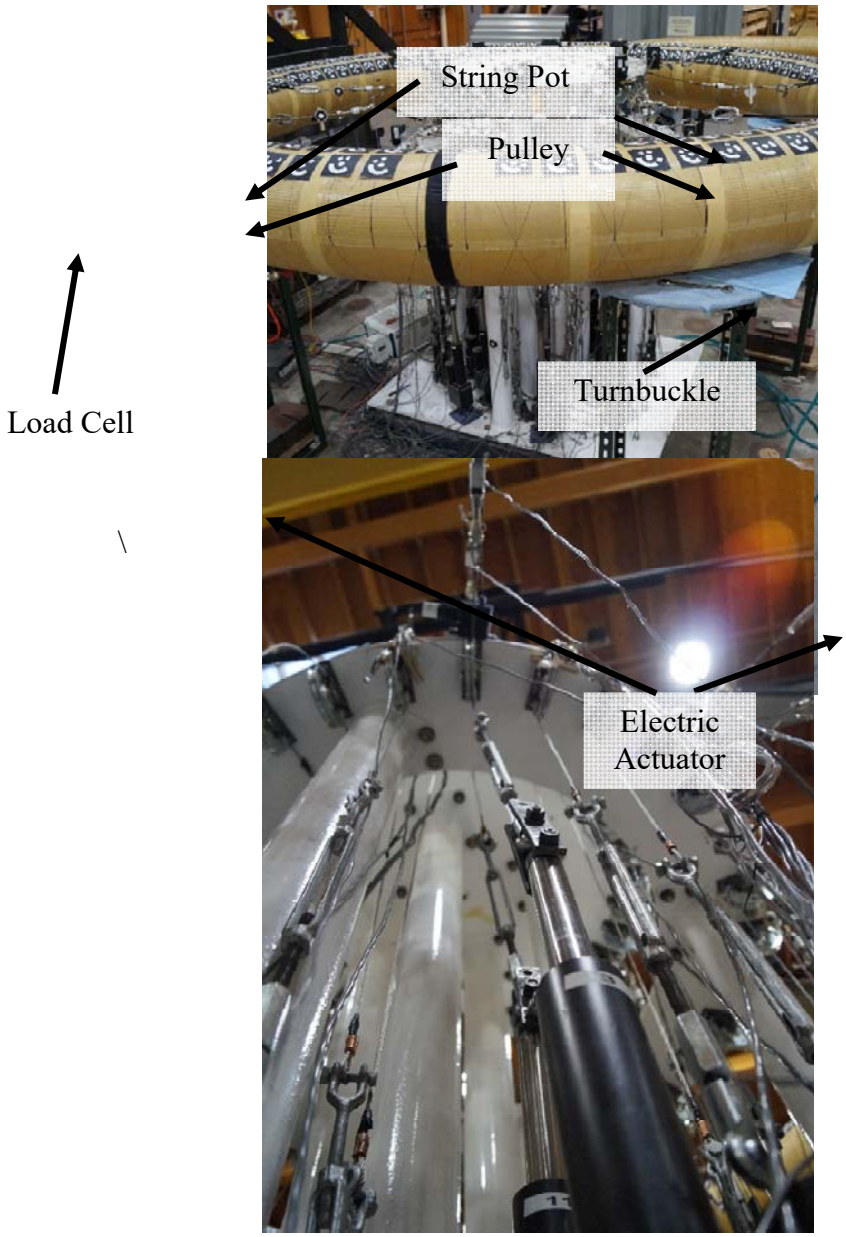

Figure 5: Torus testing Setup (left), Actuator Configuration (right)

3.1.2. 64 Load Point Configuration

The number of load cables connected to the torus affects the performance of the article during testing. To represent the loading conditions in use, a uniform load would be applied, which is best simulated by as large a number of load points as possible. The loading configuration used by NASA and for UMaine's first torus test utilized 64 cables

and load cells controlled by 16 actuators in an attempt to closely approximate uniform loading. This necessitated load splitting across four cables per actuator, which was accomplished by the use of whiffle trees. The whiffle trees spread the load across many output cables using static balancing as shown in Figure 6 below. Ideally this system allows of the load to the equally shared across all output cables regardless of their position, however in practice the load sharing is not perfectly equal.

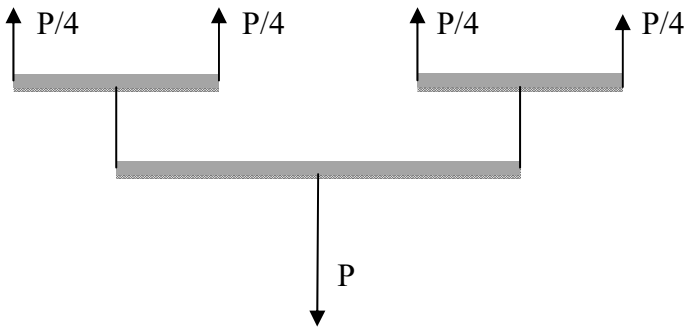

Figure 6: Whiffle Tree used for Testing

One of the issues with the whiffle tree setup was the location had to be below the pull cables so as to have parallel cables at the output of the whiffle tree. This means any loss of load in the pulleys that is not exactly the same across every cable will result in an unequal load distribution as seen by the torus during testing. This unequal loading cannot be controlled and tended to become more severe as the torus undergoes large deformations at high loads. Furthermore, the load sharing is dependent on the whiffle tree equally sharing the load across the balance, which is an accurate assumption only if there is no friction in the pivot point. Finally the whiffle tree balances the load by rotating the vertical members which results in the spacing between the cables to vary. This change of

position results in the cables becoming out of alignment with the pulleys resulting in more load losses in some of the pulleys particularly the two cables on the outside of the output.

Ultimately, the test setup was reconfigured to remove the whiffle trees, and UMaine primarily used only 16 loading points composed of eight pairs of straps located at eight equally-spaced points along the torus major radius. One loading strap of each pair was connected to the top of the torus minor radius and one strap to the bottom, which allowed torsion to be applied through unequal loads in a strap pair. This configuration gave consistent data for comparison with numerical simulations of torus response.

3.1.3. Electric Actuator Hardware

The actuators used for constructing the torus testing setup were electric actuators which allowed for the system cost to be kept low. The hardware design utilized 16 screw jack actuators from Progressive Automation (PA-17-6-2000). The PA-17 can apply forces up to 8.89 kN (2,000 lbs) at a maximum displacement rate of 0.00838 m/sec (0.3in/sec) with a total of 0.152m (6in) of stroke. This highlights the main issue of electric actuation, which is rate of displacement application. Hydraulic actuators are typically much faster, which is advantageous when testing an unstable structure such as a torus. However, appropriate hydraulic actuation was not available and could not be purchased for this project.

The chosen system allowed for the torus to be loaded according to the needs determined by the controlling algorithm. The actuators were powered using two 100A Power Max PM3-100-12 power supplies each connected through

H-bridges to 8 actuators. The h-bridges used in the control system allowed for the voltage supplied to the motors to be controlled from -12v to 12v depending on the pulse width modulated signal coming from the controlling program. Details of the actuator control system and algorithm are given in Chapter 4. Cytron technologies MD10C cards were used as the H-bridge cards in the torus testing setup.

3.1.4. Air Pressure Regulation

Regulating the air pressure inside the torus is critical for performing tests on inflated fabric structures. The hardware that was used in torus testing for regulating the air pressure in the torus was two 12V actuated Red Hat solenoid valves that allowed for the tours to either be open to the pressurized air source, held at a constant volume or vented to the atmosphere. The two ASCO red hat solenoid valves were powered using the 12V Power Max power supply and controlled using two relays controlled through an optically isolated circuit connected to an Arduino. The circuit also included a flywheel diode across the relay solenoid connection which prevented a large back EMF when the solenoid coil is disconnected. Essentially the back EMF is created by the magnetic field in the solenoid rapidly changing which results in a reverse polarity voltage spike.

3.2. Testing Procedures and Practices

Testing the tori required many methods to be developed that ensured the best possible results from torus testing. Many of the methods that were used at UMaine were adapted from initial testing performed by NASA. One specific modification that was previously discussed was the number of load points used to load the torus. There were also several methods and test protocols that were specifically developed for the testing run at UMaine which are detailed in the remainder of this section.

3.2.1. Strap Bonding

During the course of torus testing there was a need to bond straps to new specimens that were delivered to UMaine. In order to achieve consistent bonding and increase the success in bonding straps it was decided that the 3M Scotch-Weld TS230 Polyurethane Reactive Adhesive used by NASA to bond the straps to the torus might have unnecessarily high strength given the inherently low bond strength between the torus coating and braided torus fabric. Another reason for not using the TS230 bonding agent was the very short, 30 second working time of the adhesive.

During the process of torus testing it was decided that a small investigation into other methods for bonding the straps could be useful in simplifying the strap bonding process for the purpose of torus testing. A test was conducted with a strap bonded using VitaFlex and Spray90 adhesives as well as a control strap with no adhesive. The Spray90 was chosen as a potential bonding agent due to its ease of application and availability. VitaFlex was also chosen because it is already used to set the braid matrix and it was likely to bond well to itself. The straps were then loaded to 44.5N on one side and up to 1kN on the opposite side to produce a much larger torque .than would be applied to the torus during nominal testing. The results from the test can be seen in Figure 7. The loading of a single strap was accomplished using the torus testing setup with all the other straps pretensioned then held in place to restrain the article.

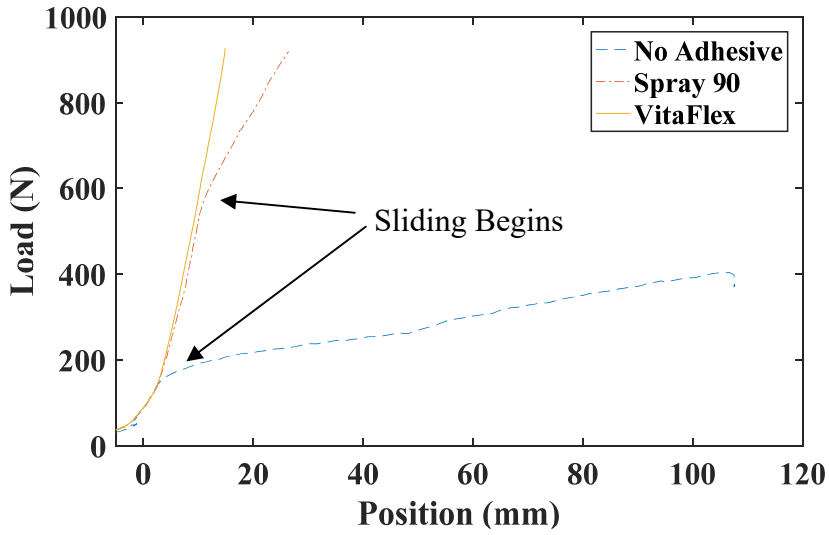

Figure 7: Strap Adhesive Performance

The best adhesive for bonding straps to the torus was determined to be VitaFlex, which is the coating substance used to coat the braid of the torus. VitaFlex was determined to possess adequate shear properties to bond the straps to the torus for the purpose of testing. During torus testing the only situation that would likely result in the debonding of the straps from the torus would be very large local deformation of the torus at a strap location.

3.2.2. Torus Centering and Specimen Configuration

In order to ensure that the torus was tested with the best possible methods many components had to be carefully aligned and centered so loading was consistent. The torus setup had cables that connected from the actuators to the torus straps. These cables could have their length adjusted by the use of in line turnbuckles allowing for the torus to be properly centered to the load frame. Before torus testing was initialized the torus was centered by first measuring the distance from the center of the load frame to the torus on

the north side and the south side and ensuring that they were the same. The process was repeated for the east and west side. Once the torus was centered the turnbuckles were adjusted to take all unnecessary slack out of the load cables. The torus does not remain at the same radius for differing inflation pressures so the cables required more slack if they are adjusted at low pressure as opposed to their maximum inflation pressure.

3.2.3. Inflation and Deflation

Inflation pressure plays a large role in the response of the torus to loading. While the pressure during the test is clearly the largest component there is some effect on the properties of the torus based on the time the torus has been inflated. There is also some amount of stiffening that occurs in the torus if the pressure is lowered allowing for the fabric to recover from the loading damage. Before the articles were tested for the first time each specimen was inflated to 138kPa and deflated to 5.5kPa three times to fully set the shape of the torus and ensure that the effects of storage were completely removed.

3.2.4. Test Matrix and Test Design

Torus testing followed an automated protocol to ensure that the tests were executed with specific wait times between each test. The torus tests were run at four different pressures covering the envelope of likely operating pressures for the HIAD. Each test was also repeated five times to ensure that the data was repeatable. For most of the articles that were tested at UMaine a displacement controlled testing method was used. The torus was first subjected to very small displacement which was repeated five

times. Between each of the five repeat tests the torus was allowed 15 minutes to recover from the previous test while being held at the test pressure. Once the test was begun the inflation pressure was not changed so that any effects due to the loading were not influenced by pressure regulation.

After the five tests had been completed on the torus the article was depressurized to 5.5 kPa, which was sufficiently low to allow the braid to slightly reorient but high enough to prevent debonding of the photogrammetry dot targets. After the torus was reinflated to the specified test pressure there was a 25 minute wait period to allow for the transient inflation effects to completely dissipate. Once the torus had been tested at 34kPa, 69kPa, 103kPa and 138kPa the next level of displacement was applied to the torus using the same methods as the previous level of displacement.

3.2.5. Photogrammetry and Dot Configuration

Determining the exact position and accurately characterizing the shape of the torus are critical in understanding the performance of the article as well as providing important data to validate numerical models. In order to achieve this level of fidelity the PONTOS photogrammetry system was used to accurately determine the position of circular targets. This system works by acquiring two photos from cameras mounted at a distance from each other as shown in Figure 8 below. Also shown in the figure are photos acquired from the cameras that have slightly differing perspectives.

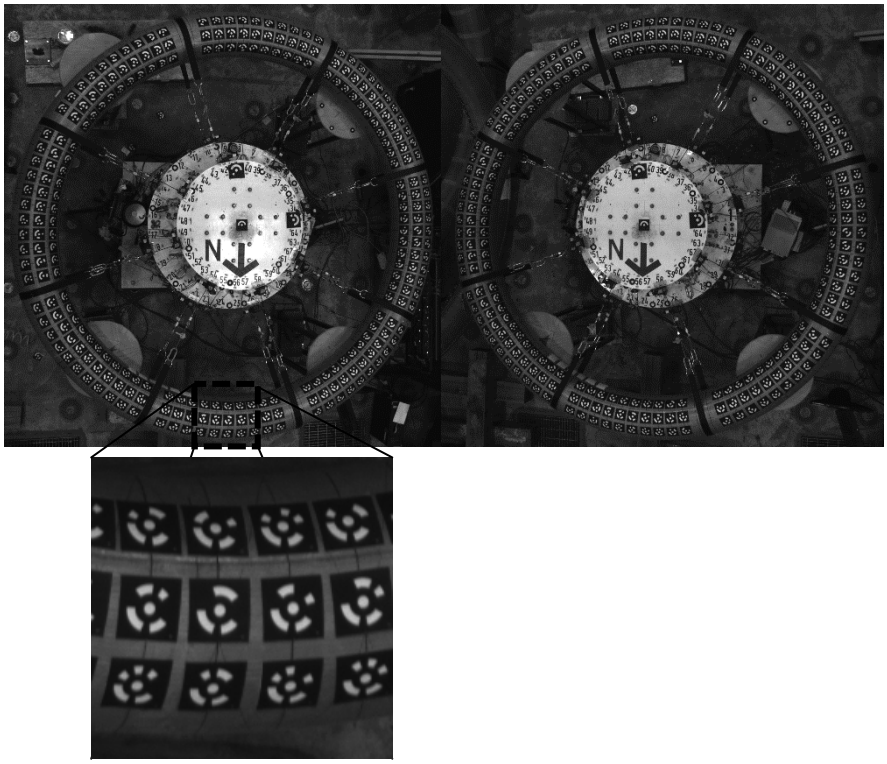

Figure 8: Photos from Photogrammetry and Pontos Dots

The two photos are then matched up by the software providing a full 3D point cloud matched to the dots in the photos. Furthermore the dots that were used for most of the tori in UMaine research were code points. These code points could each be uniquely identified because of the barcode-like pattern that encircles the center dot as shown in Figure 8. Points could be easily tracked allowing for the position of the tori to be determined including rotations of the cross-section. The resulting point cloud from the PONTOS software yields a point cloud like that shown in Figure 9.

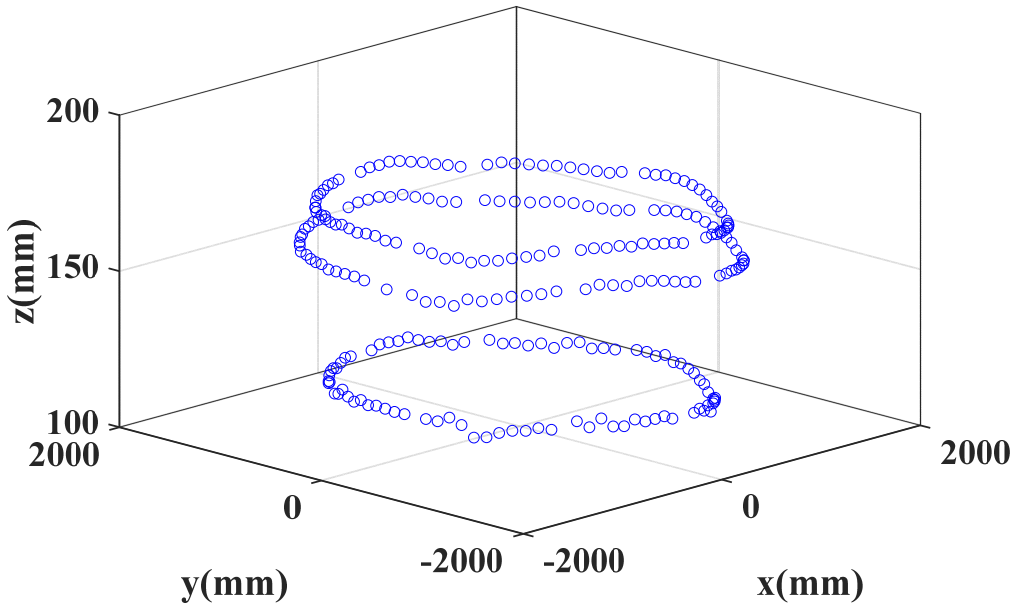

Figure 9: Torus Point Cloud from PONTOS

To ensure that the greatest amount of torus geometric information could be ascertained from the test run the dots were placed at very specific positions on the torus. The braid that the torus is constructed from has two tracer threads that run in a helical manner around the torus creating intersections as seen in Figure 10. Concentric lines were placed on the torus marking where the centers of the PONTOS dots were to be placed.

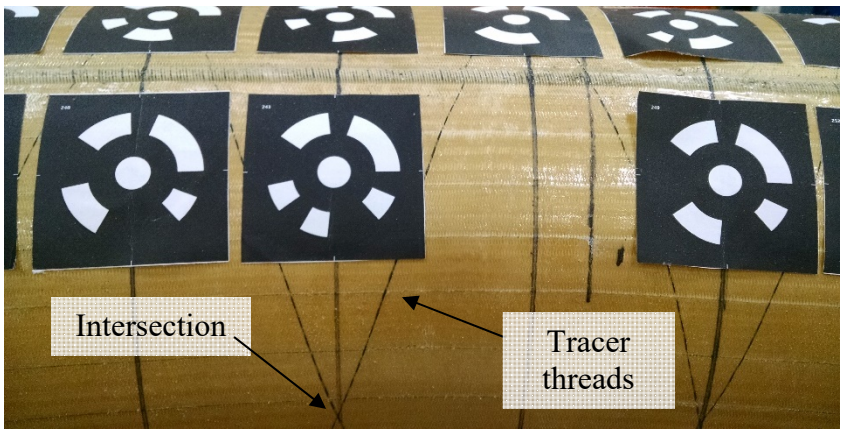

Figure 10: Dot Placing Method

The dot configuration allowed for the braid angle to be roughly approximated by the position of the dots during the test. The point cloud data however is not that useful for directly determining the position of the torus because the partially arbitrary nature of dot placement. This is because the dots cannot be used to directly measure the center axis of the article, so fitting is required to ascertain this information. Post processing routines were used to determine a best fit torus for a selected point range of the torus. This allowed for the center of the torus to be approximated during the torus testing.

3.3. Calibration and Instrumentation

Torus testing required a great deal of data acquisition equipment to allow for the full spectrum of measurements to be taken. The setup included 64 Transducer Techniques TLL-1K load cells for measuring the cable loads which were wired to eight NI TB 4330 cards. The load cells were connected in line with the load cable near the attachment to the load strap as seen in Figure 11. These load cells had a capacity of 4.4kN. The instrumentation cards allows for the data acquisition hardware to acquire 25,600

samples/second simultaneously on all channels with fully integrated hardware filtering. This maximum sample rate was used in testing to ensure that the least amount of hardware buffer time was present.

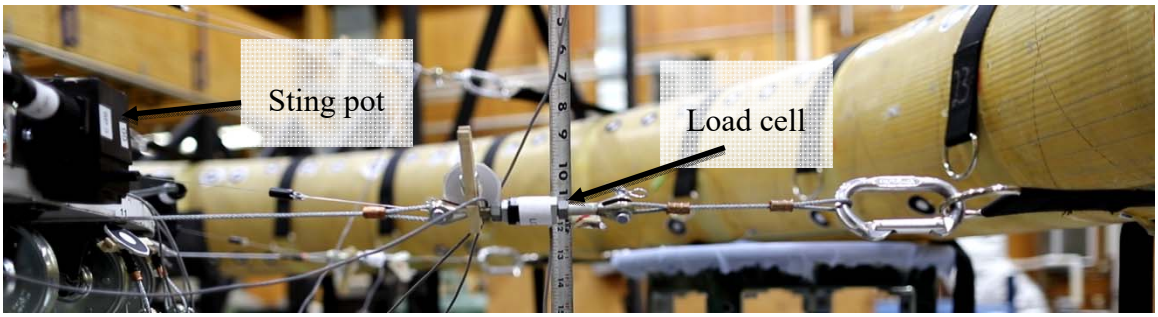

Figure 11: Load Cell and String Pot Configuration

The torus testing instrumentation also included 16 string pots to measure the cable displacements produced by each actuator as the torus was loaded. These string pots can be seen in Figure 11 on the left. Celesco PT1A-10 string pots were used wired to two 8 channel NI TB4339 data acquisition cards. The string pots allow for the cable movements to be accurately measured in real time enabling the system to run in displacement control. Because processing the photogrammetry data is so computationally intensive the position of the torus cannot be determined in real time during testing, making the string pots the only available position data for the controller (detailed in Chapter 4). In order to measure the inflation pressure in the test article a Setra Systems Model 807 transducer was connected to the same acquisition card as the string pots. The pressure transducer was powered using a Keithley 2220G-30-1 power supply set to 15V.

3.3.1. Instrumentation Verification

Before the instrumentation was used in testing, verification was performed on each instrument to ensure that the readings were as accurate as possible. All of the 64 load cells used for testing were verified using the 10kip load cell on a Instron testing rig. All the load cells that were used in testing produced correct readings while being loaded and unloaded. As a secondary precaution once the load cells were wired into the configuration and hardware used in testing a known weight was suspended from the instrument to ensure it yielded the correct reading. The string pots were also verified using a machined aluminum block that had 76.2mm, 127mm and 177.8mm steps. This allowed for the string pot to be extended to each length up and down to ensure consistent readings and accurate calibration.

3.3.2. String Pot Corrections

Instrumenting the torus testing setup with string pots presented some challenges because of the interference between the load cables and the ties for the string pot attachment. Ideally the string pots would have been placed directly in line with the load cables, however the only location at which this was feasible was directly behind the pulley after the load cable drops down to connect to the actuators. Originally it was thought that this would be an ideal location for the string pots; however, after initial investigation it became clear that the load cables would pinch the string pot lines within the wire twist of the cables as load was applied. This resulted in erroneous readings and discontinuities in the string pot data.

Finally, it was determined that the string pots would have to be placed above the cables as shown in Figure 11. Positioning the string pots as such did eliminate any issues

where the cables became intertwined with the lines for the string pots. The position used did introduce offset error in the readings. This error is a result of the fact that the measurement from the string pot is actually the change in length of the hypotenuse of a triangle formed by the load cable, sting pot and the vertical rise between the cable and the string pot position. Correcting for the actual displacement reading is possible if the height of the string pot above the cable is known along with the length of string attached to the sting pot. With these measurements acquired for each string pot attachment used in the testing setup a corrected reading was calculated and stored as output data from the test. This corrected reading was the value used to determine in the displacement to apply during a test by the controller.

One further issue with the string pot measurement is the inherent drop that occurs because the load cables sag under self-weight. This results in a somewhat significant drop in the center of the cable if the load is below 100N. In order to prevent this error from affecting the displacement readings and contributing to displacement error in a displacement controlled test, this error had to be accounted for. The results shown in Figure 12 depict the vertical drop of the load cable during torus testing.

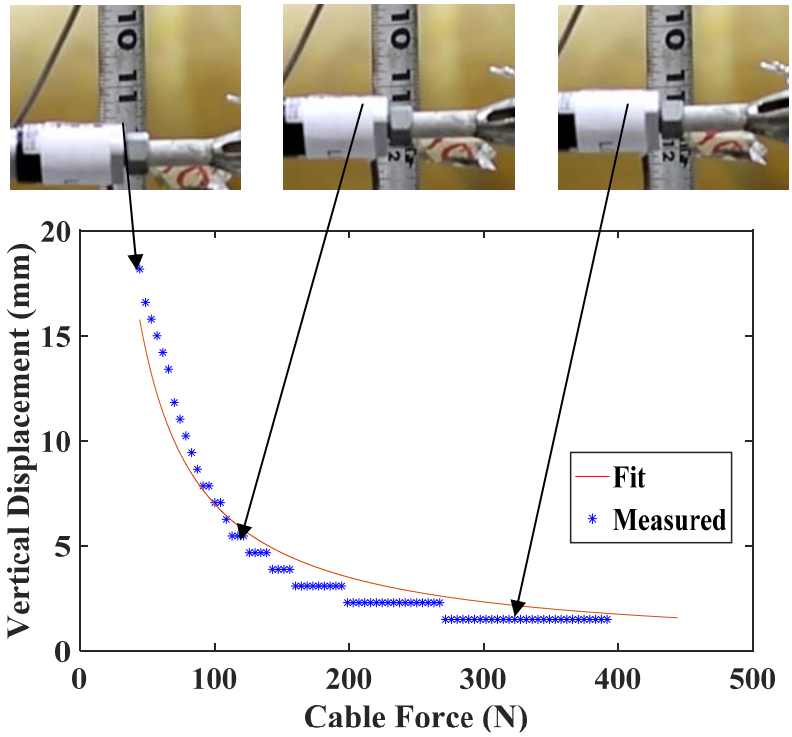

Figure 12: Vertical Drop at Low Cable Loads

The relationship between the vertical displacement of the cable and the load can be accurately approximated using an inversely proportional relationship shown in Eq. 3.1, where h_d is vertical drop, P is cable tension, and K_d is a proportionality constant. Fitting this relationship to the data collected yields 733.7mm N as the proportionality constant. This load displacement relationship only accounts for around 2mm of string pot displacement correction between 50N to 100N, however it is still important to consider in the string pot measurements.

$$h_d = \frac{K_d}{P} \quad \text{(eqn. 3.1)}$$

3.4. Summary

The test setup provides a good platform for testing the torus using many different load schemes. Through the use of overhead photogrammetry the actual shape of the torus could be attained and provided a good deal of data for the purpose of model validation. The control processes that were used to control the actuators based on the real time data are further investigated in the next chapter.

Chapter 4

HIAD TESTING CONTROL SYSTEM

Control systems of all types are used in many different situations where precise actuation is required. Many control systems rely on a Proportional Integral Differential (PID) control algorithm to determine the output based on the error of the system. This method is described in detail in the following section and the specific considerations needed for designing a control system for torus testing. This chapter explains the interworking and the basic design of the control system used in testing the HIAD single torus structures. The hardware used in designing the system as well as the software that was developed are detailed in the following sections. The control system used for torus testing at the University of Maine was developed in house and specifically designed to satisfy the constraints of torus testing.

4.1. Control System Design and Constraints

The control system was required to have multiple, independently controlled actuators in order to apply complex load cases to the torus as discussed in Chapter 3. In order to provide a robust control system at lower cost electric actuators were chosen because of the low price point and the low cost of the accessories needed to produce fine control of these actuators. For the specific application of torus testing the loads applied to the top and the bottom were independent to allow the application of torsion as well as achieve balanced loading. The largest number of actuators that could be feasibly included in the control system was sixteen because of physical size constraints imposed by the fixture as well as the difficulty of controlling a greater number of actuators.

NI hardware was used to measure the load applied by the cable to the torus as well as drive the H-bridge cards used for the actuators. String pots were also used to measure the cable displacement. This combination allowed for the control system to respond to both position as well as load data.

4.2. Control Algorithms

While there are many differing ways to determine the response of the system to the load and string pot inputs, the control system that was designed for this testing uses a load corrected PID control Algorithm. PID control algorithms depend on three parameters to scale the error in order to produce the appropriate voltage output to the actuators. The proportional parameter directly scales the actuator output based on the current error (load or displacement). The integral parameter accounts for the accumulated error over time, which means the response intensity is increased if the system has been off the set point for a large amount of time. The differential parameter scales the response based on the rate of change in the error. These relationships can be mathematically represented by equation 4.1 below.

$$u(t) = K_p\, e(t) + K_i \int_0^{\tau} e(t)\, dt + K_d \frac{de(t)}{dt} \quad \text{(eqn. 4.1)}$$

Where $u(t)$ is voltage output to the actuator, $e(t)$ is the error in either displacement or load depending on control type, K_p is the proportional constant, K_i is the integral constant, K_d is the differential constant and τ is the length of time over which the integral error is calculated. In order to attain the best results from the control system the PID control algorithm for the HIAD control system uses a load scaling algorithm. Load

scaling ensures that the control system operates very responsively but also with a good deal of stability. Inflated fabric structures do not have a constant stiffness, which is why load scaling works well for this control system. Further, the use of electric actuators means that the response of the actuator is also load dependent. The combination of the load scaling and the generic equation for a PID controller yields equation 4.2.

$$u(t) = (K_p - S_p P)\, e(t) + (K_i - S_i P) \int_0^\tau e(t)\, dt + (K_d - S_d P) \frac{de(t)}{dt} \quad \text{(egn 4.2)}$$

where $S_p$is the proportional slope, $S_i$is the integral slope and S_d is the differential slope. The control parameters can be defined with seven tunable parameters as well as the load on the actuator. P is used in the above equation to represent the load on the actuator. The three S parameters are the slopes of all the PID parameters which allows for the PID values to be scaled based on the load. It was determined that for torus testing slopes that reduced the PID parameters by approximately half the original value at maximum load level produced the best results. Since the data collected by the controller is discrete the integration length for the parameter *I* is defined by the number of control loop iterations. Table 1 gives the values for both load as well as displacement control that were determined by tuning with a previously tested article.

Table 1: Summary of Control Parameters

	Load Control	Position Control
K_P	54.925 $^{V}/_{kN}$	545.20 $^{V}/_{m}$
K_I	5.6317 $^{V}/_{kN\ s}$	83.763 $^{V}/_{m\ s}$
K_D	0.4611 $^{V\ s}/_{kN}$	7.0866 $^{V\ s}/_{m}$
S_P	1212.9 $^{V}/_{kN^2}$	141.61 $^{V}/_{kN\ m}$
S_I	933.03 $^{V}/_{kN^2 s}$	102.12 $^{V}/_{kN\ m\ s}$
S_D	758.09 $^{V\ s}/_{kN^2}$	94.829 $^{V\ s}/_{kN\ m}$
τ	60	60

The values correspond to the voltage at the motor which can be driven by ±12V to produce full advance or full reverse of the actuator. Instability is inherent in many control systems at the edge of their operating envelope; however for this particular system all actuators are influenced by the others to some degree, increasing the difficulty in producing stability for a range of testing profiles. In Figure 13 response of the controller of a single control channel during a HIAD test can be seen including the terms form the PID control. Each PID term represents the complete calculation of each term in equation such that it can be represented as displayed in equations 4.3 through 4.5 below.

$$P = \left(K_p - S_p P\right) e(t) \quad \text{(eqn. 4.3)}$$

$$I = (K_i - S_i P) \int_0^{\tau} e(t)\, dt \quad \text{(eqn. 4.4)}$$

$$D = (K_d - S_d P) \frac{de(t)}{dt} \quad \text{(eqn. 4.5)}$$

As previously discussed the initial period of the test the controller uses load control to achieve a specified preload of 44.5N on each cable. The preload period can be seen in the first minute after this the controller switches to a displacement controlled

system where the zero is set at the preload level. The test shown in Figure 13 was a uniform displacement ramp up to 76mm then a uniform unload ramp back to zero as seen by the string pot reading.

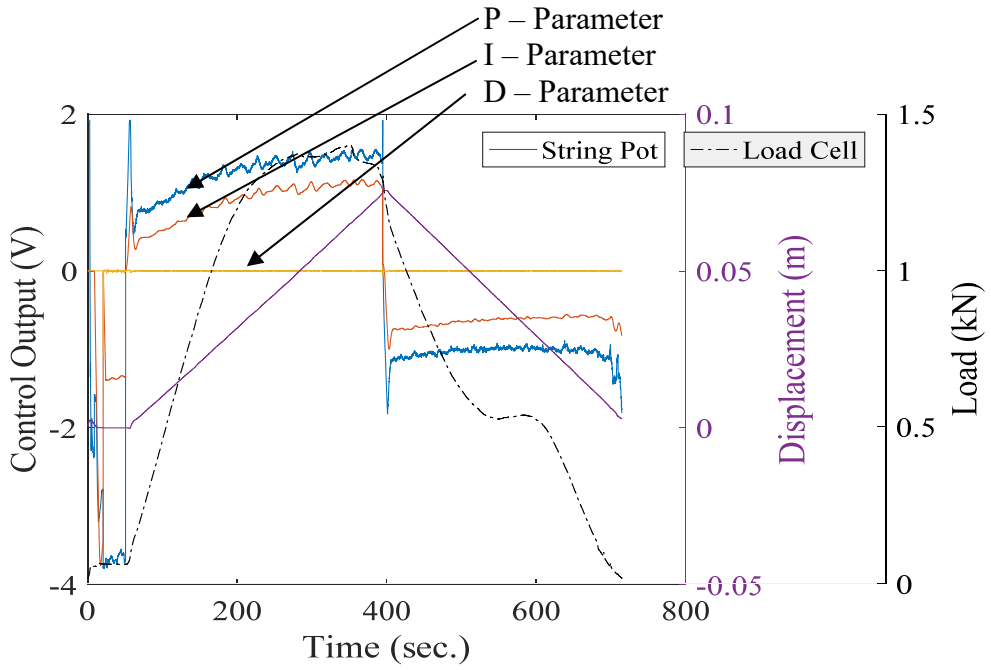

Figure 13: Control System Response during Torus Test

Clearly the controller is exhibiting good performance in the test shown in Figure 13 where the displacement ramp is very linear as specified for the test as measured by the string pot. The only parameter that cannot be seen contributing to the response in the figure is the derivative parameter; this is because the differential is only used if the test becomes unstable since it acts as a damping term in this controller.

4.3. MATLAB-based Control System

Designing a well-built control system requires a robust language that can integrate the data acquisition efficiently in real time. MATLAB provided a good platform for designing a control system because of its prebuilt hardware integrations as well as the large depth of expertise with its functionality at the Advanced Structures and Composites Center. Using MATLAB's high level programing environment allowed for the control system design to be specifically tailored to the needs imposed by torus testing.

The controlling program was based on a fixed length iteration operating at 20 Hz. The control function operates based on the input from a test matrix that is preset and passed to the controller. The test matrix is designed so that each row specifies control details for each stage of the test including a predefined execution time. The test matrix allows for the control type to be changed for each stage of the matrix as well as the control parameters if different tuning is better suited for a specific stage of execution. This is specifically used at the beginning of the test where only proportional control is used to quickly have all actuators engaged.

The flow chart shown in Figure 14 visually depicts the control logic that is used in the main control function of the HIAD control system. As seen in the flow chart the function is called from a graphical user interface (GUI) that allows the user to specify the control matrix and observe that data as it is acquired by the control computer. The control function executes the control logic specified in the test matrix as shown and collects data at the specified iteration rate of 20 Hz.

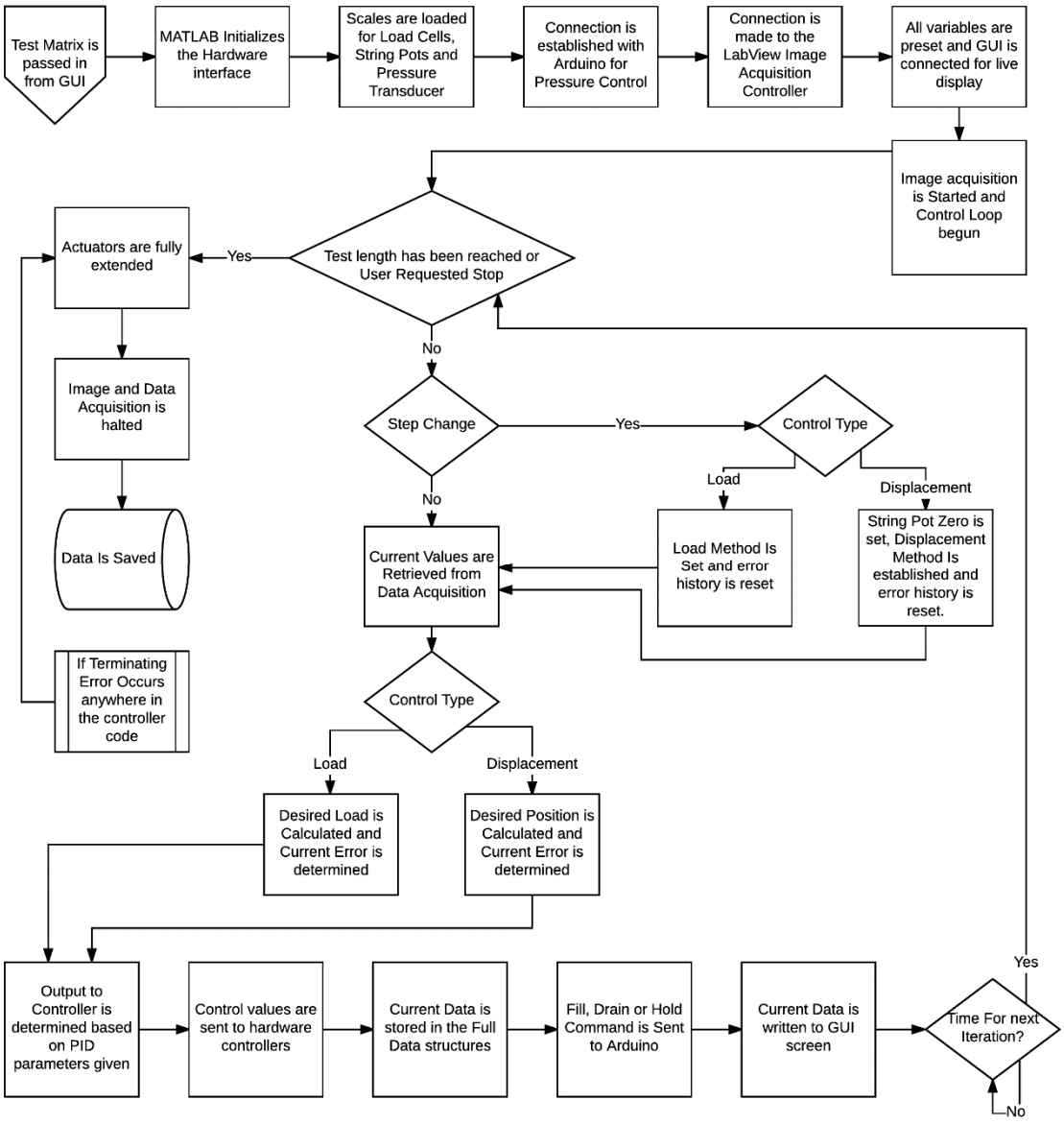

Figure 14: Main Control Function Program Flow

The control function allows for all the differing test profiles that are required for torus testing to be accomplished. The control logic used to design the main control function allows for the system to be very flexible and work through various test matrices.

This function could be easily modified to function in a variety of different testing setups and is versatile to allow for control systems to be used with more actuators as the hardware would allow. The realistic limitation would likely be 32-64 total actuators limited by communication times of the instrumentation and particularly the pulse width modulated PWM outputs.

4.3.1. National Instruments Hardware Integration

MATLAB has a built in tool box that allows for data acquisition in real time and specific functionality for National Instruments hardware. For the purpose of this control system the data acquisition runs with a session based background data acquisition method. Data is made available to the controller once the specified number of samples has been taken. Data acquisition rate is run at 20,000 samples per second which is the maximum rate of the hardware. There is an inherent lag between the time the sample is taken and the data that is sent, which is 23 samples at this rate. Using this rate ensures that there is a minimum amount of lag between data seen by the controller and the actual current values. This data is stored in a temporary global variable until it is requested by the control system iteration or overwritten by the next sample. This method ensures that there is no buffer delay since the controller will be passed the most current data regardless of timing.

4.3.2. Arduino Hardware Integration

Arduino open source hardware allows for the control system hardware to be controlled very cost effectively. Originally the control system was designed to control the actuators with two Arduino Mega boards which have fourteen (PWM) channels. These boards are capable of receiving serial commands directly from MATLAB by programing

the board with a serial interpreter and coding the specific commands on to the chip. More detail on the specific code and implementation for using Arduino controlled electric actuators can be found in appendix B.

For the purposes of driving the actuators in the torus testing control system National Instruments hardware capable of generating PWM signals was used. The Arduino platform was however still used to control the solenoid valves required to fill or drain the torus. This allowed for the torus to be regulated at a specific pressure prior to as well as during testing. The interface coded for the Arduino is capable of being used both for PWM output and pressure control.

4.4. Testing Automation

Designing a control system for testing fabric structures presents a number of difficulties that need to be overcome. One important aspect of the torus testing performed for NASA was demonstrating repeatability and consistency between multiple tests of the same torus for the same testing parameters. This required that the tests be run with specific timing and rest periods between each test run. Another consideration that made test automation an important priority was that number of test that needed to be accomplished. To data, over 1000 hours of active testing has been performed.

MATLAB provided an excellent environment for automating the testing of the tori. A function was developed that the desired test parameters could be preset for an entire series of tests including the pressure set point. This allowed the torus to be brought down to a low pressure between testing sets. The torus was also regulated to the test pressure for a specific amount of time before the tests began.

4.5. Summary

The control system design detailed in this chapter allows for adaptability and robust control of the torus setup providing consistent and well-formatted data for use in model validation. As highlighted in the previous chapter the control system is adaptable to other applications where a greater or fewer number of actuators are needed for testing. Designing the control system coding and choosing the hardware in-house allowed for customized implementation of the program and brought about the development of automation and data acquisition tools that have application beyond the scope of this work.

Chapter 5

T4 TESTING AND RESULTS

This chapter describes the testing and results from the two pristine T4 tori that were tested at UMaine as well as testing performed on the T4A-1 article previously load tested at NASA Armstrong. The testing matrix that was used for the two pristine tori that were tested is described in detail in the following section. The two tori that were tested were pristine tori without buffers. The buffers consisted of fabric bonded to the torus under the load straps to help stabilize the strap braid interaction. These two tori were constructed specifically for the testing at UMaine and had not been previously load tested. All three tori were conventionally reinforced with two-cords. This testing was directed towards determining the repeatability of the load and displacement testing as well as establishing the load displacement response for the articles tested.

Throughout the torus testing program high levels of loading would result in a loss of repeatability in the load response of the article. This loss of repeatability is referred to as damage in the following chapter; however, for all the T4 articles tested no visible signs of damage to the articles were found throughout all phases of testing.

5.1. Quantifying the Response of the Torus to Loading

Every test produces millions of individual data points between the photogrammetry system, load cells and the string pots. Many different aspects of response can be quantified with this data, however in order to compare many tests specific parameters must be calculated from the test. One of the quantities that can help to understand the response of the torus during loading is the average radius. This value can

be computed by interpolating displacements measured at discrete points on the torus to evenly spaced angular positions on the torus. Interpolation is necessary because the data is not always evenly distributed around the torus circumference, and unevenly distributed data points could result in some areas having greater influence on the average then other regions. Further, the choice of points used to interpolate radius measurements can have an effect on the final characteristics of the trend lines. As shown in Figure 15 below, data from a test run on a nominal two-cord torus to a cable end displacement of 50.1mm displays an envelope of the values that could be calculated for the average major radius for this test.

The average value at the strap uses the radius value computed by interpolating from the points immediately adjacent to the strap on both sides and computing the center of the cross sections where the loading strap is located. The same approach can be taken to determine the average radius computed at the angular position directly between the load straps. Finally the last method shown in Figure 15 is determined by interpolating data to angular points evenly spaced 0.0175 radians apart. Every method has merit when interpreting the data from a torus test, however, the evenly-distributed method was chosen for most tests because it tends to be more robust at larger levels of displacement. This is due to the fact that the strap location and region directly between the straps are the most difficult areas to fit due to high local curvature. The average computed at the strap can be useful in understanding the compliance of the strap as well as the strap-torus interaction. This compliance can be seen in the fact that the center of the torus under the strap does not achieve the 50.1mm achieved by the ends of the load straps in Figure 15.

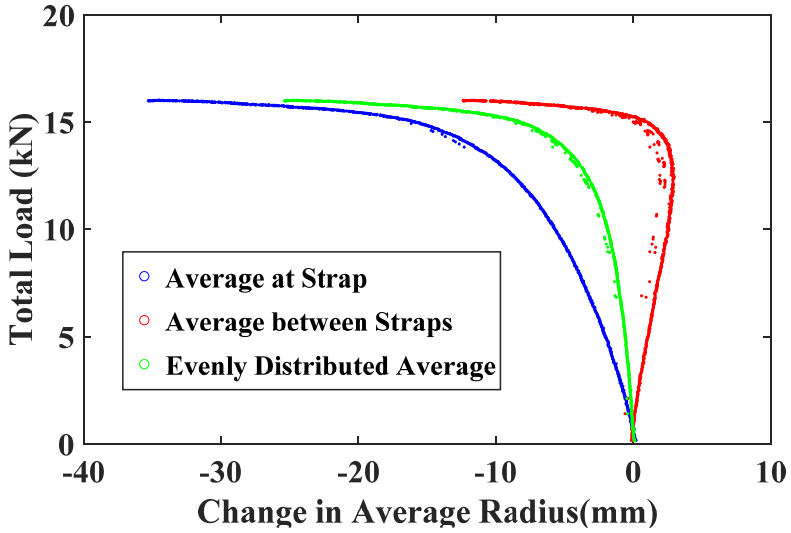

Figure 15: Average Major Radius Computation Methods

The average between the straps clearly has merit when understanding the behavior of the torus, however, tori often deform in a four pointed shape producing extremes minimum and maximum radii between different straps. This shape trend can be seen in Figure 16 where the two measurement groups deflect the opposite directions. The result of using the average between straps shown in Figure 15 is the average of these two relationships shown in Figure 16, and it can be unreliable due to local areas of bad or unavailable fit data. This can lead to data that is not consistent between sets of tori. This method of measuring the average radius of the torus does have a great deal of merit when determining the compressive response of a particular torus and can be a good predictor of the onset of permanent damage to the torus. Ultimately the evenly distributed method for calculating the average radius of the torus provided the most robust and repeatable method for quantifying the average radius of the torus.

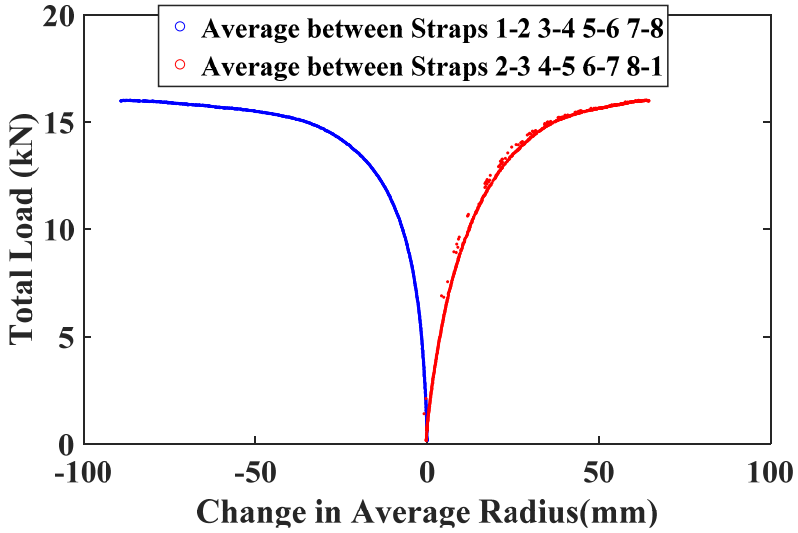

Figure 16: Four Pointed Between Strap Methods

The average radius can be influenced by parameters other than the loading on the torus. One such parameter is the inflation pressure. Since the fabric article has the tendency to stretch to a greater extent with increasing pressure. For this reason the average radius is zeroed at the start of the test in Figure 15 and Figure 16, which prevents any transient and pressure dependent changes from impacting the data trends. As seen in Figure 17 the average radius of the torus is very dependent on the inflation pressure. The figure also shows the transient behavior of the average radius once a specific inflation pressure has been reached. As seen in the figure, the article continues to expand for 15 to 20 minutes beyond the point at which the inflation pressure reached the target value. The average radius of different tori can also change because of manufacturing tolerances that make one torus slightly larger or smaller than the others.

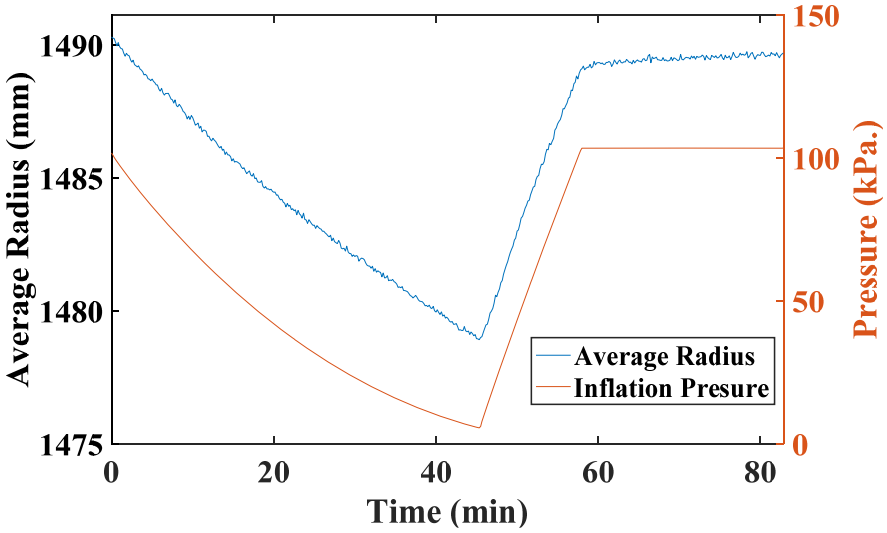

Figure 17: Pressure Dependency of Major Radius

One of the drawbacks with the average radius measurements is there is no direct relationship between this value and the damage that the torus has sustained during testing. Because the shape of the torus is impacted by damage to the torus, the shape is an important marker of the state of the torus. Shape however is difficult to quantify for something as geometrically complex as a deformed torus. In an attempt to overcome this challenge a method was developed wherein the plane deformed area of the torus was calculated. This can be computed by determining the in-plane shape of the perfect torus and measuring the area created by overlaying the actual shape of the torus as shown in Figure 18. This allows for the condition of one torus to be compared to another because the deformed area is a direct measure of the torus deformation. Further, the deformed shape of the torus can be measured in its initial state even before it has accumulated any deformation due to loading. The torus is compared to the perfect torus case since the

preexisting deformations in the pristine state may affect the response of the article so it should be considered in the measurement of deformation.

The method used for computing the deformed area used a discrete formula where the torus was angularly divided into 1000 wedges and the wedge area was computed using the center radial offset. This area is considered positive for both inside the perfect torus and outside the perfect torus perimeter and all area contributions areas are summed to get the total deformed area.

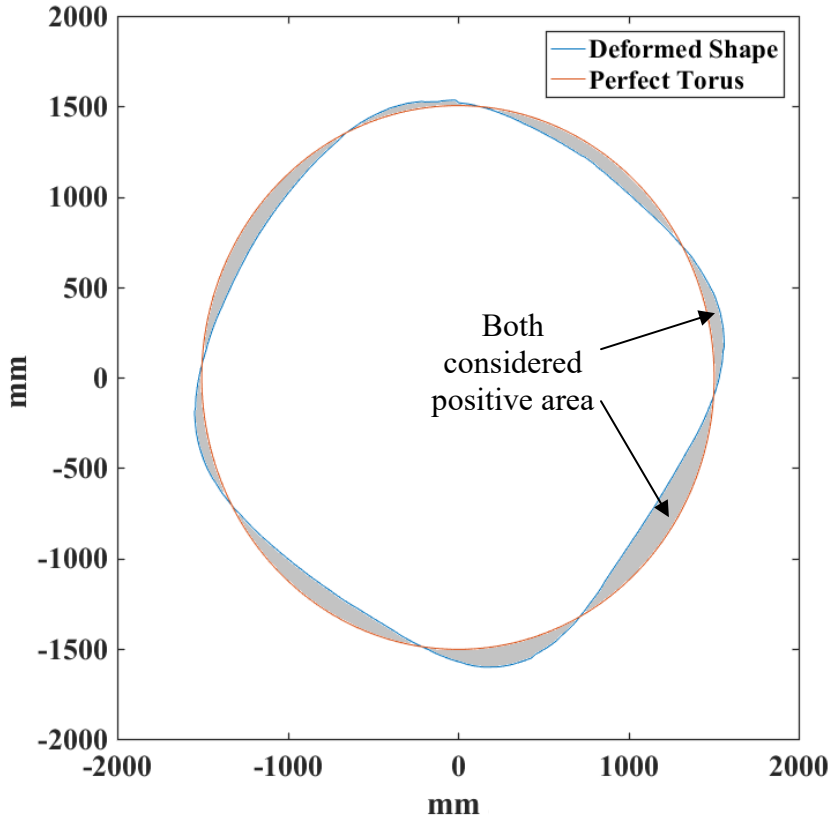

Figure 18: Deformed Area of the Torus

Using these methods, results of the torus testing can be directly compared and plotted for a variety of parameters and loading conditions. These two methods of plotting

allow for the data from the test to be used in demonstrating damage to the torus and the general effects of torus loading.

5.2. Testing Tori with 64 Cables

Torus testing initially used a 64 cable loading schemes as discussed in section 3.1.2. Loading with 64 points was accomplished using the whiffle trees shown in Figure 6 to distribute the loads across four cables using only one actuator. The tests were all run in load control so that the average load across all four of the load cells connected to a single actuator was used as the control load. This ensured that the total load achieved by the system was correct and the overall region received the correct load. The series in which the article was tested is shown in Table 2 below. Tests were stopped if a runaway condition was encountered, which can occur in load control. As seen in Table 2, two of the load cases were only tested once because they both resulted in a runaway displacement condition.

Table 2: Test Matrix for T4A-1

Number of Tests Run	Operating Pressure (kPa)	Final Total Load (kN)
2	34.5	4.4
2	34.5	6.6
2	34.5	8.8
2	34.5	11
1	34.5	13.2
2	68.9	4.4
2	68.9	6.6
2	68.9	8.8
2	68.9	11
2	68.9	13.2
2	103.4	4.4
2	103.4	6.6
2	103.4	8.8
2	103.4	11
2	103.4	13.2
2	103.4	15.4
1	103.4	17.6
2	137.9	4.4
2	137.9	6.6
2	137.9	8.8
2	137.9	11
2	137.9	13.2
2	137.9	15.4
1	137.9	17.6

Testing of the article was performed by undergraduate students operating the GUI designed in MATLAB for operating the control system. All the tests were run manually since the hardware to regulate the air pressure had not yet been implemented. The tests were also run without deflation between tests run at the same pressure, however the article was lowered to 5kPa between each test pressure. Hold times between each test

where inflation pressure was maintained but load was not applied were not regulated because automated procedures had not yet been developed for torus testing. An estimated average of one minute at no load and constant pressure elapsed between tests.

5.2.1. T4A-1 Load Control Results

The position results from the load controlled tests conducted on the T4A-1 article were computed using the torus fitting methods described in Clapp (2017). The results shown in Figure 19 show the average radius of the article at all test pressures and throughout all the tests specified in Table 4. An increase in major radius with increasing inflation pressure can be seen in Figure 19 as would be expected in these articles.

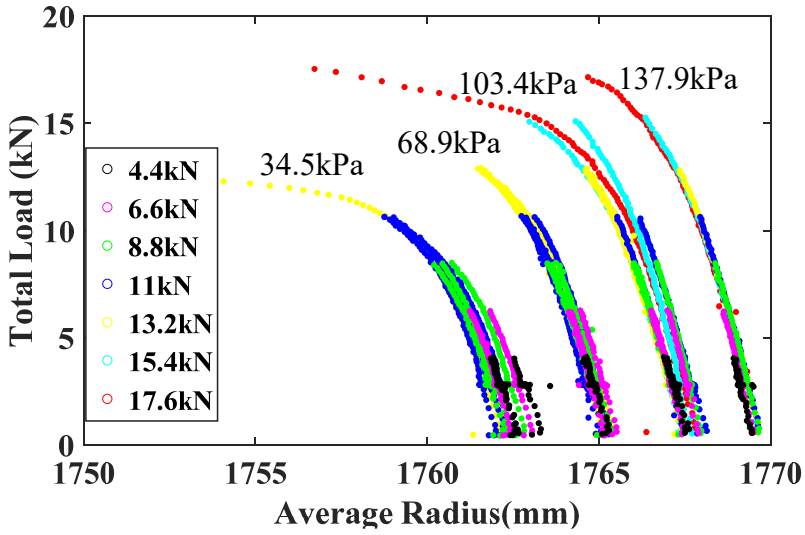

Figure 19: Average Radius Load Control Tests

As can be seen in Figure 19 there is some drift in the average radius for tests run at the same pressure. This is due to many influences that cannot be easily controlled such as length of time at the specified pressure, temperature, and viscoelastic effects from

previous tests. However as can be observed in Figure 20 these minor differences in the major radius at the same operating pressure have no noticeable effect on the stiffness response as measured by the change in average radius with applied load. Figure 20 demonstrates that this torus that had been previously tested did not accumulate stiffness measured damage from being tested even to loads that caused runaway conditions. This is likely because this torus had already sustained permanent damage under similar loading applied at a NASA facility.

One aspect of load control testing that does not occur with displacement controlled testing is runaway displacements. This condition occurs when the article can no longer sustain more loading and the actuators begin to move very quickly to try to keep up with the desired load rate. This effect can be seen in Figure 20 for a final total load of 13.2kN at 34.5kPa and a final total load of 17.6kN at 103.4kPa. An indication of a runaway condition is where the data points that are captured at 2Hz become more spread apart as a result of increasing rate of change in the average radius.

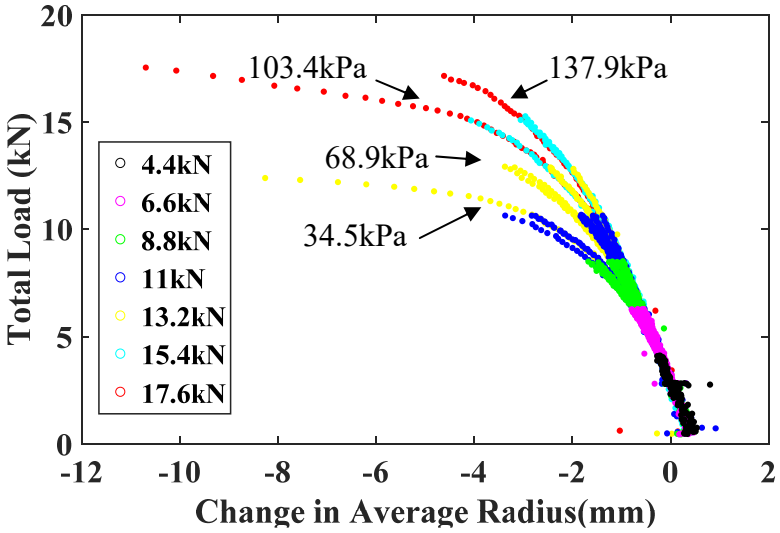

Figure 20: Change in Average Radius

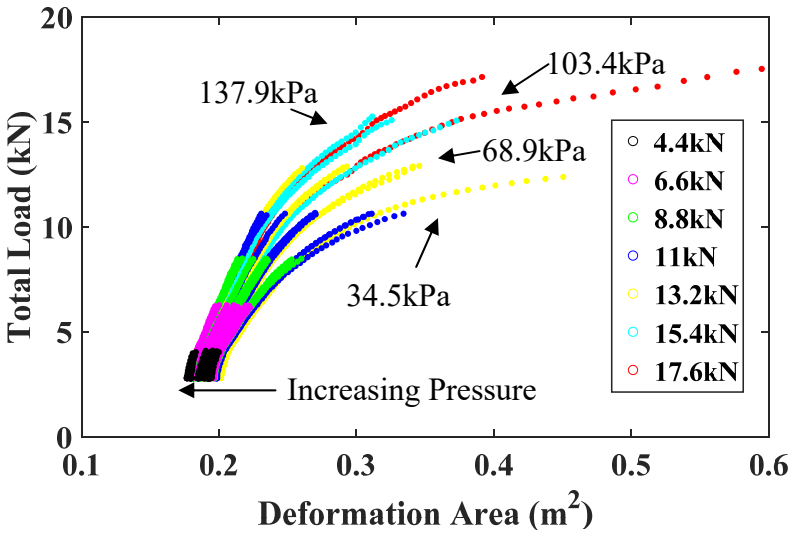

Figure 21: Deformed Area T4A-1

The deformed area of the torus can be seen in Figure 21. A trend of increasing deformed area, at the preload step, with decreasing pressure as can be seem at the bottom left of the figure. This indicates that this specific article becomes more like a perfect torus

at higher pressures, which is not the case with all articles. The torus also does not show a substantial increase in deformed area on tests run after the torus had been deformed to a large extent. This demonstrates that this article did not sustain accumulating deformations during this test series.

5.2.2. Sustained Loads on T4A-1

After the testing series shown in Table 2 the torus was tested using a sustained load protocol where the torus was held at the final total load for two minutes unless an unstable condition occurred. The motivation for this testing was to ascertain if an unstable condition would occur if the torus was held at loads that had been achieved previously but not sustained for a substantial length of time. The tests proceeded as shown in Table 3 immediately after the tests outlined in Table 2 had been run on the article.

Table 3: Sustained Loading of T4A-1

Number of Tests Run	Operating Pressure (kPa)	Final Total Load (kN)
1	137.9	17.6
1	137.9	15.4
1	137.9	13.2

As demonstrated Figure 22 there can be a significant decrease in the average radius of the torus at constant loads. The three sustained load tests all resulted in slightly different outcomes. The load test run at a final load of 17.6kN resulted in a runaway condition after the torus was held at constant load. This can be seen in Figure 22 where

the data points begin to spread towards the extreme left of the plot; consequently this test was halted by the test operator. The test run to a final load of 13.2kN also resulted in a decrease in the average radius at constant load, however unlike the test run at higher load, the torus eventually reached an equilibrium position corresponding to a constant displaced shape as indicated in Figure 22. Finally the test run at 11kN of total load did not result in any significant change in the average radius when the torus was held at the final load. This behavior is interesting and demonstrates the time-dependent response of the torus and has some implications for the overall performance of the articles in use. Load control inherently results in unstable loading situations and can also clearly result in load-rate-dependent response of the article as seen in this series of tests.

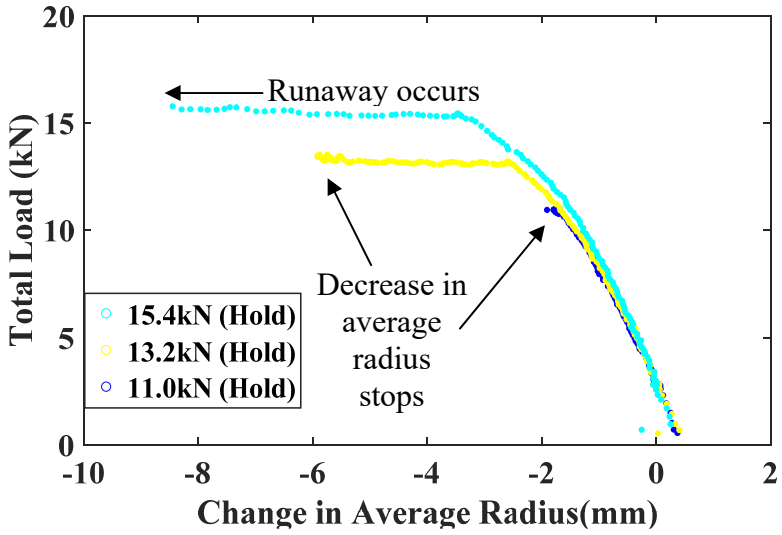

Figure 22: Change in Average Radius for 137.9kPa Load Hold Tests

Since with the use of 64 load points required whiffle trees as described in Figure 6, the load in the four cables controlled by a single actuator were not identical throughout the test. This effect can be seen in Figure 23 where the standard deviation between the

four cables controlled by each actuator was averaged to generate an average standard deviation to total load comparison. It is clear that there is a strong dependence on the total load and the deviation of load created by the whiffle tree. As shown in Figure 23 below the four tests that are plotted are all three of the sustained load tests and the runaway displacement test run at 103kPa. These test give a good understanding of the two effects that tend to exaggerate the loading differential in the whiffle tree systems the first being the magnitude of the load on the system, and the second, the magnitude of the torus deformation. During the sustained loading test the torus was held at a constant load and for two out of the tree tests had a subsequent decrease in the average radius of the torus this can be seen by the vertical trends in Figure 23. This indicates greater disagreement between cable loads connected to the same actuator with increasing deformation of the torus.

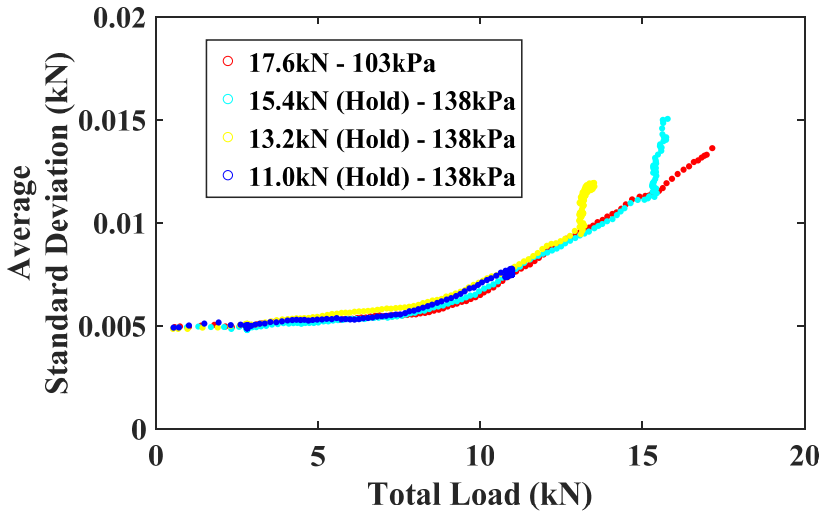

Figure 23: Whiffle Tree Load Deviation

The shapes of the torus during testing at 137.9kPa up to a total load of 17.6kN for both the nominal test and the sustained load test are displayed in Figure 24 and Figure 25, respectively. These plots show the shape of the torus before loading in green, the final shape in red with the blue region representing all the other shape data in between these extremes. The angular position is measured in radians around the torus as seen in Figure 26 which displays the zero angular position and the positive angular direction. Both Figure 24 and Figure 25 show the position of the load straps with the vertical lines and straps from whiffle tree sets shown in alternating black and red demarcation.

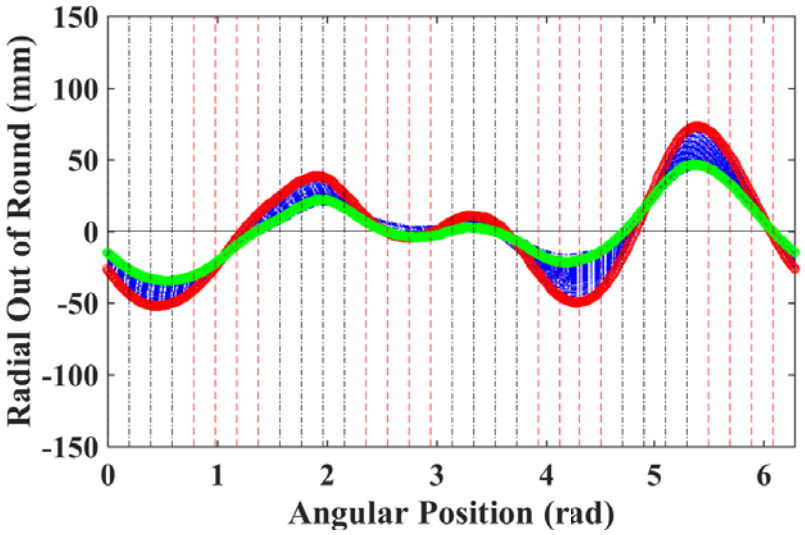

Figure 24: Deformed Shape of Torus at 17.6kN and 137.9kPa

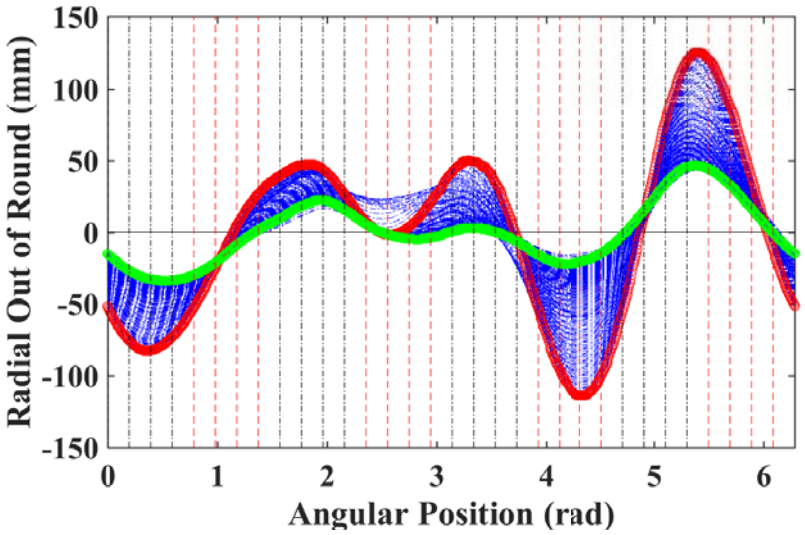

Figure 25 Deformed Shape of Torus Held at 17.6kN and 137.9kPa

The data shown in Figure 25 illustrates the increase in deformation of the torus held at constant load when compared to the data shown in Figure 24. This demonstrates the possibility that there is some bending stiffness increase of the article due to the difference in loads in in the whiffle tree. This difference in load may have resulted in some of the areas of largest deformation occurring on the sections of the torus between the whiffle trees.

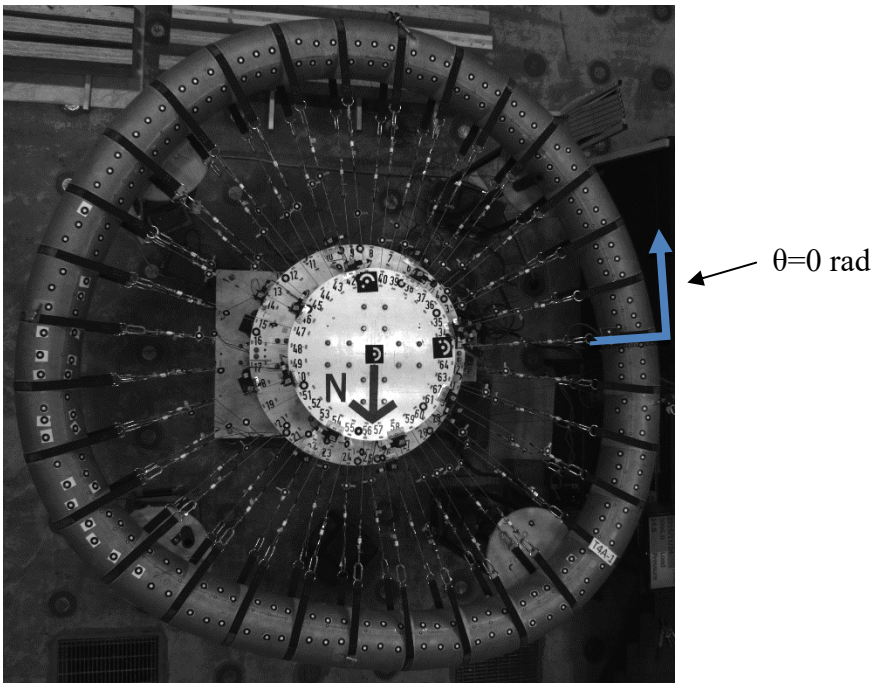

Figure 26: Deformed Shape of T4A-1

In Figure 26, the actual shape of the torus under the maximum load during the runaway 103.4kPa test at the point where the displacements began to rapidly increase is shown. After the load control tests that were run on this article it was determined that using a displacement controlled method would be more suitable for model validation and overall reliability of torus testing. This adjustment to displacement control required that only 16 load points be used for testing since there is no sensible way of splitting uniform displacements through the use of a device like a whiffle tree.

5.3. Matrix for Displacement-controlled Tests of T4AP-1 and T4AP-2

In order to produce data that can be used for numeric model validation displacement control was used for all the subsequent tests run at UMaine. This is due to

the fact that the load control tests have an inherent instability at high load which are difficult to model. Running the models using displacement control allows for the model to have the best chance to converge. The testing discussed in the following sections was accomplished using only 16 load point run in displacement control, which as previously discussed is that maximum number of load pints achievable with the hardware constraints.

The operating pressure was set to the desired value prior to the beginning of loading by the personnel running the test, and then held at constant during the test. The tests shown in Table 4 were all initiated by an operator because the software for automating the testing process had not yet been developed. Pressure regulation was not used on the testing shown in

Table 4 because the hardware was not yet developed for this task. Between each row the torus was deflated to 5kPa to allow for the torus to further recover from testing. This deflation was not used between each test as doing so would require a greater amount of time than was deemed reasonable.

Torsion testing was also performed on the T4AP-1 specimen after the uniform displacement tests on the article as shown in Table 4. The torsional test was run by applying 12.7mm of displacement to all the torus cables at which point top cables were advanced 2.5mm inward and the bottom cables were released 2.5mm (termed top advance). The torsional test matrix also includes what was termed bottom advance where all cables were displaced to 12.7mm after which the top cables where released 2.5mm

and the bottom cables were advanced 2.5mm. Torsion testing terminology is further denoted in Figure 27.

Figure 27**:** Torsion Test Terminology

Table 4: T4AP-1 Test Matrix

Phase 1: Displacement Testing			
	Number of Tests Run	Operating Pressure (kPa)	Final Displacement (mm)
This section repeated 5 times	1	34.5	12.7
	1	68.9	12.7
	1	103.4	12.7
	1	137.9	12.7
	5	137.9	19.05
	5	137.9	25.4
	5	137.9	31.75
	5	103.4	19.05
	5	103.4	25.4
	5	103.4	31.75
	5	103.4	38.1
	5	68.9	19.05
	5	68.9	25.4
	5	68.9	31.75
	5	68.9	38.1
	5	34.5	19.05
	5	34.5	25.4
	5	34.5	31.75
	5	34.5	38.1

Table 4: Cont

Phase 2: Torsion Testing			
Number of Tests Run	Operating Pressure (kPa)	Displacement Bottom Cables (mm)	Displacement Top Cables (mm)
5	34.5	10.16	15.24
5	68.9	10.16	15.24
5	103.4	10.16	15.24
5	137.9	10.16	15.24
5	34.5	15.24	10.16
5	68.9	15.24	10.16
5	103.4	15.24	10.16
5	137.9	15.24	10.16

The T4AP-2 article was tested using the matrix shown in Table which was designed to not inflict any permanent damage to the specimen such that it could be used in further testing of stacked tori. The displacement that was applied to T4AP-2 was well under the damage threshold for the article based on previous testing.

Table 5: T4AP-2 Test Matrix

Number of Tests Run	Operating Pressure (kPa)	Final Displacement (mm)
5	68.9	12.7
5	103.4	12.7
5	137.9	12.7
5	34.5	12.7
5	34.5	19.05
5	68.9	19.05
5	103.4	19.05
5	137.9	19.05

The tests run on the T4AP-2 specimen were accomplished using a fully automated protocol that was developed to help provide better data. The internal pressure of the torus was held at the specified pressure for 15 minutes between each test in a specific row of Table . This hold period allowed the torus to recover from any testing-induced deformations that the torus obtained. The hold period also allowed for the torus to be brought to the appropriate pressure if any air was lost during testing allowing time for the transient effects of inflation to dissipate. Between each row the torus was deflated to 5 kPa to allow for the torus to further recover from testing.

5.4. Displacement Testing Results

The testing of the pristine T4 gives a better understanding of the properties of tori than the initial load-controlled tests. It provided a clear path from a pristine or untested article to the damaged state that is produced by large displacement loading on the torus. The testing was performed at four operating pressures as discussed in the previous section. This allows for the pressure dependence of the torus response to be better understood. This section describes in detail the results from testing the two pristine T4 articles and analyzes the findings from this series of tests.

5.4.1. T4 Results for 138kPa

As previously described the testing progression of the pristine specimen testing resulted in the torus being damaged at high displacements on the T4AP-1 article. The T4AP-2 article was not subjected to displacements as large as the T4AP-1 article and therefore was not damaged during testing. As can be seen in Figure 28 the first article was damaged as the cable enforced displacement exceeded 25 mm. Indicated on the figure is a region of the average radius plot where subsequent tests did not follow the

same stiffness curve as previous tests. This is considered the condition of first damage to the torus where a significant loss of repeatability occurs.

During the process of testing these specimens it became clear that consistent timing and control over air pressure was necessary to achieve high fidelity results. This lack of fidelity can be seen in Figure 28 where the average radius of the article varies from test to test at the same pressure. This could potentially influence the repeatability of the test and it is important to eliminate any time-dependent effects from impacting the shape or response of the torus if possible.

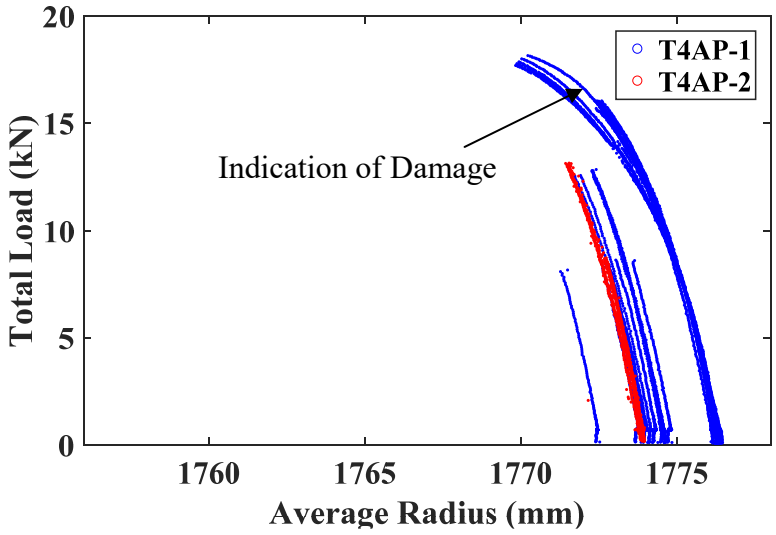

Figure 28: Average Radius 138kPa

Repeatability is clearly demonstrated in the trends shown in Figure 29 where 20 T4AP-1 and 10 T4AP-2 loading cases are plotted with their respective average radius zeroed at the beginning of the test such that the apparent stiffness of the tori can be seen aligned with on another. As can be seen in the figure both tori followed the same trend

and final load level on each run as well as being in good agreement with each other. The loading curve that resulted in damage can be clearly seen after T4AP-1 was displaced past 25mm at the cable ends. In this test series the first test that achieved a new higher displacement level of 32mm follows a different stiffness curve then the following tests at the same displacement. After subsequent tests were performed to the same level of displacement the torus clearly settled in to the new stiffness curve after damage occurred. Figure 29 also shows the maximum total load for each of the displacement tests, taken as the peak value of the five test runs that were undertaken for each article at the given level of displacement.

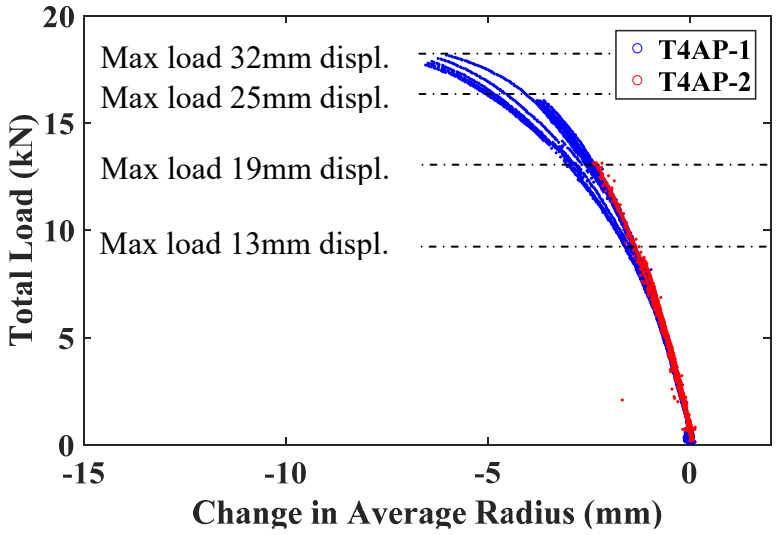

Figure 29: Change in Average Radius 138kPa

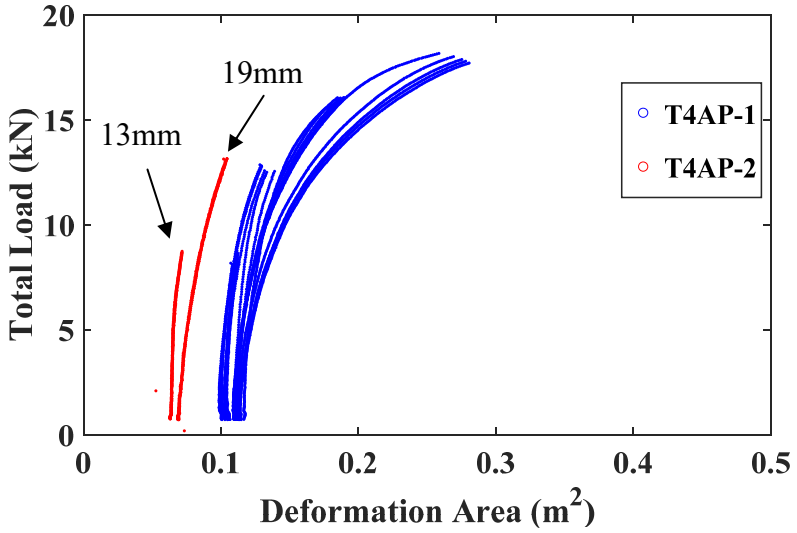

Figure 30: Deformed Area of the Torus 138kPa

Loading of the articles progressed in the order previously described in Table 4 and Table . The influence of this test order on the data is evident in Figure 30 can be seen in the deformed area of the T4AP-2 article at zero load between the 13mm displacement and 19mm displacement tests. This increase in deformed area did not occur due to testing at this pressure, however, as the article was tested at other pressures between the 13mm and the 19mm displacement test at 138kPa as shown in Table . A justification why the jump in deformed area did not result from the loading at 138kPa is because each of the two apparent red lines in Figure 30 are comprised of 5 individual test runs. This indicates that any increase in the deformed area of the torus would result in a different starting point for subsequent tests at the same enforced displacement which is clearly not seen here.

5.4.2. T4 Results for 103kPa

The loading on the T4AP-1 article at 103kPa further progressed to 38mm of displacement which had not been previously enforced. This increased displacement resulted in more permanent damage to the T4AP-1 article as can be seen by the drop in stiffness that occurred after the first 38mm test at 103kPa. Figure 31 also shows the approximate ending position of the plots at each displacement level. These positions indicate that torus was behaving in a very repeatable manner up until the enforced displacement exceeded the level that had been applied at a higher pressure.

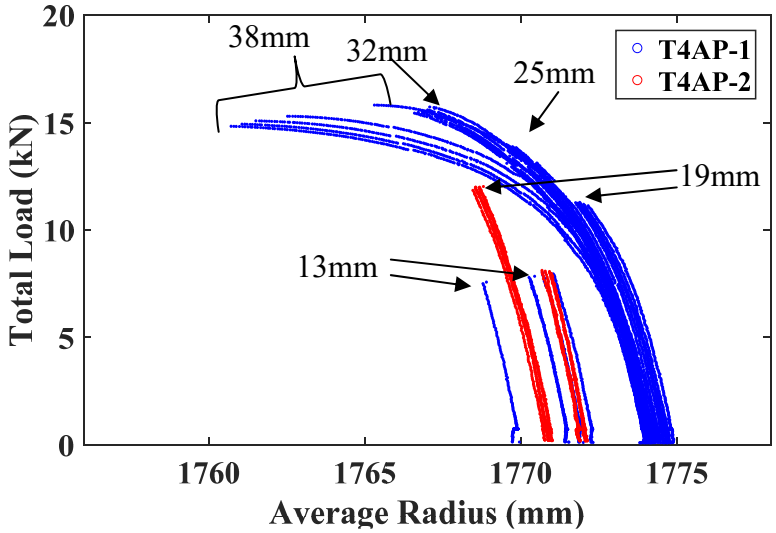

Figure 31: Average Radius 103kPa

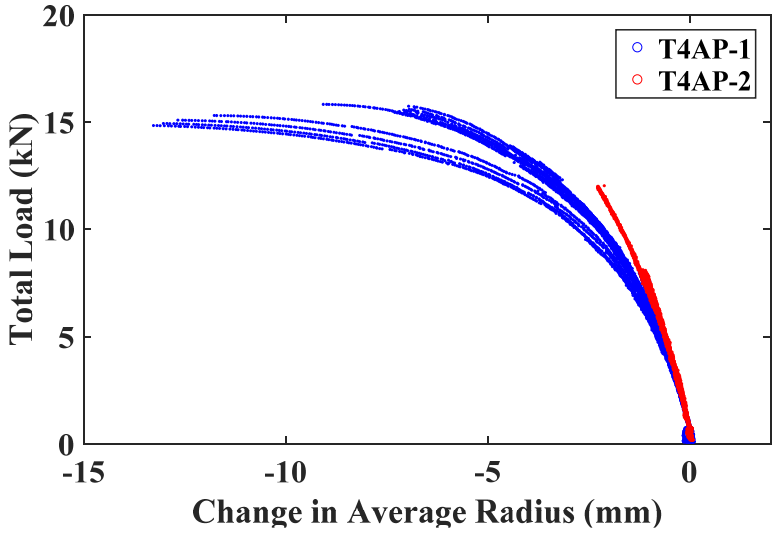

Figure 32: Change in Average Radius 103kPa

As seen in Figure 32 the stiffness of the T3AP-1 article began to diverge from that of the T4AP-2 article for the same level of displacement. This is a result of damage that the torus had been subjected to previously at 138kPa. This does indicate that the damage that the torus undergoes at other pressures affects its response for all subsequent tests. This may seem like an obvious outcome of damage to a structure, however, the damage mechanism is not well understood since it only is seen in loss of repeatability of the load-average radius response and is not visibly observable.

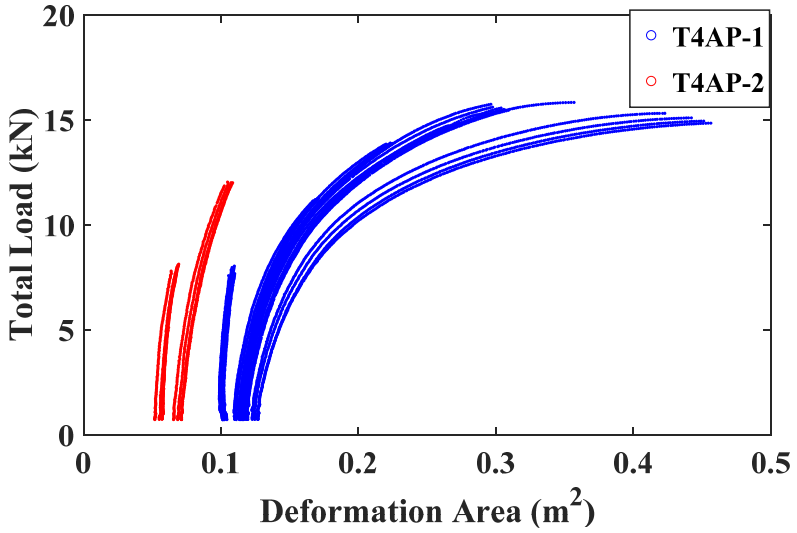

Figure 33: Deformed Area of Torus 103kPa

The deformation area of the torus shown in Figure 33 does not exactly follow the same trends as the average radius. As can be seen in both the articles even at low levels of displacement, such as 13mm and 18mm, a small amount of drift in deformed area is observed in the load sets. This suggests that there is some amount of accumulation of deformations with repeated testing, however small, that occurs before the previously described damage occurs. This accumulation of deformation does not seem to have a large impact on the load response of the torus observed at the strap or as measured by the average radius versus load data.

5.4.3. T4 Results for 69kPa

The stiffness response of the T4AP-1 clearly was changed due to loading at other inflation pressures. As can be seen in Figure 34 as well as in Figure 35 the stiffness of the T4AP-1 article has a very similar trend to that of the other article for the initial five

13mm displacement tests. Once the T4AP-1 article was tested at other displacements it had already been damaged at other pressures resulting in the measured drop in stiffness.

The results at 69 kPa show similar trends to the other pressures however there was not any apparent damage as determined by the change in average radius shown in Figure 35. The test series run at this pressure did not at any point exceed the enforced displacement level that had been previously applied at a different pressure. As such it would not be expected to exhibit any trends indicating more damage occurred to the torus. As can been seen in Figure 35 the stiffness of the T3AP-1 article is significantly diminished from that of the T4AP-2 article to the extent that the maximum load of the T4AP-2 article is near that of the T4AP-1 article in spite of half the enforced cable displacement on T4AP-1.

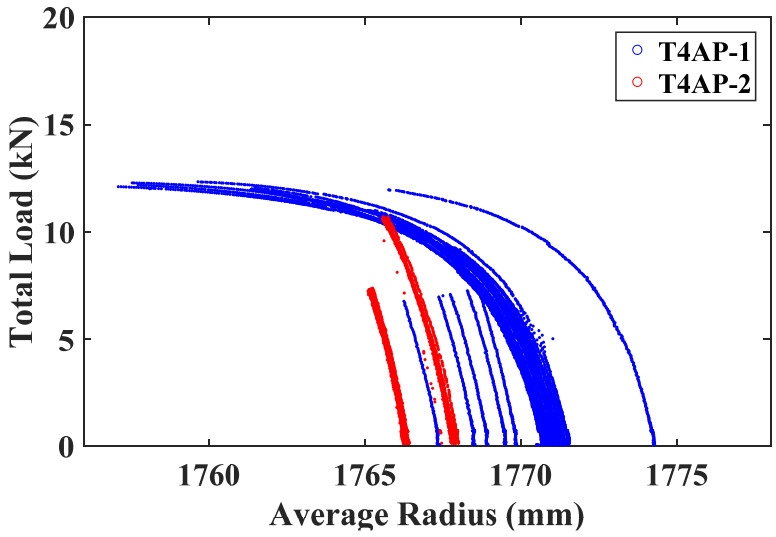

Figure 34: Average Radius 69kPa

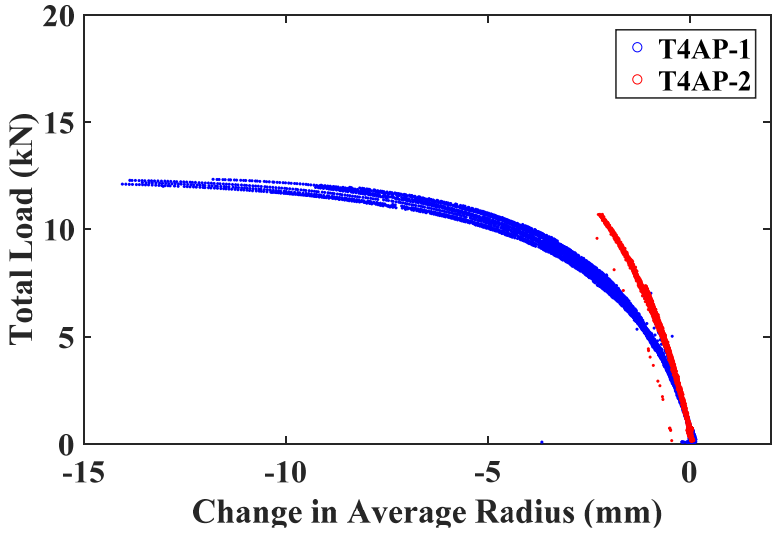

Figure 35: Change in Average Radius 69kPa

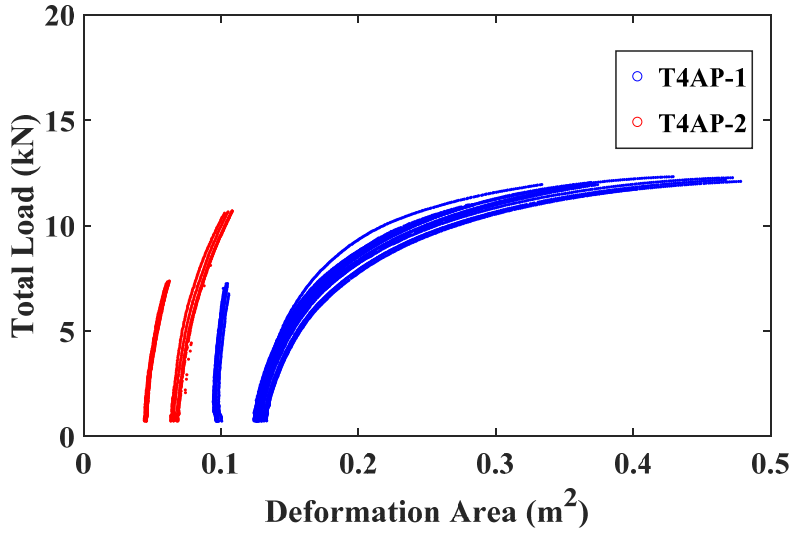

Figure 36: Deformed Area of Torus 69kPa

During the process of testing these specimens at 69 kPa there was an observed drift in the deformed area of the torus. This trend can be seen in Figure 36 where it is

clear that the torus did experience accumulating deformations for all tests run at this pressure.

5.4.4. T4 Results for 34kPa

Results from 34kPa testing generally match those obtained at the other pressures exhibiting repeatability and good agreement between stiffness of both specimens prior to damage. As can be seen in Figure 38 the test results with 13mm of enforced displacement for both specimens follow the same stiffness trend and arrive at similar load levels as would be expected. The response of the T4AP-1 article has clearly been affected by higher displacements at other pressures.

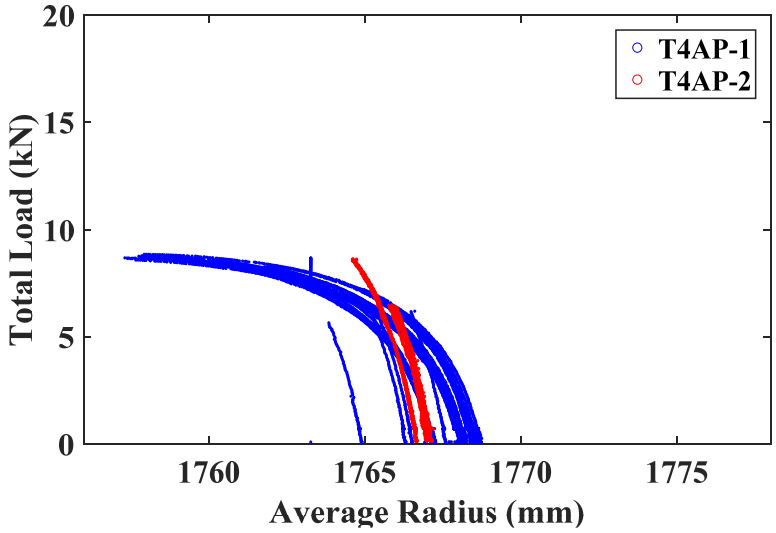

Figure 37: Average Radius 34kPa

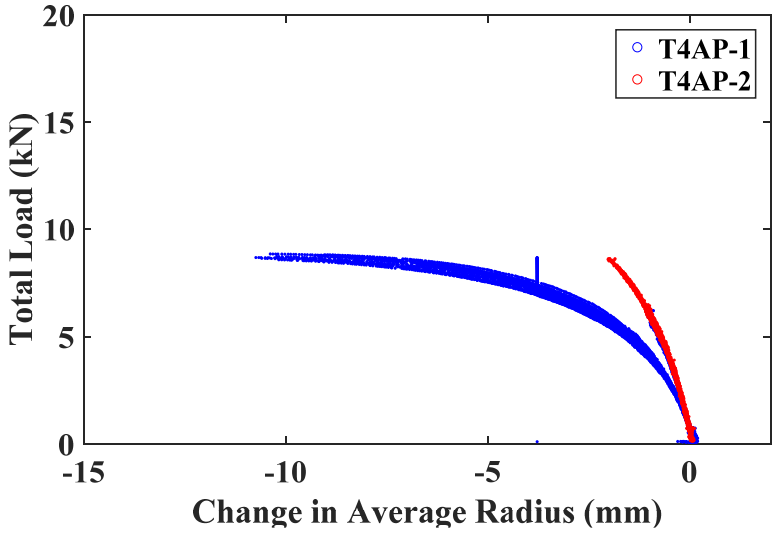

Figure 38: Change in Average Radius 34kPa

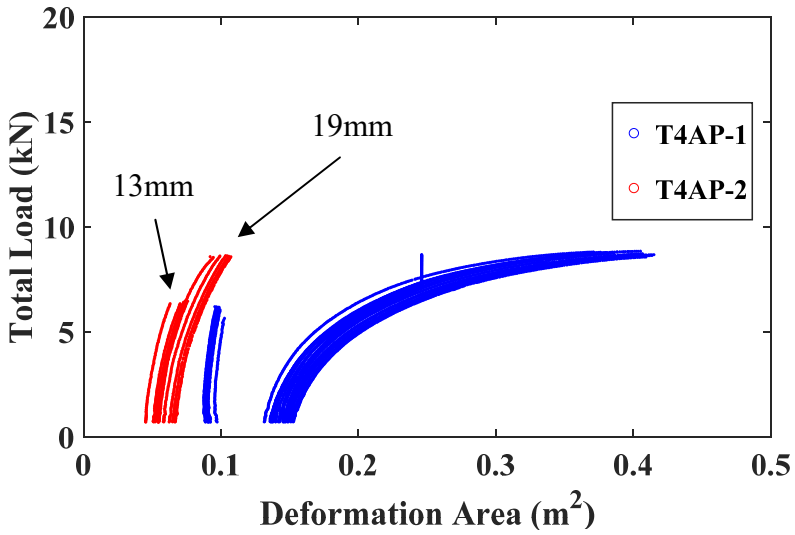

Figure 39: Deformend Area of torus 34kPa

The deformed area of the torus as shown in Figure 39 indicates that there was a measured drift in the deformation area as the article was tested at this pressure even for small displacements. Since the article was tested to 13mm of displacement and 19mm of

displacement at 34kPa, as previously indicated, the drift can be clearly seen as theT4AP-1 article is loaded. This does indicate that especially at low pressures the articles are susceptible to induced deformations that are not entirely recovered.

5.5. Torsion Testing of T4AP-1

The testing setup for the HIAD also allowed for many loading schemes to be used in the torus testing, including torsional loading in order to better understand the properties of the torus. Torsion testing on the T4AP-1 article was performed using displacement control where the top and bottom cables were displaced in opposite directions.

The first step of torsion testing was to displace all cables to 12.7mm allowing for all the cables to achieve some preload. Preload is important in order to ensure there is a drop in the load carried by the retracted strap when it is slowly released during the test. Torsion testing consisted of two distinct phases termed top advance and bottom advance as previously discussed.

A typical displacement vs time plot for the torsion test is shown in Figure 40. The controller appears to do a good job applying the correct displacement ramp for the first step of the test procedure. There are however some areas of interest once the controller starts to apply the 2.5mm ramp up and down. As shown on Figure 40 a flat portion of displacement can be seen where all the actuators that had previously been retracting need to begin extending. This stalled effect on the displacement response is partially due to some backlash in the mechanical gearing in the actuators. This backlash is particularly difficult to correct for in the controler due to the very slow operation of the actuators required for this testing. Furthermore there is also a voltage threshold under which the actuator DC motors will not spin. This flat section in the response is a result of both of

these physical phenomena and was observed every time the actuators need to reverse direction.

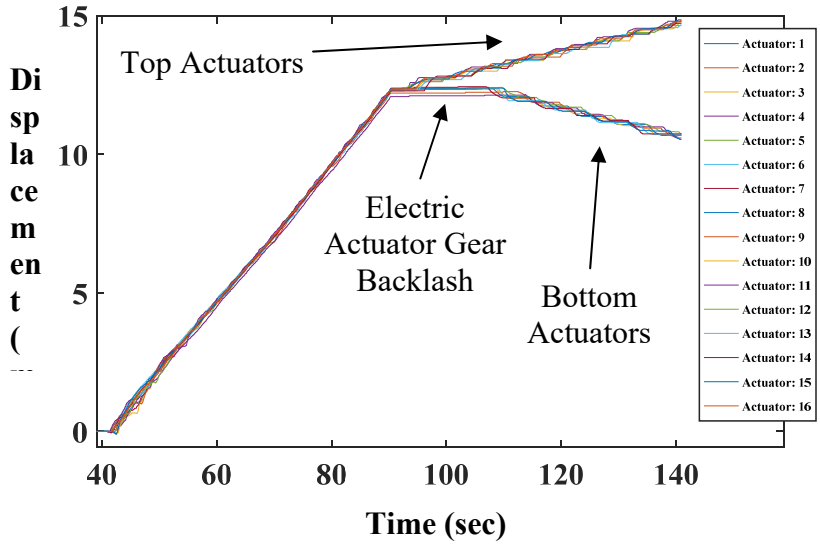

Figure 40: Typical Displacement verses Time

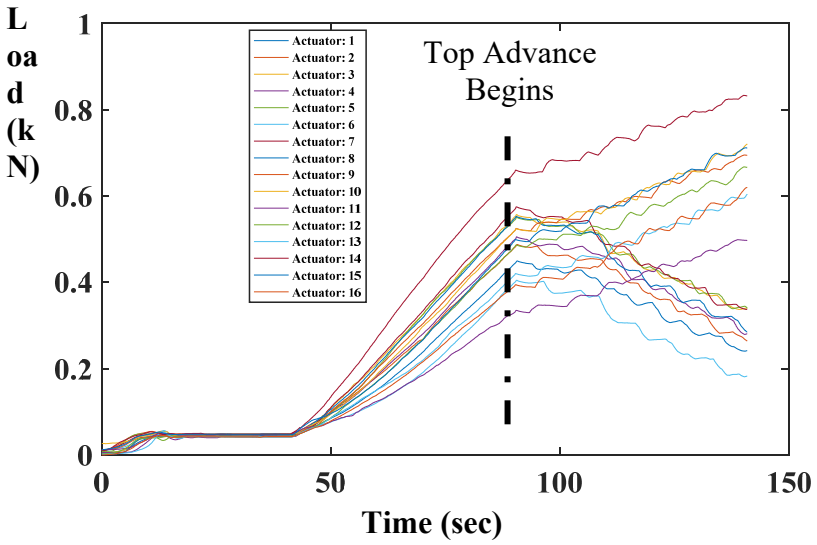

Figure 41: Typical Cable Load Distrubution

Individual cable load data shown in Figure 41 demonstrate the load distributions typical in a displacement-controlled torsion test of one of the torus articles. The spread in the loads applied are due to small stiffness variations of the torus. One of the interesting features of the data shown in Figure 41 is the jagged nature of the loads applied to the torus during the torsion portion of the test. This load response was typical for all the torsion tests run on the article and was attributed to the displacement ramp rate. The total enforced displacement for this portion of the test was 2.5mm; since the control system operated at 20Hz for the 60 second portion of the test, the displacement rate of increase per control loop iteration was 0.002mm/iteration. The string pot resolution achieved by the instrumentation setup used in the testing was 0.01mm, and as such, the resolution was not sufficient to accurately achieve the desired displacement rate, resulting in somewhat jagged load results. This is not likely to impact the results from the torsion testing because of the magnitude of the load fluctuations with respect to the total applied loads are small.

5.5.1. Results from T4AP-1 Torsion Testing

The response of the article to torsional loading can be seen in Figure 42 where the average radius of the torus clearly changes in both the top advance and the bottom advance testing. Interestingly, the figure shows that the average radius continues to decrease for torsion testing with bottom advance protocol. For the top advance method it can be seen that the average radius increased for all the tests run in top advance testing. It is also clear in Figure 42 that the total load on the torus drops in both cases of top advance and bottom advance when the torus is being subjected to torsion. This drop in

load is most likely due in large part to a drop in load seen when a torus is held at a constant displacement, a reflection of the viscoelasticity of the material.

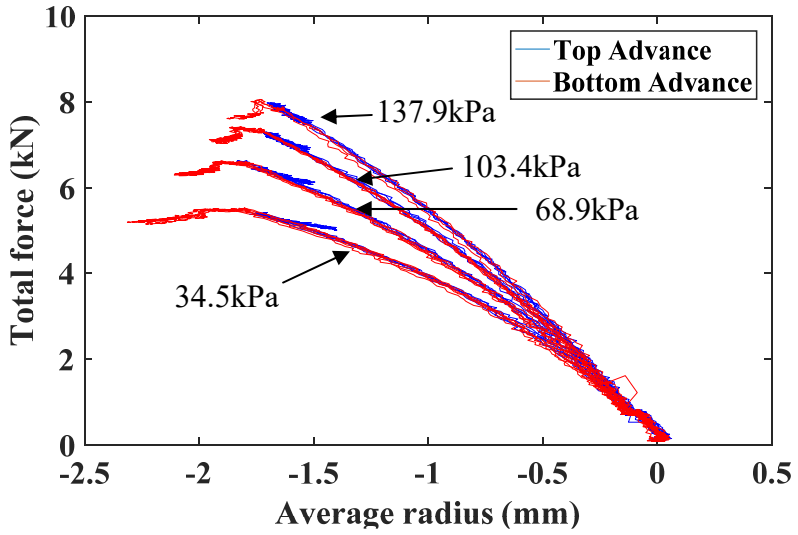

Figure 42: Average Radius During Torsion Testing

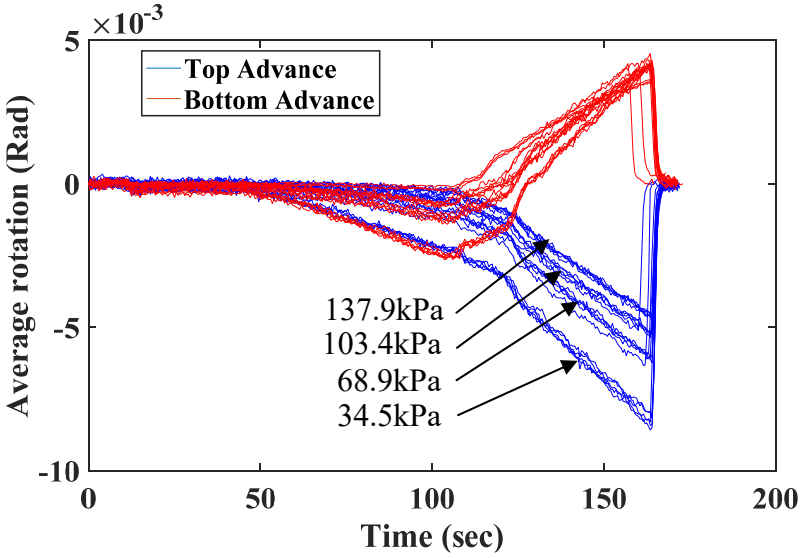

Figure 43: Rotation Time History T4AP-1

As can be seen in Figure 43, the rotation of the torus is dependent on the inflation pressure in that more rotation of the cross section occurs at lower pressures regardless of

the same enforced displacement at the cable ends. It can also be seen in Figure 43 that the torus undergoes rotation during the initial displacement control period to 12.7mm of displacement. This effect decreases as inflation pressure increases.

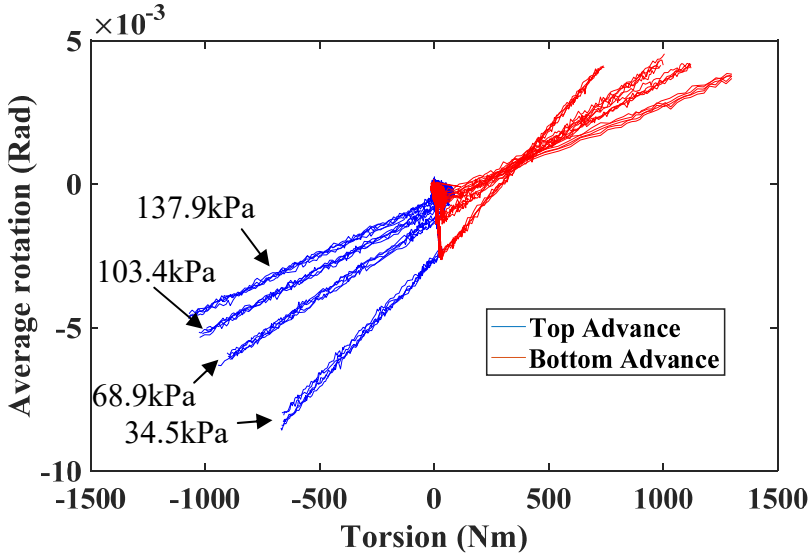

Figure 44: **T4AP-1 Torsional Stiffness**

Torsion testing allowed for the torsional stiffness of the articles to be back calculated from the linear response observed in Figure 44 is very linear. This stiffness is dependent on the inflation pressure and increases with increasing inflation pressure.

Table 6: T4AP-1 Torsional Stiffness

Pressure (kPa)	Torsion Stiffness (kN-m/rad)	Modulus (Clapp 2015) N/mm	Ratio
34.5	112	224	1
68.9	182	329	0.904
103.4	229	420	0.917
137.9	265	468	0.883

As can be seen in Table the torsional stiffness increases non-linearly with increase in inflation pressure, with the largest jump in stiffness occurring between 34.9kPa and 68.9kPa. Figure 44 shows that the torsional stiffness is very similar for both top advance as well as bottom advance, and as such, the data displayed in Table is calculated using information from both tests. Considering the shear properties enumerated in Clapp (2015) a comparison can be made to the pressure dependent response of this article to this torsion case. This response showed similar pressure dependency to the values given however this torsion case is directly comparable to tension torsion results and as such no further relations can be drawn.

5.6. Summary of T4 Testing

Torus testing in both load and displacement control can provide valuable information on the response of the torus articles. For the purpose of creating high fidelity data for modeling as well as achieving good control over the desired test parameters displacement control was chosen to perform the majority of tests run at UMaine. Testing on pristine articles resulted in accumulating deformations and a loss in the stiffness as measured by the average radius. This was not seen in testing of articles that had previously been loaded, indicating that there is permanent damage that occurs to pristine tori when loaded to a high level.

Chapter 6

TESTING RENFORCING METHODS ON T3

As a part of the tori that were tested at UMaine some alternative reinforcing methods were used to construct two of the T3's in the test series (Figure 45). This allowed for the reinforcing methods to be evaluated as compared to the nominal two-cord method. This chapter discusses the results from the testing series and the different ways by which reinforcing effects the results of the testing. The method of reinforcing is highly critical to the performance and can have a large impact on the bending response of the articles. However, reinforcing is also determined by manufacturability as it is very difficult for more complicated reinforcing schemes to be constructed without encountering an unstable inflated state.

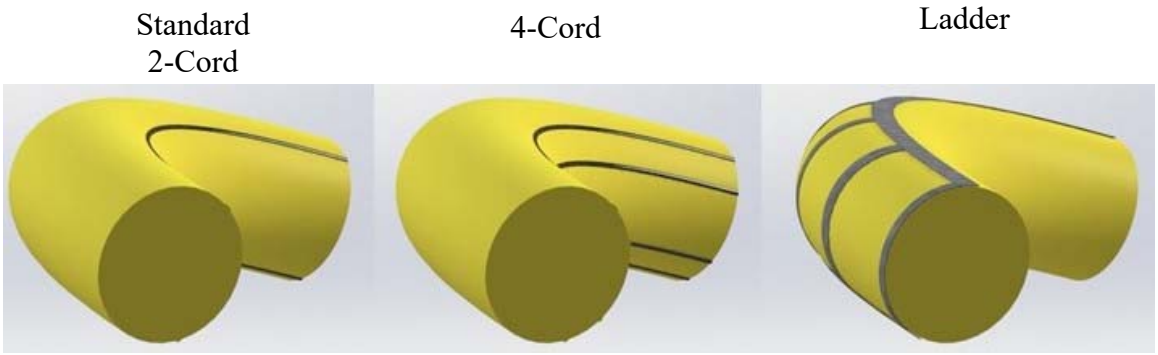

Figure 45: Reinforcing Methods

It can also be very difficult to avoid minor manufacturing errors during the construction of the torus articles. Included in the test series was a T3 torus constructed deliberately with two-cords of slightly different lengths. This range of constructions allowed for many of the important aspects of the performance of the articles to be

quantified during testing. All of the two-cord articles tested are configured as shown in Figure 45, as standard two-cord, and the description of each article can be found in Table .

Table 7: T3 Articles Tested

Article	Reinforcing Members	Description
T3AP-1	4	Four smaller than nominal cords, not previously tested
T3AP-2	2	External reinforcing ladder, not previously tested
T3AP-3	2	Nominal two-cord, not previously tested
T3AP-5	2	Nominal two-cord, not previously tested with buffers
T3A-2	2	Two unequal length cords, not previously tested with buffers

6.1. T3 Series Testing Matrix and Testing Goals

In order to fulfill the objectives of this study, several tests were run to ascertain the repeatability of the article. For this reason multiple tests were run at every displacement and significant care was taken to ensure that the condition of the torus prior to, and during, testing was strictly regulated and specified. Tori subjected to large displacements have a tendency to exhibit damage producing altered responses in subsequent testing of the article. As a part of this research effort this effect was quantified by performing large displacement tests on the tori. It was also very important to understand the effect that differing reinforcing methods have on the overall performance of the articles. Data that was collected from these tests is also critical for validating numerical models used to better understand the response of these structures to different loading scenarios.

6.1.1. Test Matrix

Torus testing followed a predefined test matrix in order to demonstrate repeatability and ensure that the torus could be fully tested before the torus suffered any permanent damage. The air pressure was regulated by the controller between tests to ensure that the correct testing pressure was achieved. During testing no additional air was added to the article so that the pressure change due to the loading could be measured. The internal pressure of the torus for all the tests was held at the specified pressure noted in Table between each test with a 15 minute hold period between each test. This hold period allowed the torus to recover from any testing induced deformations. The hold period also allowed for the torus to be refilled to the appropriate pressure if any air was lost during testing allowing time for the transient effects of inflation to dissipate. Between each row of tests noted in Table the torus was deflated to 5kPa to allow for the torus to further recover from testing. This deflation was not used between each test as it would produce a prohibitively long testing campaign.

Table 8: Nominal Testing Matrix for T3 Torus

Phase 1: Small Displacement Testing		
Number of Tests Run	Operating Pressure (kPa)	Final Displacement (mm)
5	34.5	6.35
5	68.9	6.35
5	103.4	6.35
5	137.9	6.35
5	34.5	9.53
5	68.9	9.53
5	103.4	9.53
5	137.9	9.53

Table 8: Nominal Testing Matrix for T3 Torus (Cont)

5	34.5	12.70
5	68.9	12.70
5	103.4	12.70
5	137.9	12.70
5	34.5	15.88
5	68.9	15.88
5	103.4	15.88
5	137.9	15.88

Phase 2: Torsion Testing			
Number of Tests Run	Operating Pressure (kPa)	Displacement Bottom Cables (mm)	Displacement Top Cables (mm)
5	34.5	10.16	15.24
5	68.9	10.16	15.24
5	103.4	10.16	15.24
5	137.9	10.16	15.24
5	34.5	15.24	10.16
5	68.9	15.24	10.16
5	103.4	15.24	10.16
5	137.9	15.24	10.16

Phase 3: Large Displacement Testing		
Number of Tests Run	Operating Pressure (kPa)	Final Displacement (mm)
5	34.5	15.9
5	68.9	15.9
5	103.4	15.9
5	137.9	15.9
5	103.4	19.1
5	103.4	25.4
5	103.4	38.1
5	103.4	50.8
5	103.4	76.2
5	103.4	101.6

The testing for all the T3 specimens was run using automated protocol such that the testing proceeded with exact timing and often overnight. The testing consisted of three distinct phases as can be seen in Table the first phase of was small displacement testing which was aimed particularly at determining the repeatability of the tests. As seen in prior testing tori began to lose stiffness when loaded to high displacements, and therefore, the displacements were chosen to be less then would be expected to cause damage. The first pristine torus that was tested was the T3AP-3, which used the matrix as shown in Table for phase 1 (small displacement) testing. This matrix was set to achieve slightly higher displacements than should be used for tori with untested reinforcing schemes, and thus all the other T3 tori used the first phase of the matrix shown in Table was used. The second phase of the testing was to establish a better understanding of the torsional response of the torus without damaging the torus.

Table 9: Testing Matrix used for T3AP-3 Phase 1

Number of Tests Run	Operating Pressure (kPa)	Final Displacement (mm)
5	34.5	12.70
5	68.9	12.70
5	103.4	12.70
5	137.9	12.70
5	34.5	19.05
5	68.9	19.05
5	103.4	19.05
5	137.9	19.05

The third phase of testing consisted of large displacement testing where the torus was pushed past the point where permanent damage would occur as determined by the loss of repeatability in the achieved load-displacement response. The matrix shown in Table for phase three was used of all tori except T3A-2 which was tested at all pressures as shown in Table 5.

Table 5: Large Displacement Tesing T3A-2 Phase 3

Number of Tests Run	Operating Pressure (kPa)	Final Displacement (mm)
5	34.5	15.9
5	68.9	15.9
5	103.4	15.9
5	137.9	15.9
5	103.4	19.1
5	103.4	25.4
5	103.4	38.1
5	103.4	50.8
5	*34.5*	*50.8*
5	*103.4*	*50.8*
5	*137.9*	*50.8*
5	103.4	76.2
5	103.4	101.6

Italicized rows correspond to changed matrix for this article

T3 testing focused on establishing the repeatability of testing and on determining what types of damage the torus underwent during the course of the testing program. The T3A-2 article was tested using the matrix shown in Table 5. Since this test method resulted in a discontinuous load-displacement response between 50.8mm and 76.2mm further testing was conducted only at 103.4kPa.

6.2. T3 Testing Results

This section examines the results from all five of the T3 tests run on specimens with differing reinforcing schemes. The test results from the test matrices given in Table - Table 5 are shown and discussed. Tests run at lower levels of displacement (phase 1) on the articles resulted in good repeatability as measured by the change in average radius change of the articles. This is also true for the torsion tests run on the articles which all exhibited good repeatability as well as demonstrated consistent response before and after torsion testing. However, for tests run during phase 3 of the testing matrix, damage was seen both in the response for the stiffness based on average radius change as well as observation of physical damage at extreme displacements. This damage was generally abrasion of the coating or small areas of braid bunching or stretching as can be seen in Figure 59.

6.2.1. T3AP-1 4-Cord

All three phases of the test matrix were performed sequentially on this article yielding a good understanding of the response of this system to loading. This article was comprised of 4 axial reinforcing cords placed at 30 and 60 degrees off the plane as shown in Figure 46. The cords used on this article were smaller than the axial reinforcing cords used to construct the two-corded specimens.

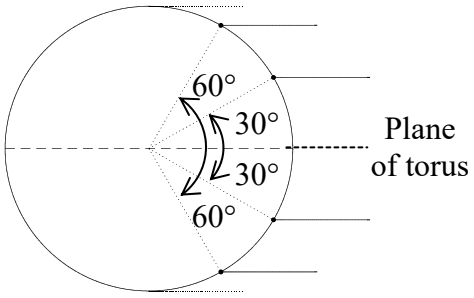

Figure 46: Cord Position of T3AP-1

The cords used in the four-corded tori were incorporated using the same method used for other tori wherein the axial cords were constrained in the braid by threading the cords through the fibers of the fabric braid. This method of incorporating the reinforcing cords allows the cords to be very well contained and robustly attached to the matrix of the braid. In addition a high level of shear transfer between the cord and the braid is created which is critically important for these fabric structures.

6.2.1.1. Small Displacement Testing T3AP-1

The small displacement testing on the four-cord torus exhibited good repeatability as can be seen in Figure 47. The influence of pressure on the response of the torus can also be seen as the average radius of the torus clearly increases with increasing inflation pressure.

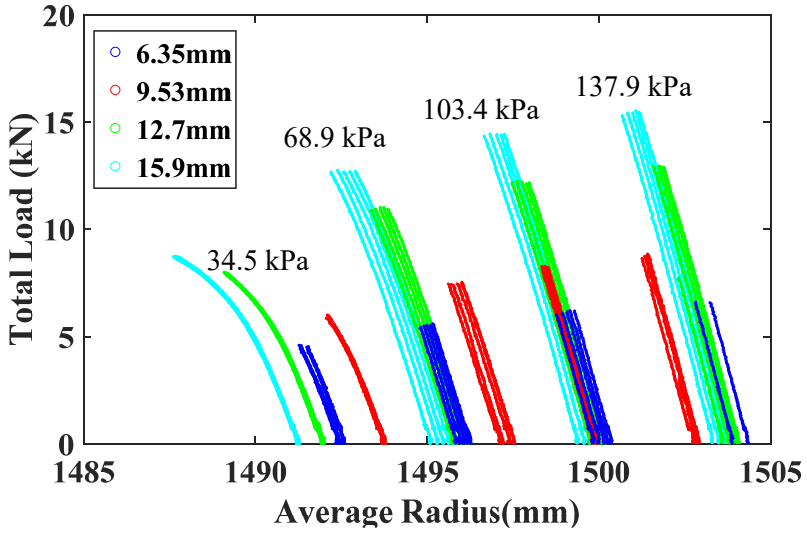

Figure 47: Average Radius T3AP-1 Four-Cord Torus

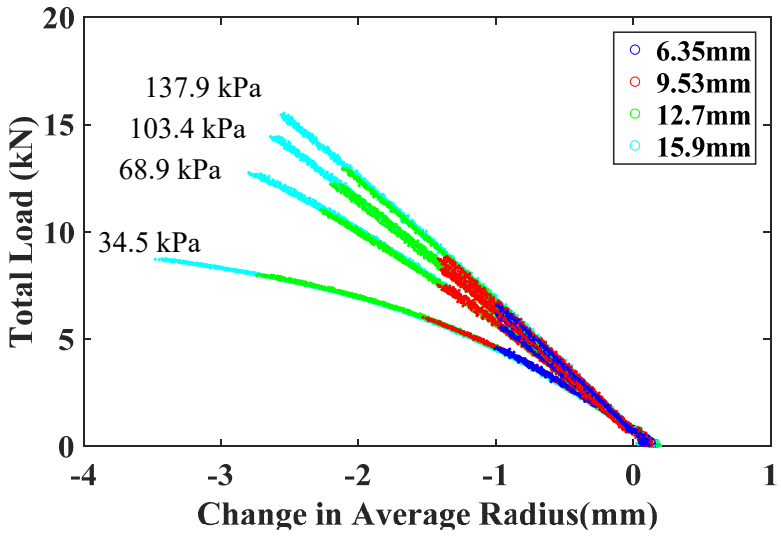

Figure 48: Change in Average Radius of T3AP-1

Results shown in Figure 48 highlight the repeatability of this test article performed to small displacements. All the trends shown at the four pressure levels possess the same stiffness throughout all test run.

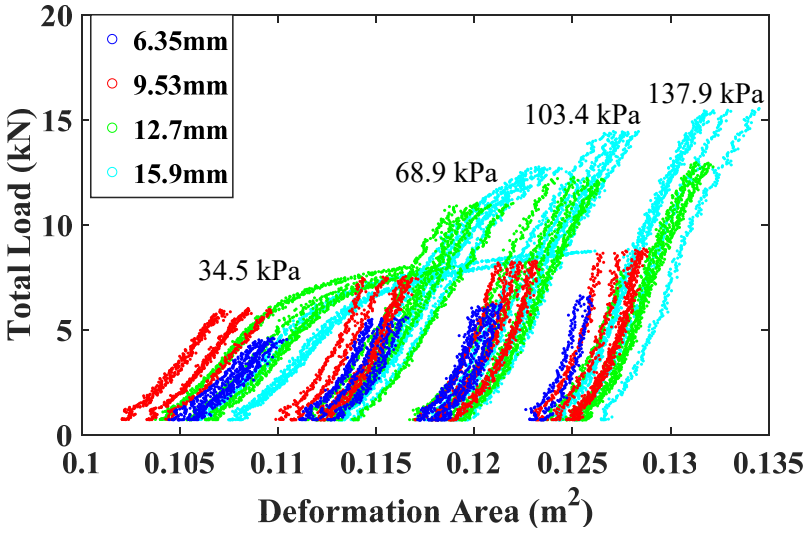

Figure 49: Deformed Area of T3AP-1

As can be seen in Figure 49 the deformed area of the four-cord torus increases with increasing inflation pressure. The small displacement testing can be seen to have a cumulative effect on the deformed area of the torus especially at the lower pressure of 34.5kPa. The deformed area also increases the most during tests run at lower pressures.

6.2.1.2. Torsion Testing T3AP-1

Torsion testing on the four-cord torus was performed using the same method as had been used on the T4AP-1 article and was used for all the torsion tests initially run on the T3 articles in this chapter. The first step of torsion testing was to displace all cables to 12.7mm allowing for all the cables to achieve some preload. Preload is important so there is a drop in the load carried by the strap when it is slowly released during the test.

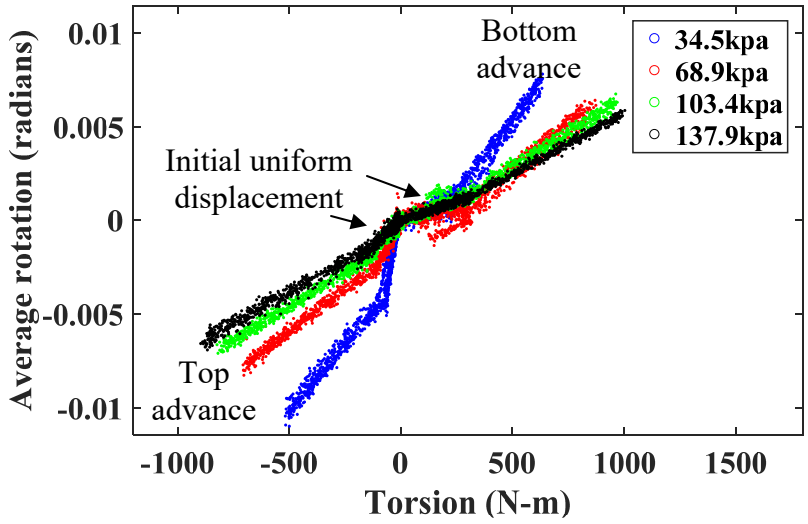

Figure 50: Torsion Results from T3AP-1

As can be seen in Figure 50 the torsional response of the torus in very linear and is very similar for both top advance and bottom advance testing. The rotation produced by top advance is negative and the rotation for bottom advance is positive as defined by the chosen convention. It is also evident from the figure that in the initial uniform displacement of this article the rotation of the specimen was not the same for top advance testing as it was for bottom advance testing. These two test types should respond in the same way since the uniform applied displacement was prescribed to be the same; however, because of an issue with one of the actuators in the system the uniform displacement resulted in one of the strap sets applying torsion for the bottom advance testing. This problem resulted in the torsion and rotation response of the torus not following different trends for bottom and top advance testing.

6.2.1.3. Large Displacement Testing T3AP-1

After it had been established that the torus exhibited good load repeatability at smaller displacements as well as during torsion testing, the article was loaded to increasing levels of displacement at a single operating pressure. The operating pressure of 103.4kPa was chosen for all the large displacement tests performed on the T3 articles as it is likely to be close to the operating pressure of these articles during actual use.

The method that was used to determine the center of the torus cross section for the large displacement tests involved fitting circles to the line of points placed on the torus and constraining the circles to the nominal minor radius as well as completely vertical. The line of points that was used for circle fitting was placed on the radial marks as defined by the tracer intersections as previously discussed. Fitting was accomplished by allowing for the radius from the center of the torus to the center of the fit circle to vary as well as the angular rotation of the fit circle to vary until the best fit is found. These two conditions are very consistent during tests and help to eliminate noise that is caused by the imperfect placement of the dots. Circle fitting is required at large displacements because of the large curvatures that can occur in the article. The method for calculating the center of the torus for most tests fit a three-dimensional perfect torus to a region of points in a small angular region of the torus. This is a highly robust method that does allow for a large number of points to be used in a fit; however it is not effective when the curvatures become large and non-uniform.

As can be seen in Figure 51 there is a rapid loss in stiffness that occurred during the first test performed at 76mm of displacement. Prior to this drop no significant loss of repeatability had been observed during testing of this article. The cause of this loss in

stiffness and loss of repeatability is that two of the load straps began to dig into the torus as illustrated in Figure 52.

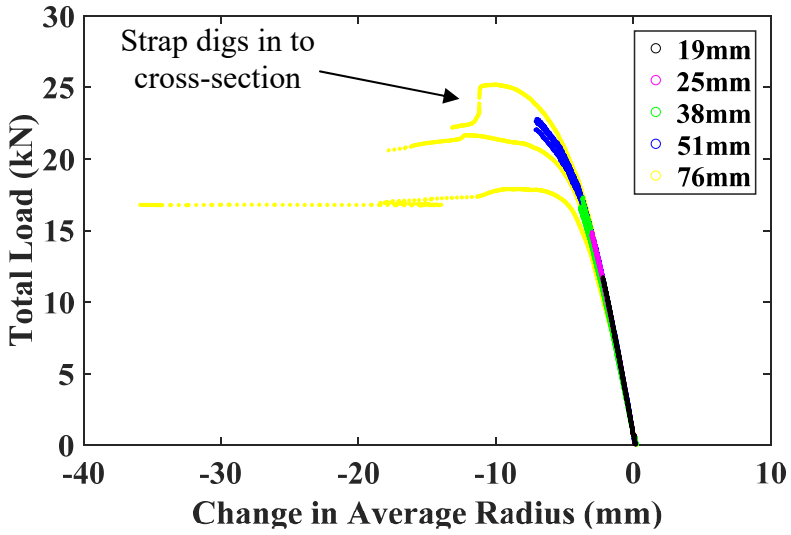

Figure 51: Change in Average Radius of T3AP-1 Large Displacment

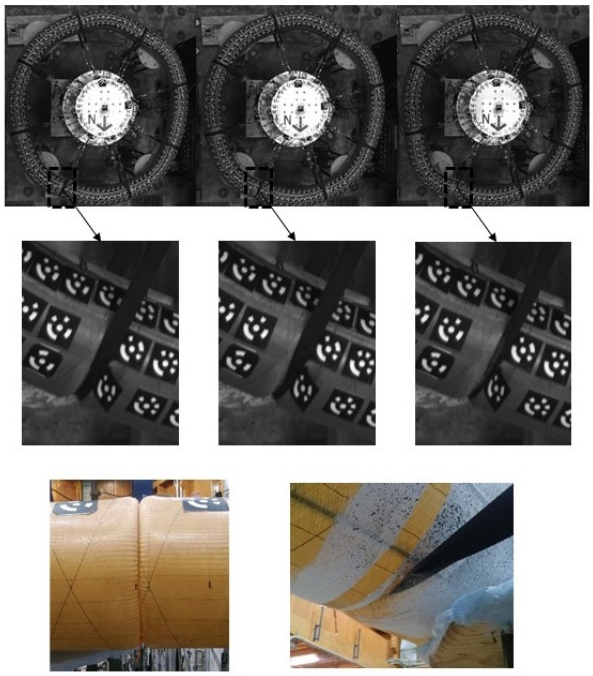

Figure 52: Strap Intrusion of T3AP-1

This strap intrusion into the cross section of the torus resulted in rapid loss in load and a large drop in the total load achievable in subsequent tests. It can be seen in Figure 52 that the strap rapidly plunged into the cross-section as shown by the three adjacent pictures all taken a second apart. The strap intrusion occurs because of the strap load exceeding what could be carried by the internal torus pressure and was only achievable on this article because of the high loads reached during testing. As shown at the bottom left of Figure 52 the depth that the strap became embedded into the torus became very significant and prevented further testing of the torus.

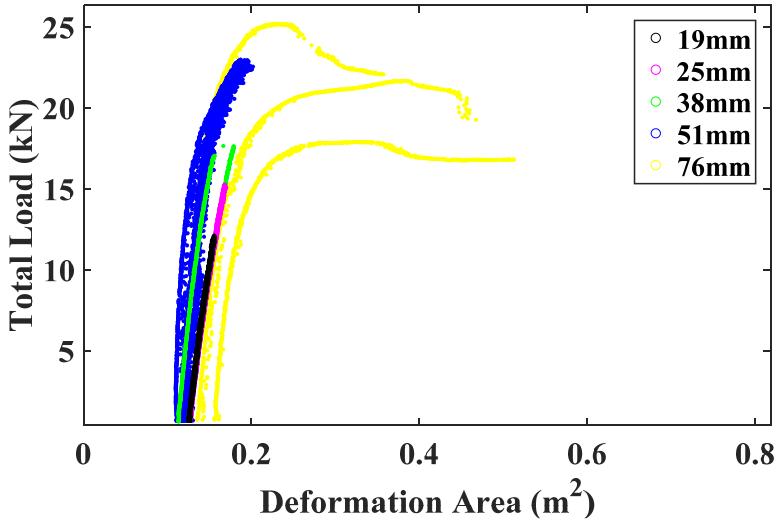

Figure 53: Deformed Area of T3AP-1 Large Displacement

As displayed in Figure 53 the deformed area of the article increased quickly after the article could no longer support the strap loads which resulted in a rapid and permanent increase in the deformed area of the torus.

6.2.2. T3AP-2 Ladder

One of the other reinforcing methods that was used to construct the torus was the ladder, which consisted of externally bonded straps on the outer area of the torus. This configuration was used to construct the T3AP-2 article which possessed reinforcing straps resembling a ladder since the connecting straps were used to connect the two reinforcing straps keeping then firmly attached to the article.

6.2.2.1.Small Displacement Testing T3AP-2 Ladder

The T3AP-2 article was tested using the same method used for the other T3 articles as described in Table . As shown in Figure 54 the average radius of the article increases at with increasing pressure.

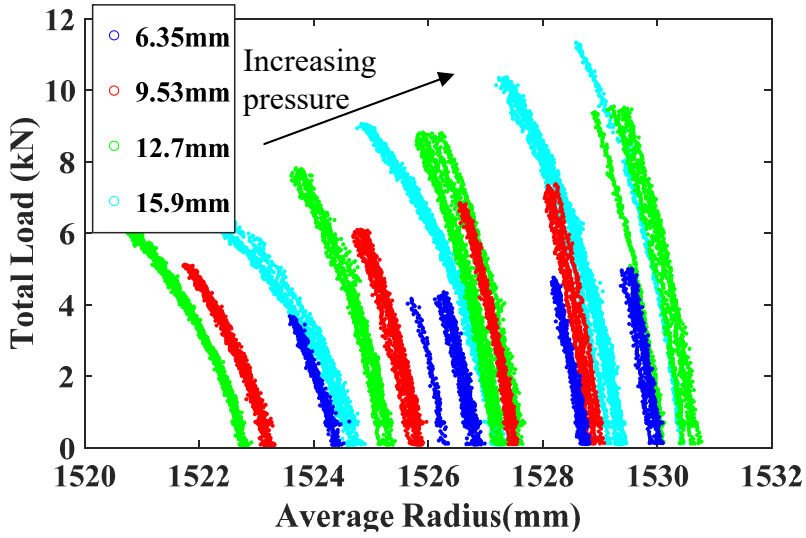

Figure 54: Average Radius of T3AP-2 Small Displacement

Testing on the ladder article resulted in a clear demonstration of repeatability as seen in Figure 55 where all tests run at the same pressure resulted in the same load-deformation response. It is also evident that there is more noise in the data found in the

previous tests. This is primarily due to the fact that the ladder reinforcing strap is located such that it interfered with the optimal PONTOS dot locations. This forced the dots to be placed further down on the torus cross-section creating more noise from partially obscured targets.

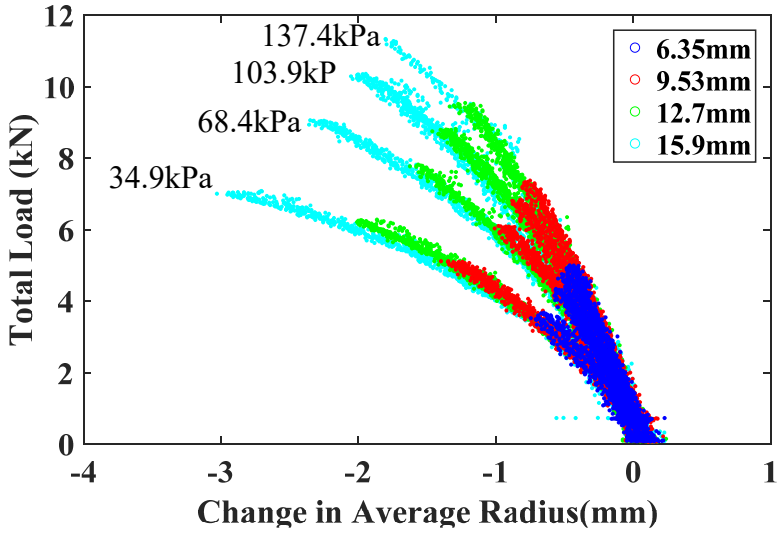

Figure 55: Change in Average Radius of T3AP-2 Small Displacement

The deformed area response of the ladder torus as shown in Figure 56 did not exhibit the same level of pressure dependent response as the four-cord article. There is also a trend towards less deformed area at higher pressure for this article indicating that the article reinforcement is well attached and yields evenly distributed loads.

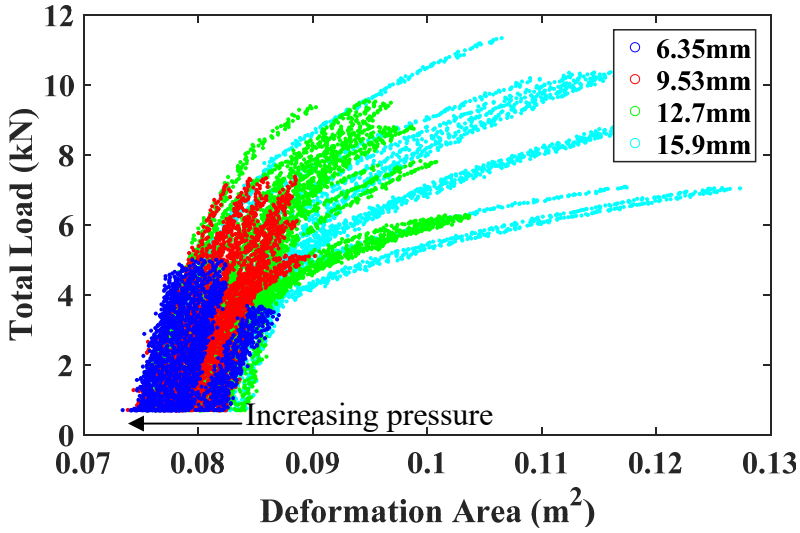

Figure 56: Deformed Area of T3AP-1 Small Displacment

This article demonstrated a good deal of repeatability with only very small changes in the deformed area after loading to small displacements. The tightly clustered nature of the data shown in Figure 56 makes it difficult to distinguish the individual tests; however, this demonstrates the lack of large change in the deformed area of the article as a function of the inflation pressure.

6.2.2.2. Torsion Testing T3AP-2 Ladder

Torsion testing of the T3AP-2 ladder article was accomplished using the same methods used for torsion testing as described previously. The testing showed good repeatability and consistent response for the torus testing of the ladder. The noise resulting from the non-ideal dot placement can be seen in the rotation data in Figure 57. This coupled with the small amount of rotation of this article makes it difficult to measure without the displayed noise.

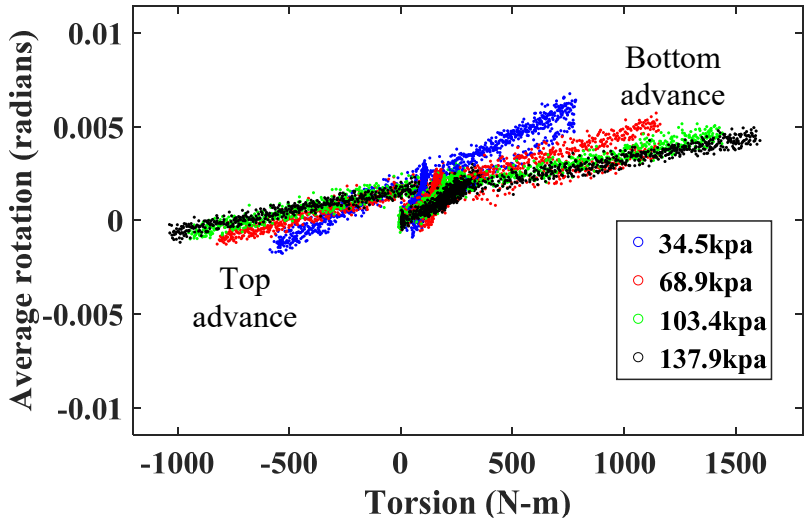

Figure 57: Torsional Response of T3AP-2

The initial response of the article during torsion testing is also different from what was observed for the other articles. It can be seen in Figure 57 that the initial uniform loading of the torus results in a positive rotation of the torus. The response of the ladder torus also shows a fairly linear and consistent response for both the top advance and bottom advance testing.

6.2.2.3. Large Displacement Testing T3AP-2 Ladder

Large displacement testing of the ladder article produced a loss of repeatability after it had been established that the torus exhibited a repeatable load-deflection response at smaller displacements. All of the large displacement tests run on the ladder torus were done using 103.4kPa inflation pressure as had been used for the four-cord torus. The large displacement test of the ladder torus resulted in the first measureable damage occurring during the first 38mm displacement test as seen in Figure 58. This damage

initially could only be seen in the loss of repeatability in the measured value from testing and did not result in any observable damage to the braid or reinforcing of the article.

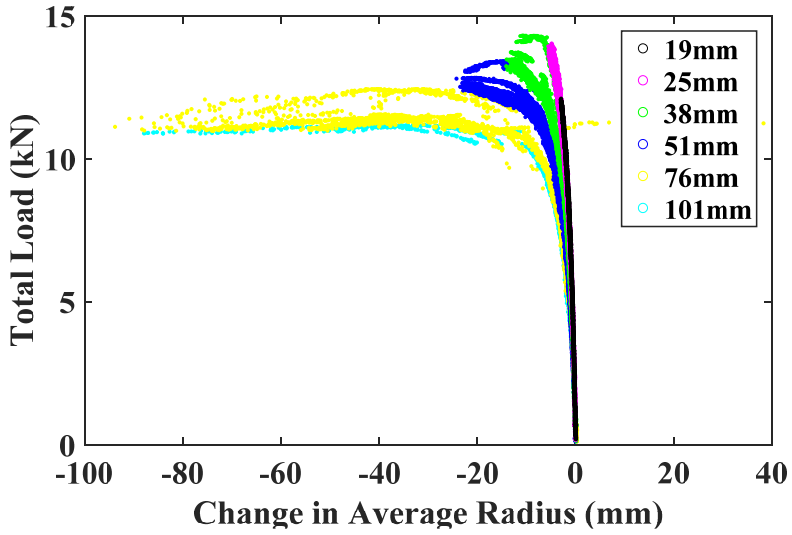

Figure 58: Change in Averge Radius of T3AP-2 Large Displacement

As illustrated in Figure 58 a loss of repeatability occurred during the first test to 38mm, 51mm, 76mm and 101mm of displacement. There was no observable damage until the 76mm displacement test where the braid began to show signs of bunching and a loss of coating which gradually increased in severity until it resulted in the damage shown in the top right of Figure 59. The deformations that resulted during the 103mm displacement tests were very extreme and much greater than the deformations seen during testing of the other articles. The left side of Figure 59 shows that the torus had one area where a kink formed this area is also shown top of the figure form another angle. All of the pictures shown in the figure are taken from the region of highest curvature during testing.

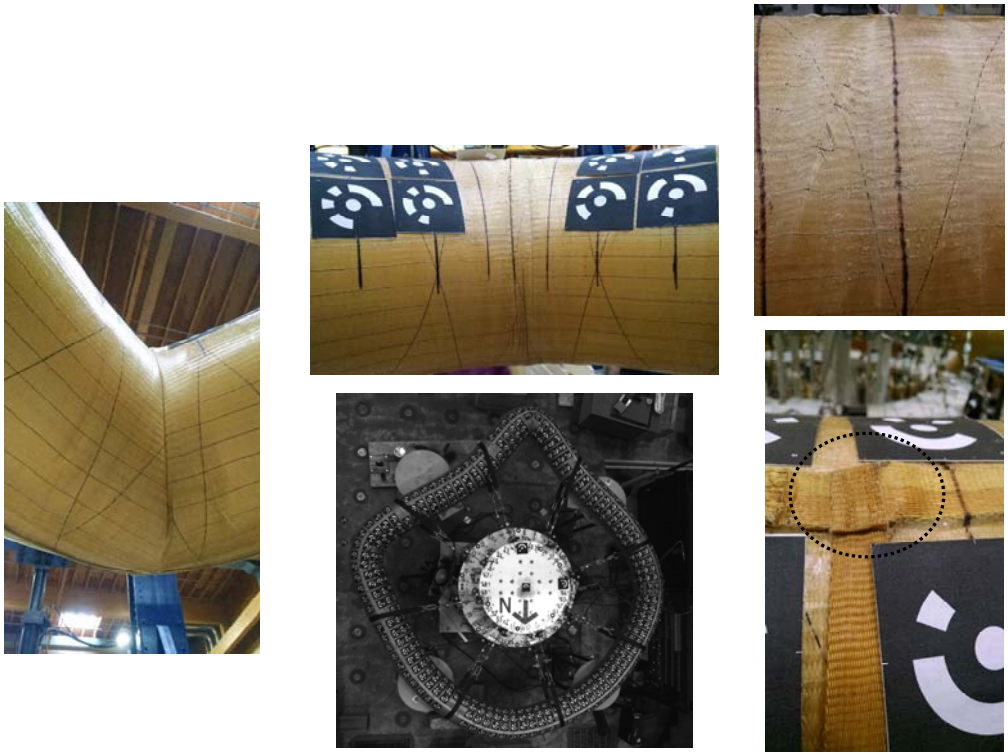

Figure 59: 101mm Displacment Test of T3AP-2 Ladder

The only damage that can be observed to the reinforcement is shown at the bottom right of Figure 59. This damage occurred where the strap and the torus debonded where the ladder straps were connected by the vertical webbing. This created small bumps in the reinforcing straps at inflation pressures of less than 5kPa however it was not noticeable at higher pressures. This debonding occurred at some point during the 76mm displacement test as the damage was only revealed once the pressure in the torus was lowered. Only a small portion of the strap debonded leaving a majority of the reinforcing strap properly bonded to the torus.

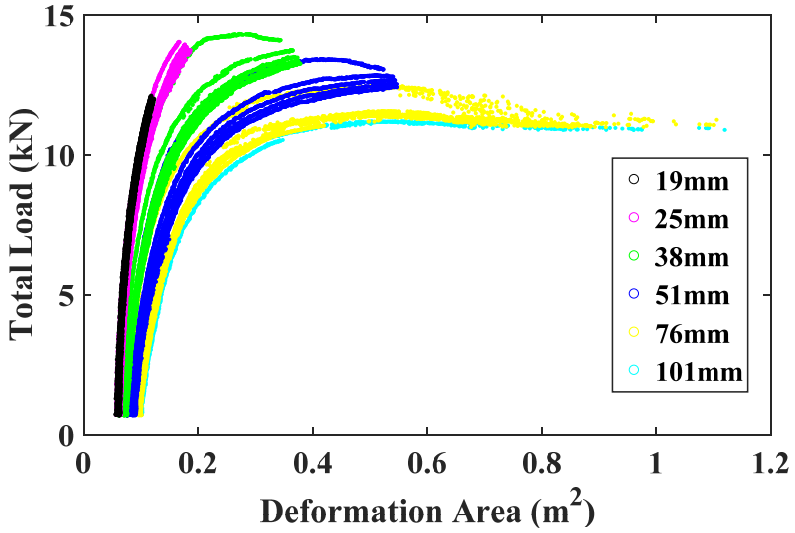

Figure 60: Deformed Area of T3AP-2 Large Displacment

The deformed area of the torus can be seen increasing as the torus was tested to larger levels of displacement as shown in Figure 60. The initial deformed area of the torus gradually increased after the article was unloaded as indicated in the figure. The deformed area plot also shows the point at which a loss of repeatability occurs during the first run at 38mm of displacement.

6.2.3. T3AP-3

The T3AP-3 article was constructed using nominal 2-cord reinforcing. T3AP-3 article had initial small displacement testing before the test matrix was fully developed, and the tests shown in Table were performed afterward this initial testing. It was determined that in future tests the articles would not be initially displaced past 15.9mm of displacement to ensure that no loss of repeatability occurred before the torus had been fully tested to small displacements. This resulted in fewer small displacement tests being

performed on this article. Nevertheless good repeatability was still demonstrated with only two levels of displacement being tested for this article.

6.2.3.1. Small Displacement Testing T3AP-3

The response of the T3AP-3 article showed good repeatability through all the small displacement tests. The average radius as shown in Figure 61 clearly increases as expected with increasing inflation pressure. The average radius for the torus does drift during some of the tests more than others, however, it is not very clear why this happens during testing even with good pressure regulation. There is no measureable effect on the load-deformation response of the torus even with small changes in the average radius of the torus between tests.

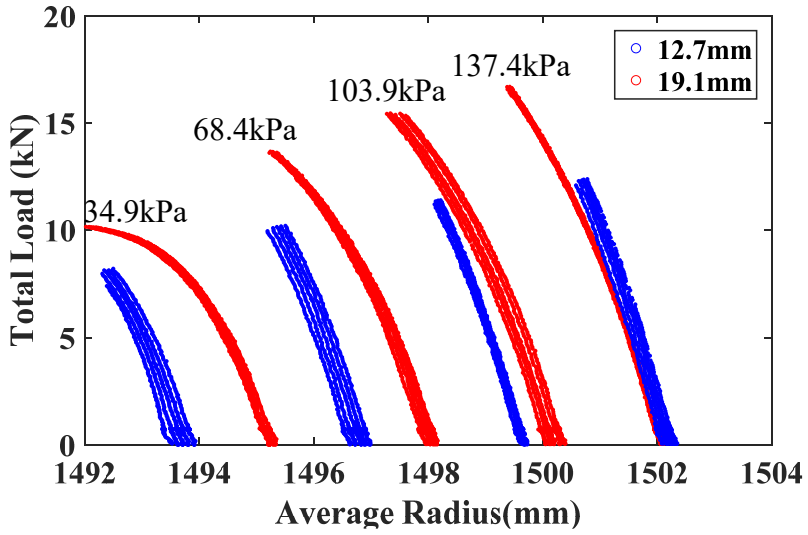

Figure 61: Average Radius of T3AP-3 Small Displacement

Figure 62 displays the repeatability for the small displacement tests run on this article. The stiffness measured by the average radius is the same for all five runs performed at all four pressure levels. The stiffness of the torus is strongly pressure

dependent observed in Figure 62. The test run at the lowest pressure shows the greatest extent of load dependent loss in stiffness.

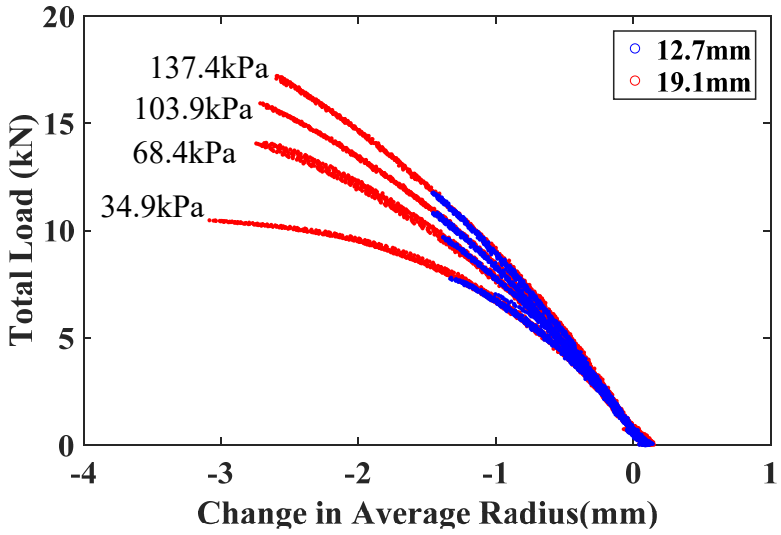

Figure 62: Change in Radius of T3AP-3 Small Displacment

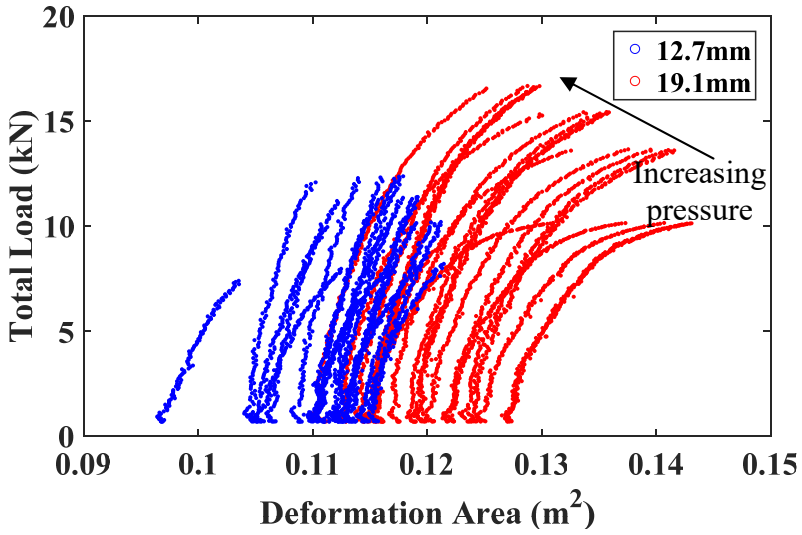

Figure 63: Deformed Area of T3AP-3 Small Displacment

The deformed area of the torus during testing can be seen in Figure 63. The deformed area did increase as the testing proceeded on the article to a small extent as the larger displacement tests all initially exhibited more deformed area. It is also evident that the deformed area of the torus decreases with increasing inflation pressure. This trend can be better observed in the larger displacement tests as the four pressure level groups are more distinguishable.

6.2.3.2.Torsion Testing T3AP-3

Torsion testing on the article was performed using the same method that had been used for all the other articles testing with first top advance then bottom advance. This torsion testing was performed after the small displacement testing and yielded a linear and repeatable response shown in Figure 64.

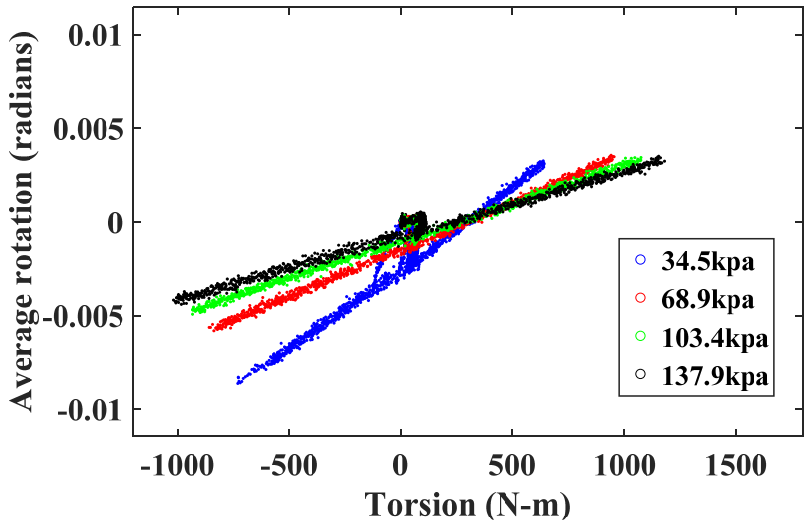

Figure 64: Torsion Response of T3AP-3

The torsion results given in Figure 64 show the same linear trend in both the top advance and the bottom advance testing and can be used for constructing a trend line to

determine the torsional stiffness of the article. The T3AP-1 article rotated during the uniform displacement loading the torus rotates as can be seen by the drop in rotation angle shown at the center of Figure 64. This effect becomes more pronounced at lower pressures.

6.2.3.3. Large Displacement Testing T3AP-3

The large displacement testing of the T3AP-3 article resulted in damage measured by the loss or repeatability of the average radius which occurred on the first test run at uniform displacement of 38mm as can be seen in Figure 65. The torus clearly shows damage when the torus was loaded to a higher level of displacement then had previously been applied to the article. The article however also settled into a new stiffness profile after being loaded multiple times at the same displacement.

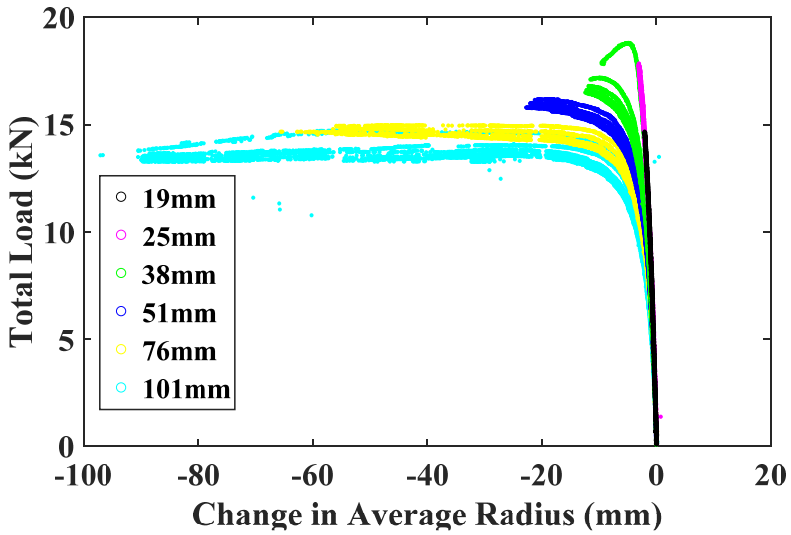

Figure 65: Change in Average Radius T3AP-3 Large Displacment

The large displacement test performed on the article did not result in any observable damage to the torus, however, as previously noted the damage was apparent

by a loss of response repeatability. It is also evident that for the initial loading of the torus there is not a strong correlation between the magnitude of the displacement as applied at the end of the load straps and the change in average radius. However, once the torus response softens because of increased loading there is more agreement between the applied displacement and the average radius. Finally for the highest displacement test, the 101mm prescribed strap displacement caused an average radius change of nearly 100mm.

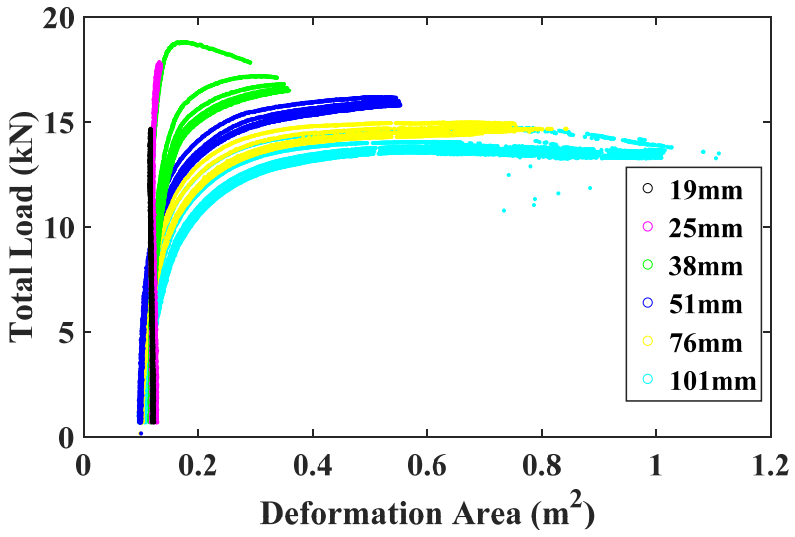

Figure 66: Deformed Area of T3AP-3 Large Displacement

The deformed area of the torus actually has a slight trend towards slightly less deformed area as testing progressed than its initial deformed area. This is likely because there may have been some deformation in the article that was initially reduced by strap loading. The deformed area of the torus also clearly had a change in trend during the first 38mm where the deformed area during the test began to increase rapidly after the loading on the torus was increased.

6.2.4. T3AP-5

The T3AP-5 article was constructed using two reinforcement cords at 60 degrees off the plane of the torus, this being the nominal reinforcing scheme used on these articles. This article was manufactured for previous testing performed at NASA Armstrong, however, it was never actually tested by NASA. This article was nominally identical to the T3AP-3 specimen with the exception of 32 buffer straps that had been wrapped around the 32 locations where loading strap were to be placed on the article.

6.2.4.1. Small Displacement Testing T3AP-5

Small displacement testing on the article resulted in nominal performance similar to what was observed with similar, previously tested articles. The response of the T3AP-5 article showed good repeatability through all the small displacement tests. The average radius as shown in Figure 67 clearly increases with increasing inflation pressure as expected.

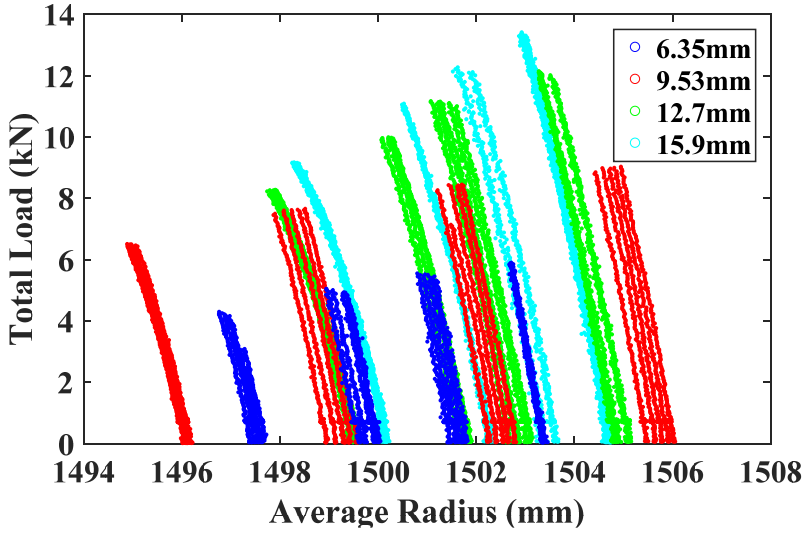

Figure 67: Average Radius T3AP-5 Small Displacement

The change in average radius for this article was repeatable as shown in Figure 68 where the trend lines all pass through similar points for a given pressure. This repeatability has been seen in all the articles tested to small displacements and highlights the robust nature of the articles' construction. There is also a fair amount of photogrammetry noise as illustrated in Figure 68, this likely being the result of non-ideal placement of the tracking dots.

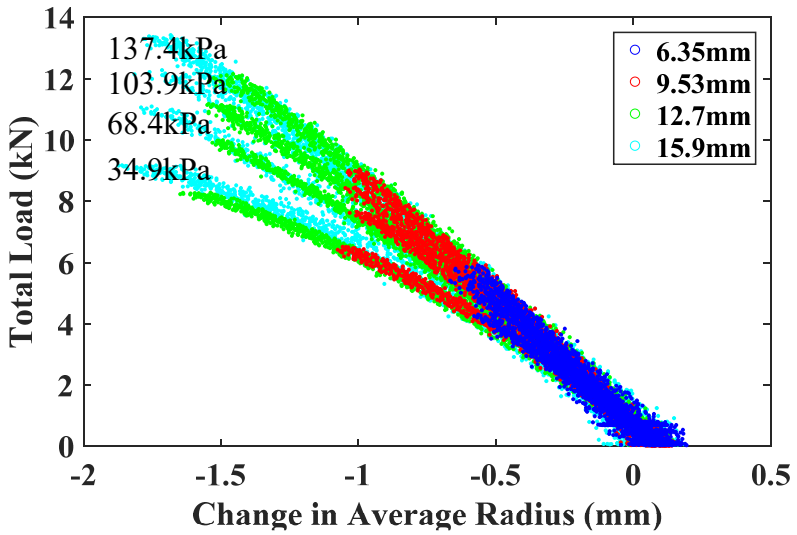

Figure 68: Change in Average T3AP-5 Small Displacment

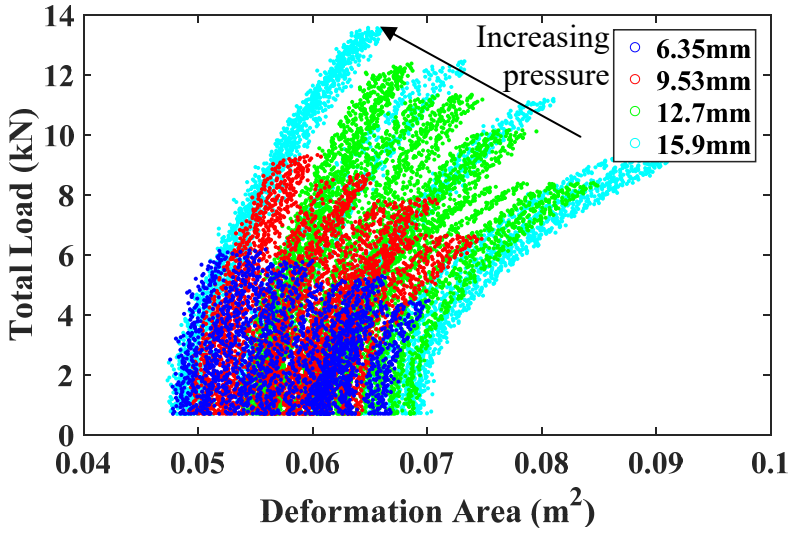

Figure 69: Deformation Area T3AP-5 Small Displacement

The deformed area of the torus can be seen in Figure 69 where the small spread in deformed area measured during testing indicated that the torus did not accumulate a significant amount of deformation during testing. This is apparent since the deformed area is clearly less affected by previous tests than the four-corded article and shows more dependency on pressure and natural drift. This torus also exhibits a pressure dependent decrease in deformed area when the inflation pressure is increased.

6.2.4.2.Torsion Testing T3AP-5

Torsion testing on the article was performed using the same test matrix that had been used for all the other specimens. The tests yielded good repeatability and linear load-deformation response similar to what had been seen previously in other articles.

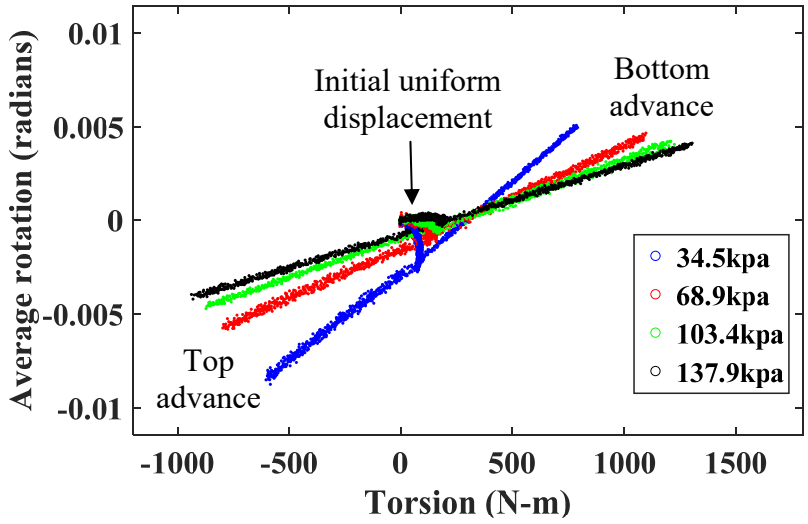

Figure 70: Torsional Response of T3AP-5

As observed in Figure 70 the article responded in a very consistent manor when it was torsionally loaded. The article also responded with a fair amount of rotation when uniformly loaded at the start of the torsion test with the effect strongest at lower pressures. This trend can be seen at the center of Figure 70 where uniform displacement is indicated. The torus also exhibited the same pressure-dependent stiffness for both top and bottom advance loading.

6.2.4.3. Large Displacement Testing T3AP-5

Large displacement testing on the T3AP-5 article showed consistent response compared to the other test performed on similar articles. The first test where the specimen began to exhibit a loss of repeatability was on the first run of the 38mm displacement test. However this loss of repeatability was very minor compared to the relative change that occurred when the article was first loaded to a displacement of 51mm.

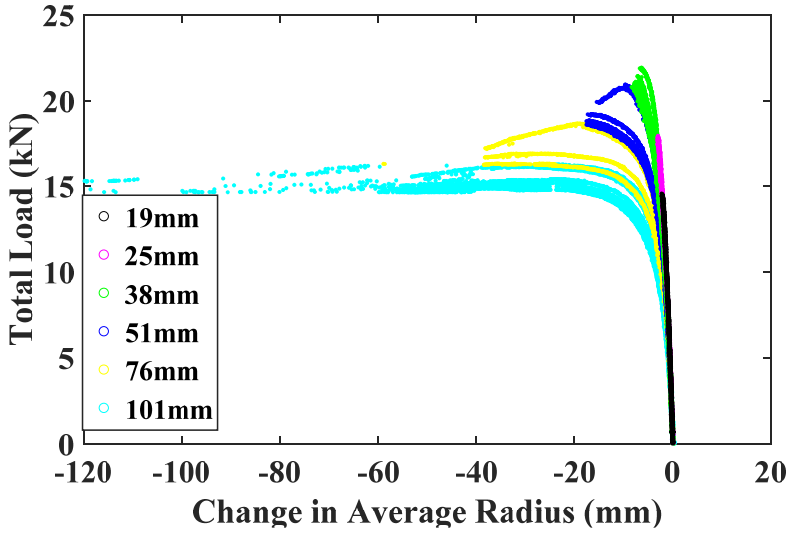

Figure 71: Change in Average Radius T3AP-5 Large Displacement

As observed in Figure 71 the average radius response of the torus showed a loss of repeatability on the first test run to displacements of 38mm and larger. It is found that once the torus is tested to larger displacements, the torus settles into the same response until it is later loaded to a greater displacement then it had previously been loaded.

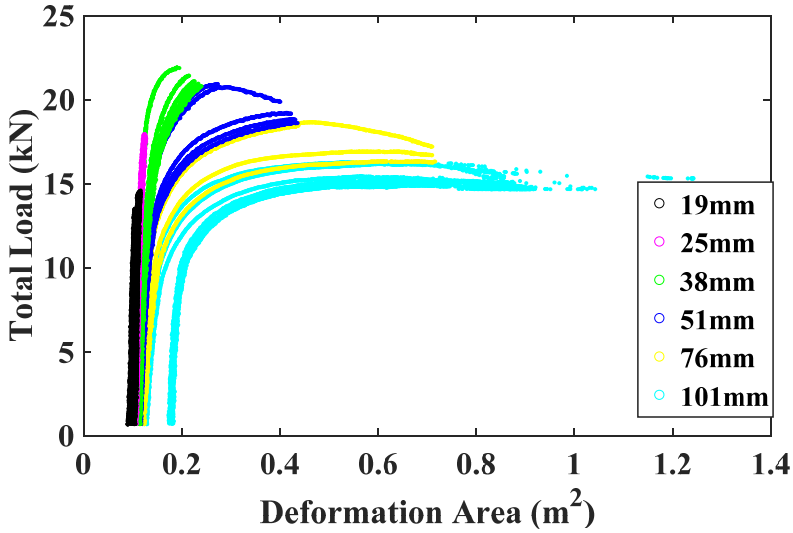

Figure 72: Deformed Area T3AP-5 Large Displacement

In Figure 72 large jumps in deformed area can be seen on the first loading at all displacements 38mm and greater. The largest jump in deformed area occurs between the 76mm displacement test and the 101mm displacement test. This coincided with the first observable damage which occurred between these two levels of displacement. As highlighted in Figure 73, the buffer straps had bond failure where the curvature was very large during the test. This may have prevented the torus from being able to fully restore itself to the shape it possessed prior to the buffer straps debonding from the braid.

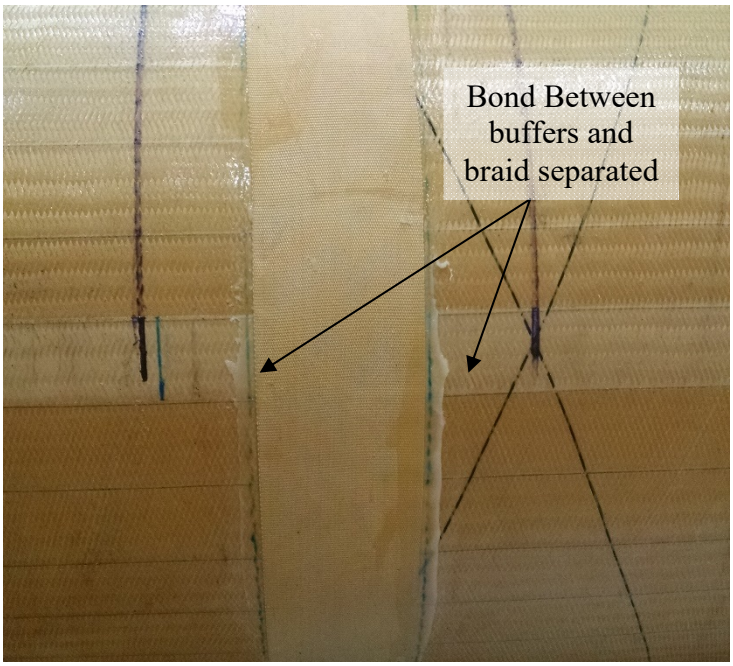

Figure 73: T3AP-5 Buffer Strap Bond Failure

6.2.5. T3A-2 Differential Cord

The different length reinforcing cord torus was constructed using the nominal two reinforcing cord method used for most of the articles tested in this work. However, this article was constructed with one axial reinforcing cord that was 50mm shorter than the

other. This resulted in the angular position of the cords not being at the nominal 60 degrees off the horizontal plane as is typical for these articles. This specimen was constructed and tested to assess the sensitivity of the response to inaccurately sized reinforcing cords.

6.2.5.1. Small Displacement Testing T3A-2

Small displacement testing on the T3A-2 article showed good repeatability and consistent performance throughout all stages of the testing. The article also clearly increased in average radius with an increase in pressure.

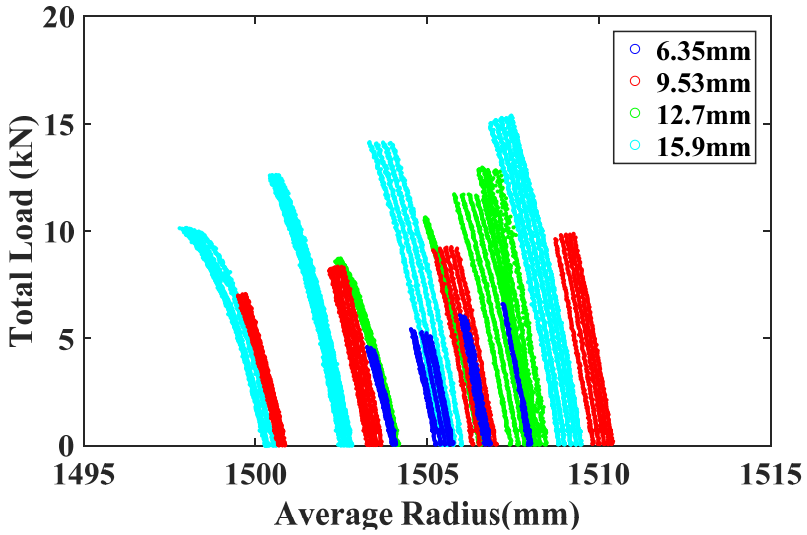

Figure 74: Average Radius T3A-2 Small Displacement

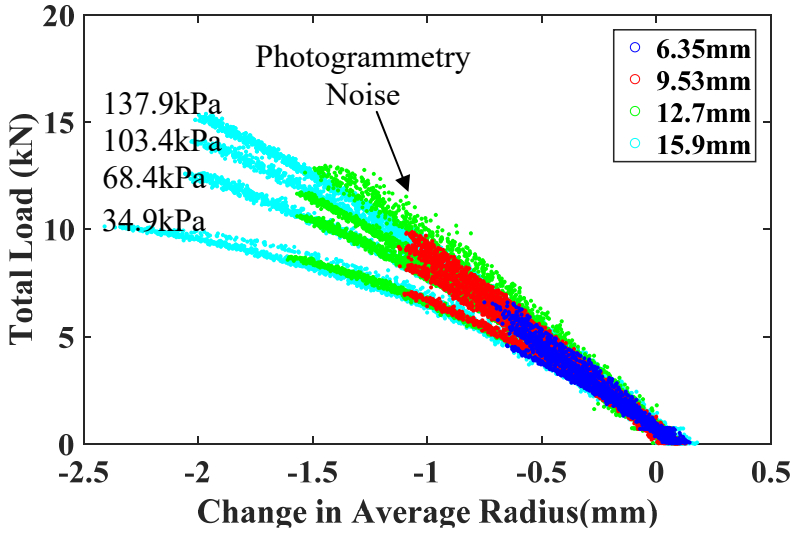

Figure 75: Change in Average Radius T3A-2 Small Displacment

The change in average radius given in Figure 75 demonstrates the consistency of the stiffness response of this article. The response of the article shown in Figure 75 has the same load-deformation trend for tests at a given pressure level. The tests run at 12.7mm displacement and 137.9kPa inflation pressure possess a good deal of data noise which resulted from over-exposure of the photogrammetry dots caused by direct sun light on the torus during testing.

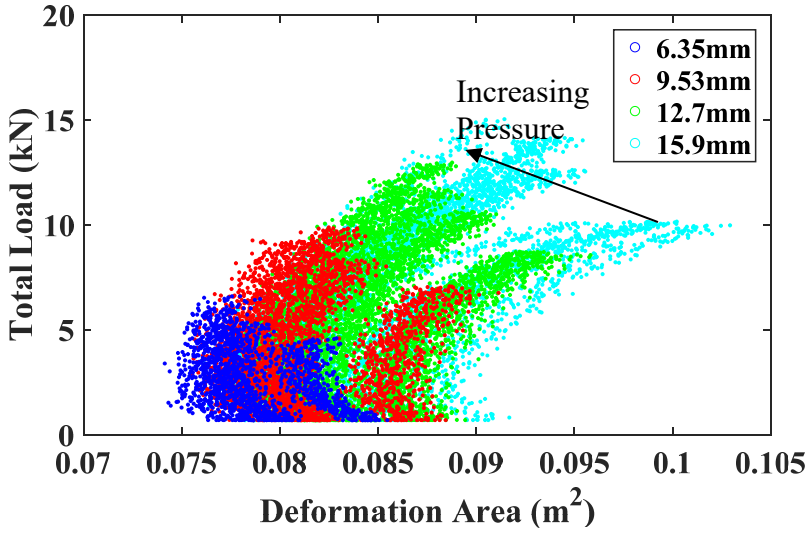

Figure 76: Deformed Area T3A-2 Small Displacment

The deformed area response of the torus is given in Figure 76. Because of the very small amount of change in deformed area, with increasing load, there is a large amount of noise in the data. Some interesting trends can still be observed in the response, primarily the small amount of decrease in deformed area upon initial loading. This decrease in the deformed area was unique to this article and could have been a result of the two uneven cords. This article also clearly shows a decrease in the deformed area with an increase in inflation pressure.

6.2.5.2. Torsion Testing T3A-2

The torsion testing of the T3A-2 article yielded consistent and linear performance during torsion testing. This consistent performance permitted the torsional stiffness of the article to be determined for all the pressures considered.

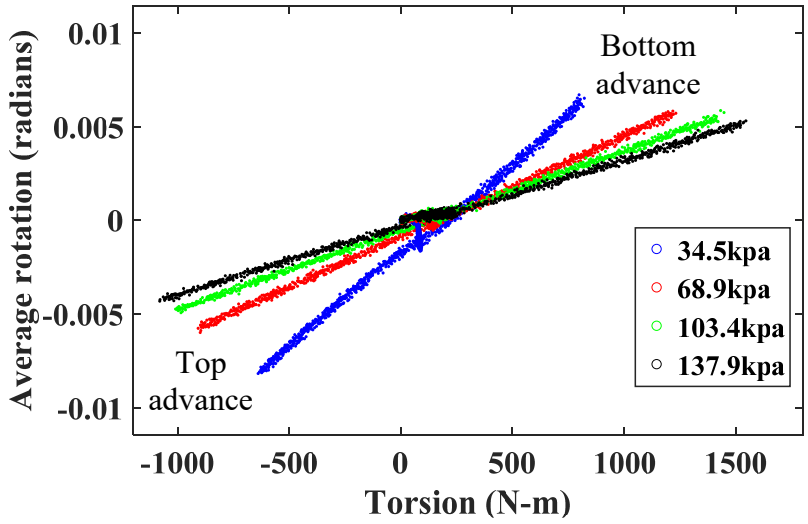

Figure 77: Torsional Response T3A-2

The torsional response of the differential cord article closely resembled that of the other two-corded articles. As can be seen in Figure 77 both the bottom advance testing and the top advance testing have the same slopes at a given pressure indicating that the torsional stiffness in consistent when loaded in either torsional direction.

6.2.5.3. Large Displacement Testing T3A-2

The large displacement tests run on the T3A-2 article resulted in very similar outcomes to the response of the other two-corded articles tested in this configuration. This article experienced a loss of repeatability to a small degree during the 38mm displacement tests. However, this was only observed as a drift in the stiffness curve as shown in Figure 78. The first test that was performed at 51mm of displacement resulted in a significant loss in stiffness and repeatability at high loads. Furthermore, this article was tested at other inflation pressures to a displacement of 51mm between finishing the 51mm displacement test at 103.4kPa and the 76mm displacement test as specified in

Table 5. This testing at other pressures affected the response of the torus at 103.4kPa, and as such it was the only torus tested at other pressures between the 51mm and 76mm displacements.

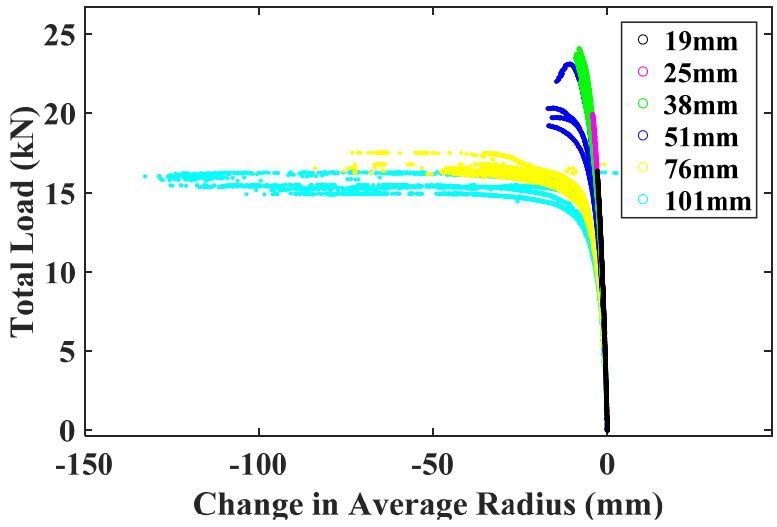

Figure 78: Change in Average Radius T3A-2 Large Displacement

As can be seen in Figure 78 the response of the first test at 76mm of displacement resulted in only a very small amount of drop in stiffness for subsequent tests. Generally the other articles had a significant drop in stiffness between the 51mm and 76mm displacement tests.

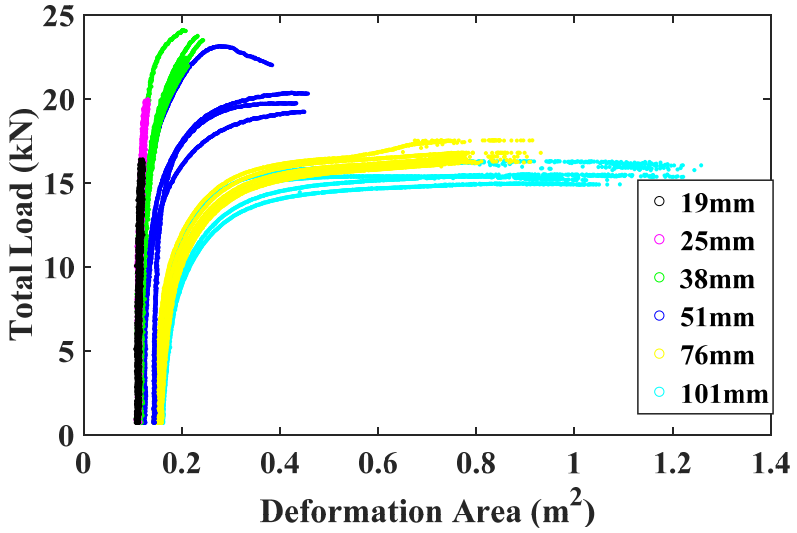

Figure 79: Deformed Area T3A-2 Large Displacement

The deformed area response showed a marked change when the article was displaced to 38mm. The response of the torus also exhibited a drift in the deformed area of the torus as the test increased in displacement.

6.3. Small Displacements Response comparison

This section compares the response of the T3 articles for the small displacement tests initially performed on all specimens. This section includes the small displacement that were the first test run on the article at 15.9mm of displacement at four of the operating pressures with the exception of the T3AP-3 article which was only run at 19.1mm of displacement. All small displacement tests on the T3 articles established good repeatability in the average radius response at all the tested inflation pressures.

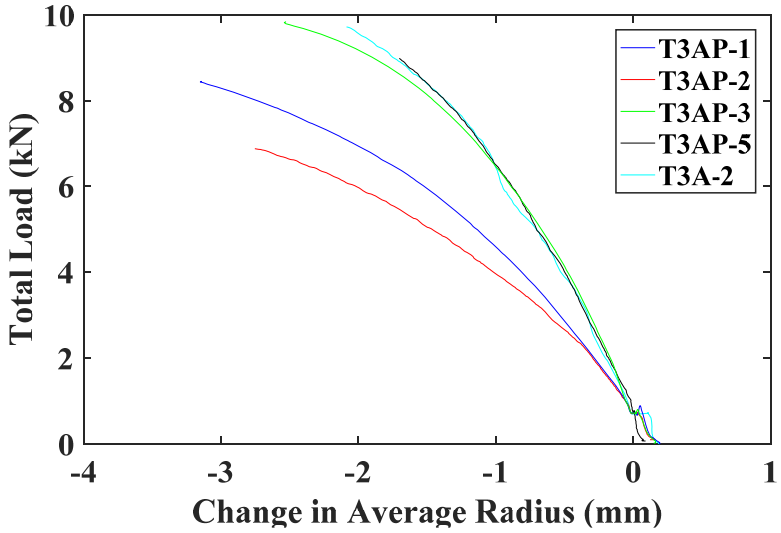

Figure 80: Change in Average Radius 34.9kPa

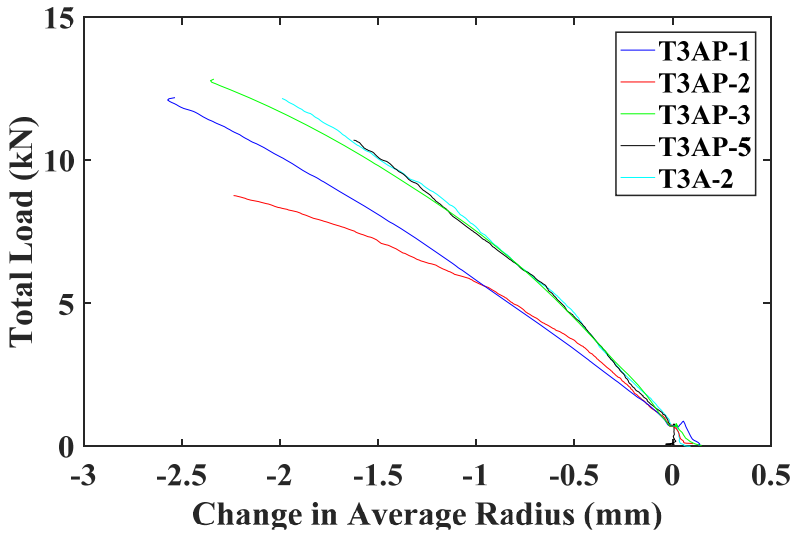

Figure 81: Change in Average Radius 68.4kPa

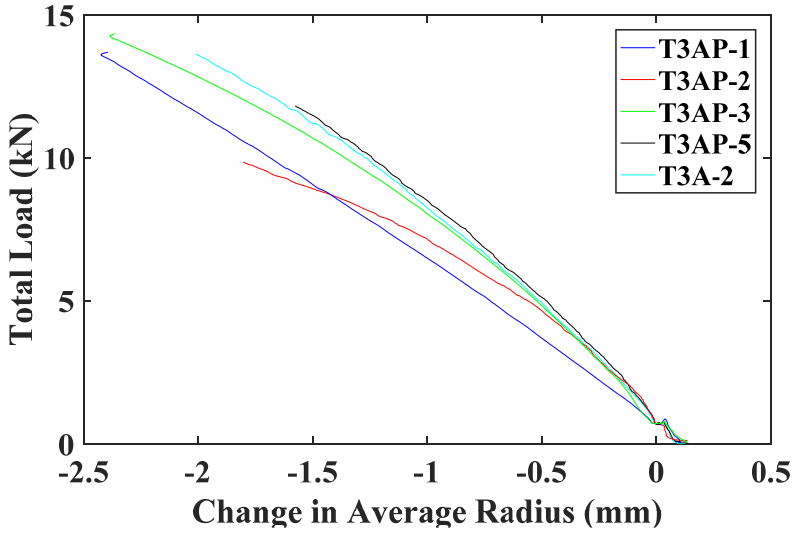

Figure 82: Change in Average Radius 103.9kPa

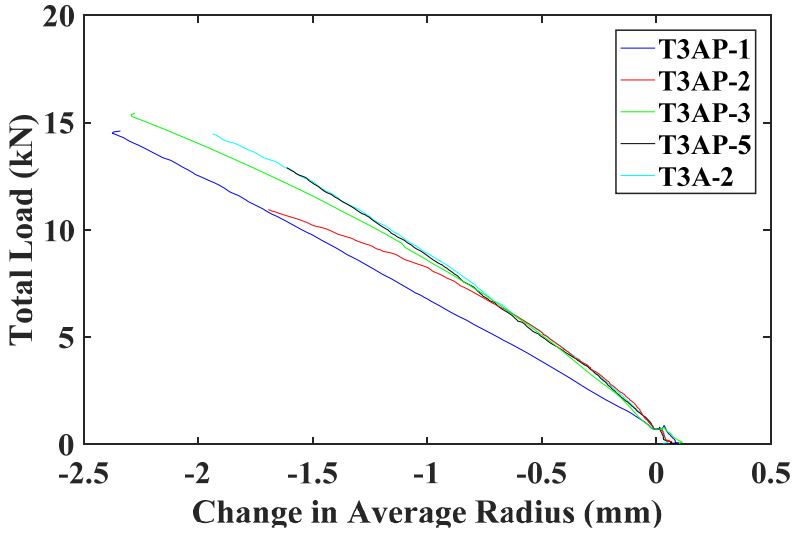

Figure 83: Change in Average Radius 137.4kPa

As can be seen in Figure 80 through Figure 83 the average radius stiffness of the five articles was different for each specimen when subjected to small displacement. All three of the articles that had only two reinforcing cords possessed very similar stiffness

responses at all the pressures shown in Figure 80 through Figure 83. Interestingly, the stiffness of the T3AP-1 four-corded article is less than that of the two-corded articles despite the fact that it carried the most load out of all the tori during large displacement testing. As illustrated in Figure 83 the four-corded article was less stiff than the nominal two-corded articles at 137.4kPa albeit displayed a more linear load-deformation response then any of the other articles. Observed in Figure 80 through Figure 83 the ladder torus (T3AP-2) generally exhibited the softest and most non-linear response at all the tested pressures.

6.4. Torsion response comparison

All the articles tested using the torsion test scheme that was described previously yielded linear and highly repeatable torsional responses of the article. The torsion tests subjected the torus to uniform torsion which generally resulted in a uniform rotation response of the article. Because of the nature of the braid mechanism the uniform article rotation easily adjusts the fibers allowing for this rotation to occur with little torsional stiffness contribution from the braid. The reinforcing cords do contribute significantly to the torsional response as a result of the need to axially strain to permit the cross section to rotate. The torsional stiffness for the articles was calculated as the slope of the torsion versus rotation data. These values are tabulated for all the T3 articles in Table 6.

Table 6: Torsional Stiffness of T3 Articles

Pressure (kPa)	Torsion Stiffness (kN-m/rad)				
	T3AP-5	T3AP-3	T3A-2	T3AP-2	T3AP-1
137.9	276	287	375	493	157
103.4	232	255	238	415	139
68.9	177	201	184	317	107
34.5	104	117	99	176	71

The torsional stiffness displayed in Table 6 was calculated using both the top advance and bottom advance testing from the T3 articles except for the four-cord article which only used data form the top advance testing because of test setup issues that could have affected the data. The stiffness data clearly indicates that the ladder torus has much more torsional stiffness than the other articles. Interestingly, the article that exhibited the smallest torsional stiffness was the four-corded specimen which had nearly half the torsional stiffness of the other nominal two-cord articles. The data shown in Table 6 also demonstrates the pressure dependency of the torsional response as well as a good agreement between all the two-corded articles.

6.5. Large Displacement Comparison

Large displacement tests on the T3 articles provides valuable insight into the effects of differing reinforcing schemes on the response of the inflated articles to large displacements. The four-cord article (T3AP-1) achieved the maximum load during testing, however, its ultimate capacity was limited due to strap intrusion into the cross-section. Buffer straps or another method of distributing applied loads would likely have increased its capacity further.

As shown in Figure 85 the four-cord article stayed the most circular during the displacement test. The straps created one local region of high curvature at the bottom left of the torus as seen in the figure. From the data presented thus far, it is evident that the reinforcing scheme used to construct the torus has a large impact on the performance of the article. However, it is also interesting that all three of the articles constructed with the two-cord reinforcement did not all achieve the same level of load. Furthermore as can be observed in Figure 84 the T3A-2 article which was constructed with the two uneven cords actually performed the best in both total load and deformed load carrying capacity of all of the two-corded articles that were tested. The worst performer of the nominal two-corded articles was the T3AP-3 article which was constructed most recently of the three. This could indicate that the article may actually benefit in some way from unevenly sized cords for this loading configuration, or it could indicate that construction effects other than differential cord length play a more significant role in behavior.

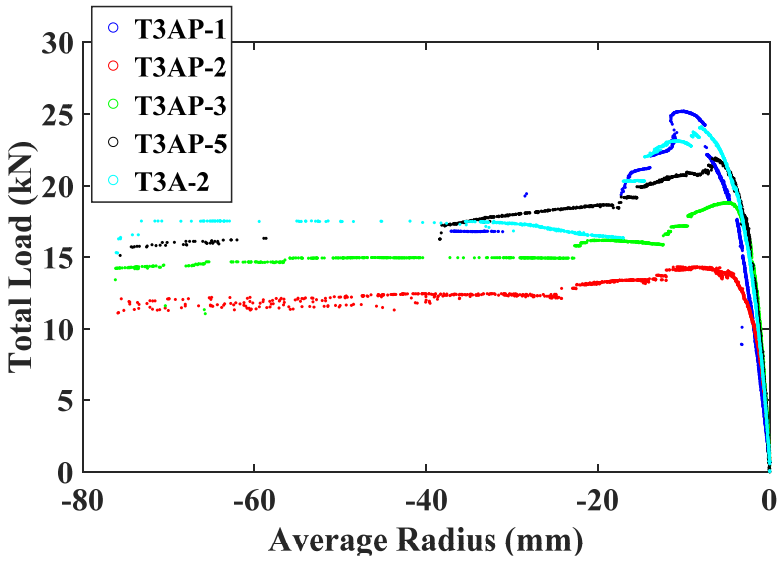

Figure 84: Average Raduis Upper Performance Envolope

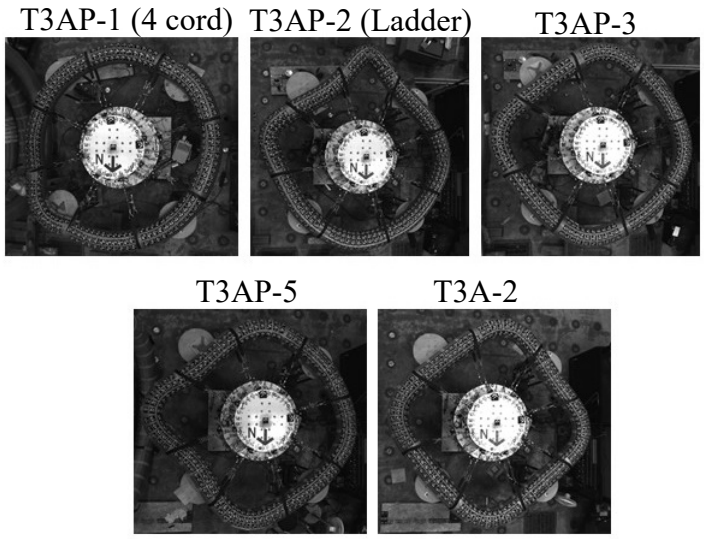

Figure 85: Most Extreme Deformed Shape of All T3

The deformed shape of all the articles shows slightly differing characteristics as can be seen in Figure 85. The articles all deformed to a four-noded square shape similar to a square with the exception of the T3AP-1 article which remained very circular up until local bending caused by the straps induced the buckled shape shown. The ladder torus shown in Figure 85 possesses the displaced shape with the largest localized curvatures and deformations of all the articles tested. This is consistent with the ladder article exhibiting the lowest load carrying capacity and average radius stiffness throughout the testing program.

The bending response of these articles is important to the overall response of the tori. Select images of the bending response of the articles are shown in Figure 86 where there is an observed difference in the neutral axis position of the differing reinforcing methods. As would be expected, the neutral axis position of the ladder and the two-cord torus positioned at the reinforcing location. The location of the reinforcing cords and

straps can be seen in Figure 86 as indicated. As was seen during torus testing the ladder torus had far more compression on the inner face of the article than any of the other articles that were tested. It is also interesting to consider the bending response of the four-cord torus which has a higher bending stiffness resulting from the offset of pairs of cords that significantly increases the cross-sectional moment of inertia.

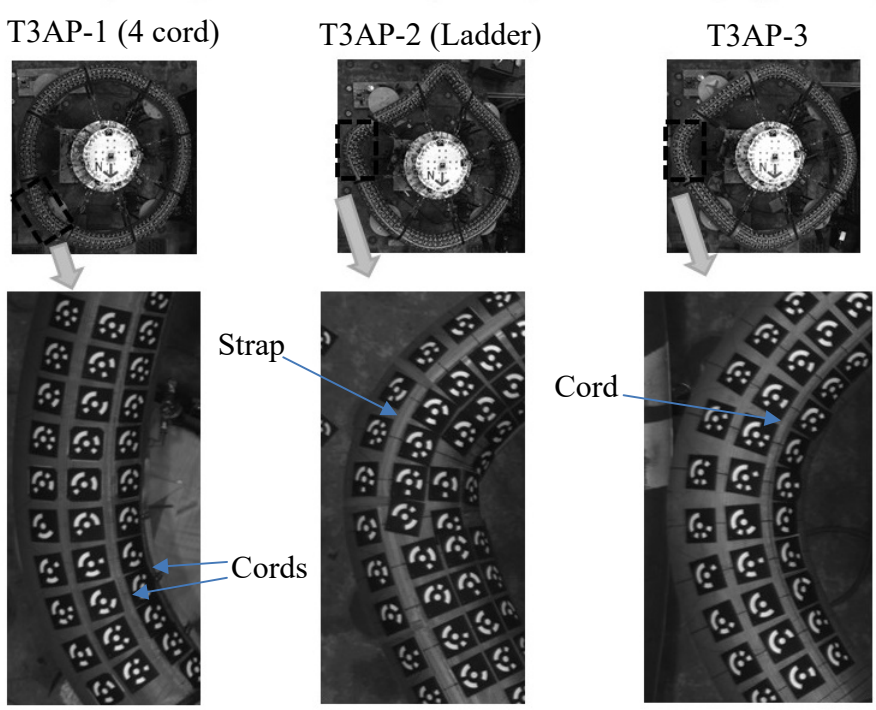

Figure 86: Bending Response with Varying Reinforcing

Overall the large displacement testing response of the T3 articles resulted in interesting and somewhat unexpected results in that the articles that were of similar construction did not have exactly the same response. This was apparent in the large range of total load achieved by the three two-corded articles. Furthermore, the article with intentionally mismatched cords performed better than those with evenly balanced cords.

6.6. Out-of-Plane Loading of T3AP-3

In order to produce more out-of-plane response from the torus, testing was conducted where dead weights were used to subject the torus to out-of-plane loading. This loading provided additional data to be collected for assisting with numerical model validation. For the out of plane testing the T3AP-3 article was chosen to be loaded with dead weights because it was constructed with nominal reinforcing and is likely to have properties most closely matched to the articles used in the final HIAD construction.

Out-of-plane loading was produced by placing hanging weights of 0.8kN, 1.3kN and 2.1kN hanging on both sides of the torus as indicated in Figure 87. After the weights had been placed on the torus it was then uniformly displaced to 51mm of cable end displacement at a rate of 12.7mm/minute and then unloaded at the same displacement rate. All three out-of-plane tests were conducted with an inflation pressure of 103.4kPA in order to produce comparable results to the large displacement tests previously run on the article.

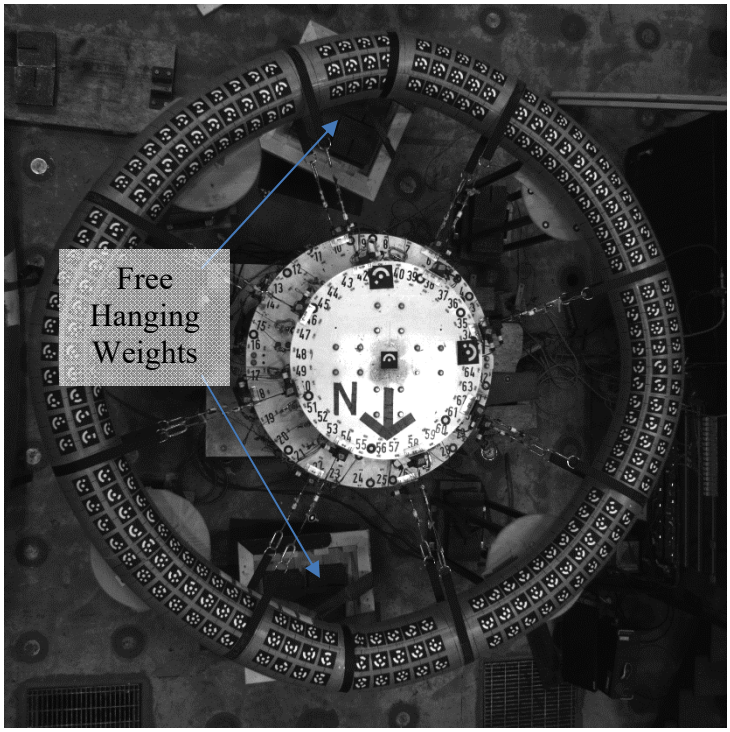

Figure 87: Out-of-plane Load Configuration

As can be seen in Figure 88 the out-of-plane load did result in an apparent stiffness change of the article with the 2.1kN test showing significantly less stiffness for the latter portion of the test. It is also observed that the 1.3kN test achieved a slightly higher final load than the previous 0.8kN test which was likely due to the friction increase caused by more contact force at the supports. This friction is also apparent in the slightly more sluggish unloading response of the 1.3kN test as compared to the 0.8kN. The rapid drop in load is clearly seen in Figure 88 and occurred just as the cord began to slide inside the torus braid resulting in rapid out-of-plane bending. This failure happened just as the control system reached 50.7mm of displacement and caused the test to be quickly aborted to prevent further instability.

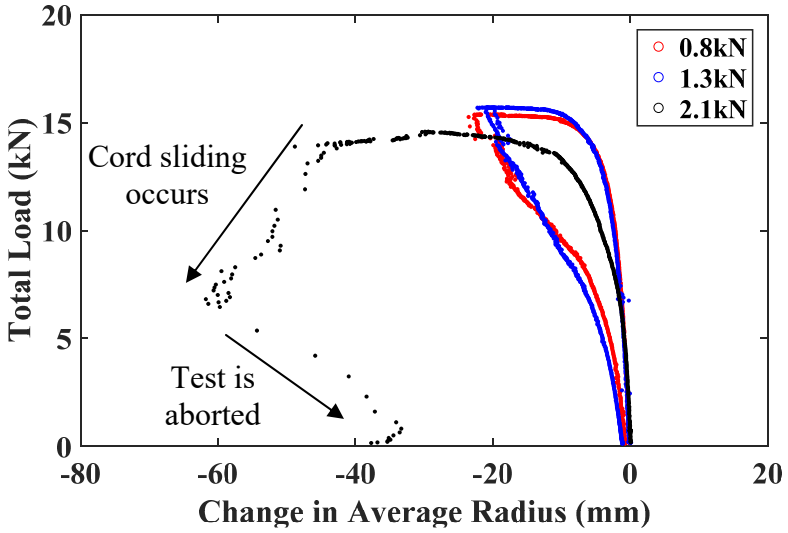

Figure 88: Change in Average Radius for Out-of-plane Loading

As shown in Figure 89, the torus starts the test with significant out-of-plane deflections caused by the loads as indicated by the arrows on the plot. The positions of the supports are also shown in Figure 89 and are indicated by black bars. The supports in this configuration work with the free-hanging weights to produce significant out-of-plane loading on the article. As can be seen in Figure 89, the out-of-plane deflections of the article became very significant during the test, particularly at 1.3 radians where cord debonding occurred.

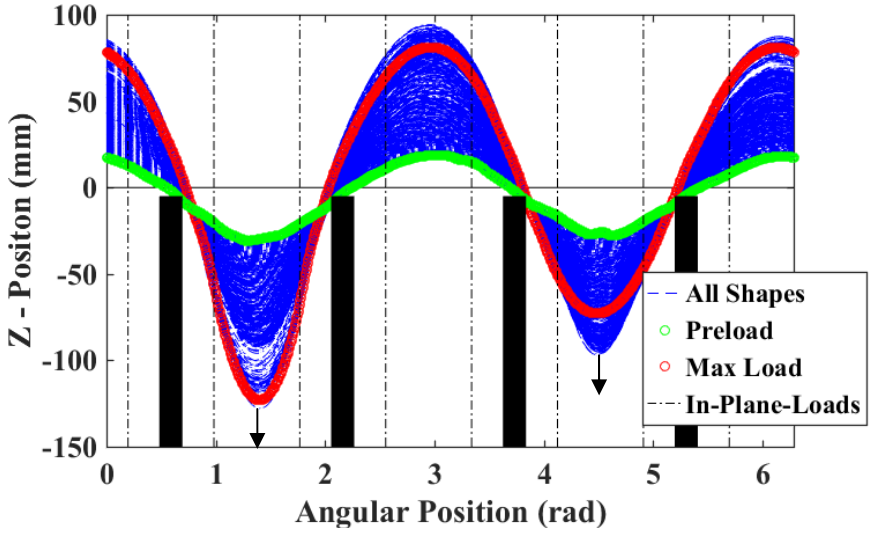

Figure 89: Vertical Deformation 2.1kN Test

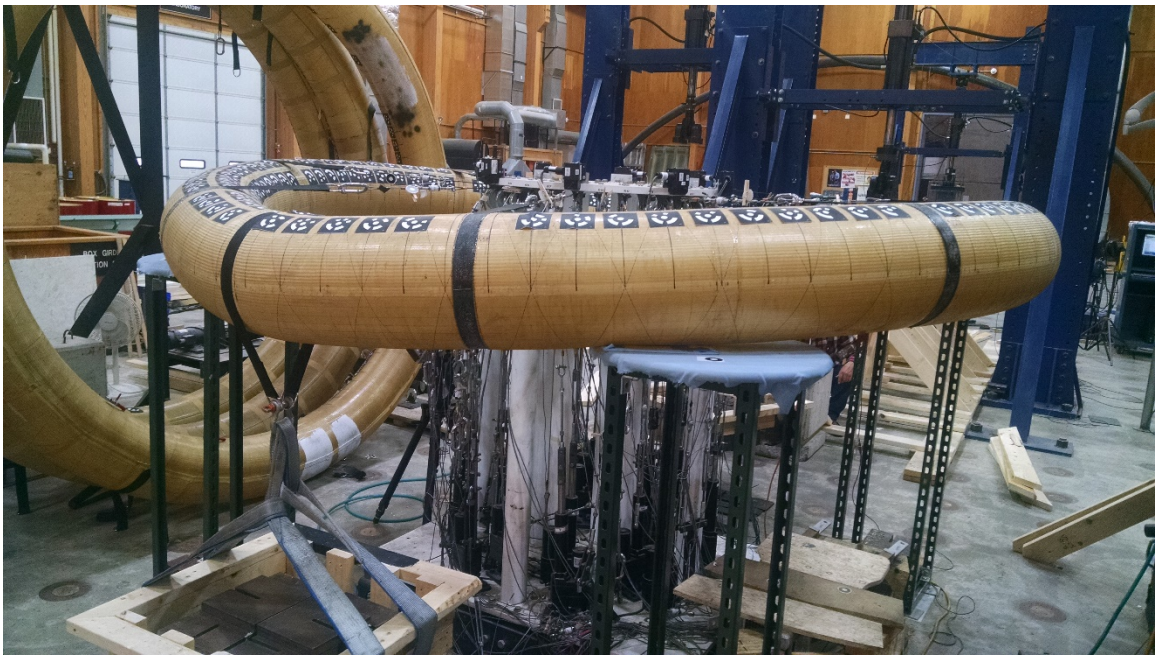

Figure 90: 2.1kN Out-of-plane Test Just Prior to Failure

It was observed that the torus experiences a rapid loss of strength when the shear stresses between the braid and the axial reinforcing cord exceed the bond strength

yielding a rapid contraction of the braid occurs at the cord location. This loss of bond between the cord and the braid significantly reduces the load carrying capacity of the torus and results in significant and permanent damage to the torus.

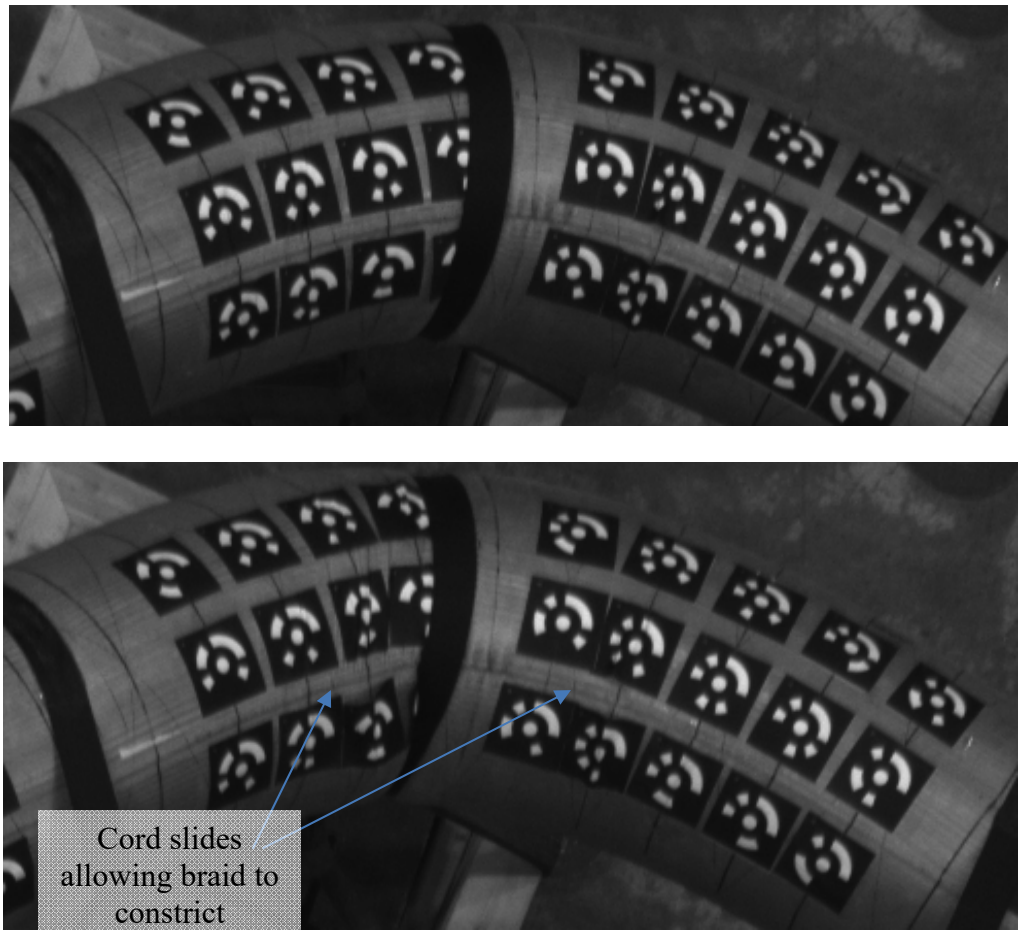

Figure 91: Cord Debonding During 2.1kN Test

The top image of Figure 91 shows the torus just prior to the loss of bond between the cord while the bottom picture shows the same location two seconds later. The region of the torus near the free-hanging weight at 1.3 radians shows signs of the cord debonding from the braid as constriction of the braid in these regions occurs. The article can support a significant amount of out-of-plane loading without experiencing significant

deformation or loss of load carrying capacity. This test demonstrates that these articles are robust and capable of supporting varied and complex loading.

6.7. Torsion testing of T3AP-5

The torus testing conducted on the T3 articles did not include torsion tests to high levels of torque. In order to create more out-of-plane loading the T3AP-5 torus was loaded with high levels of torsion after other testing had been completed. The operating pressure used in the test was 103kPa to maintain consistency with other testing efforts. As can be seen in Figure 92 the torus was uniformly displaced to 25.4mm in order to allow for more significant torsion to be applied.

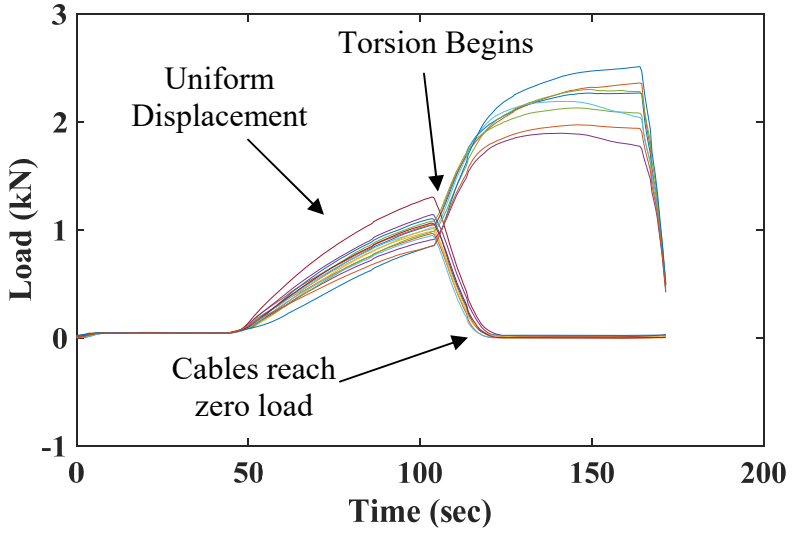

Figure 92: Cable Loads During Torsion Test

After this initial displacement was reached, alternating pairs of straps were torqued to 102mm of displacement as shown in Figure 93. This forced the torus to displace out-of-plane. During the test the cable that was being unloaded in the torsion pair reached zero load as indicated in Figure 92.

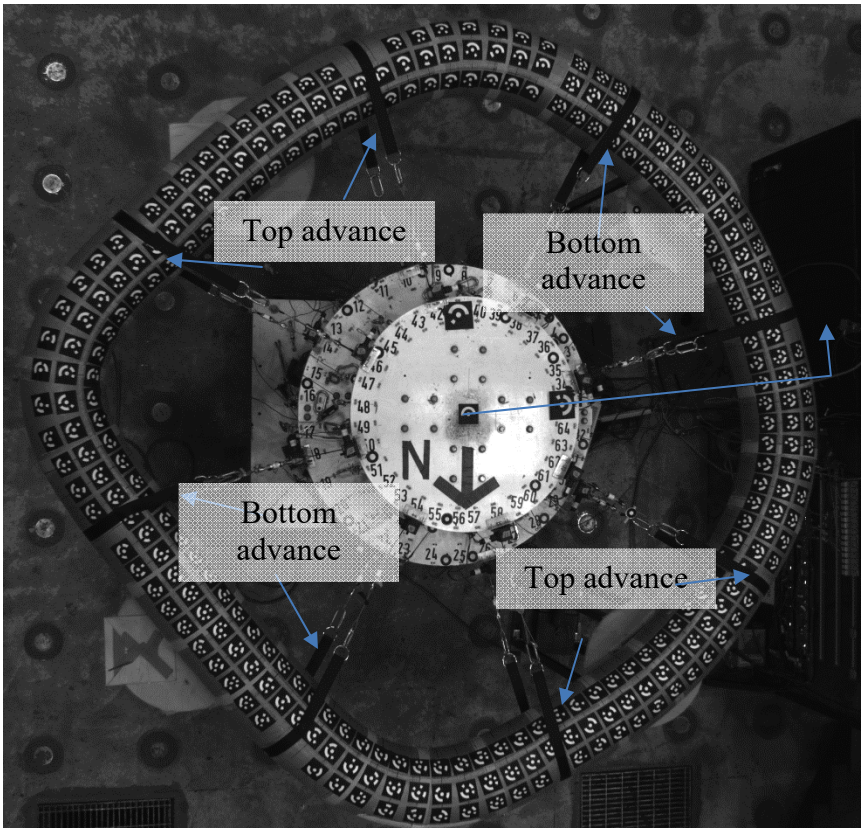

Figure 93: Torsion Loading Scheme T3AP-5

The resulting in-plane deformed shape of the torus was similar to the shape produced during large displacement testing. As seen in Figure 93 and Figure 94 the torus had four extreme nodes and four flat sections similar to what is shown in Figure 85.

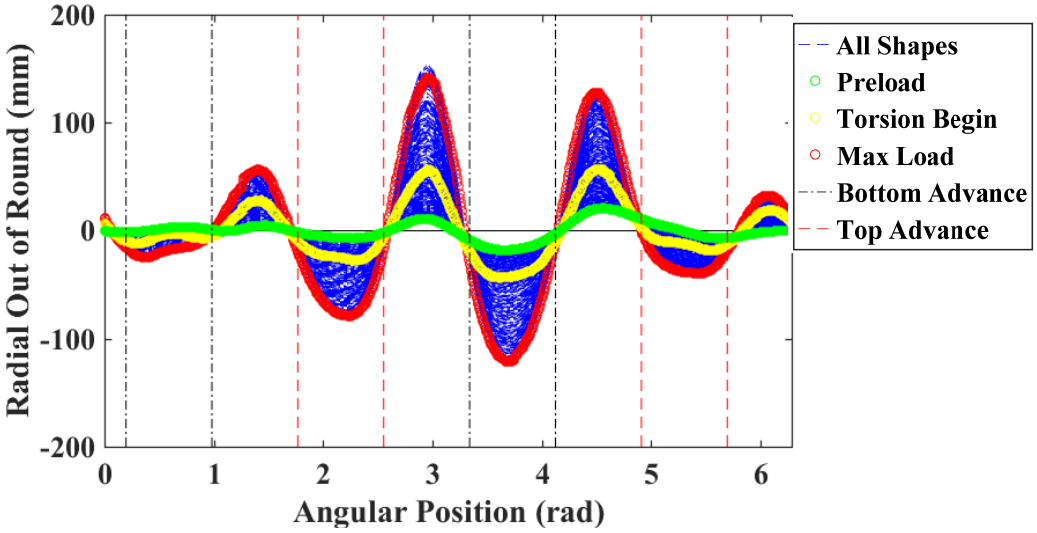

Figure 94: Radial Deformation During Test

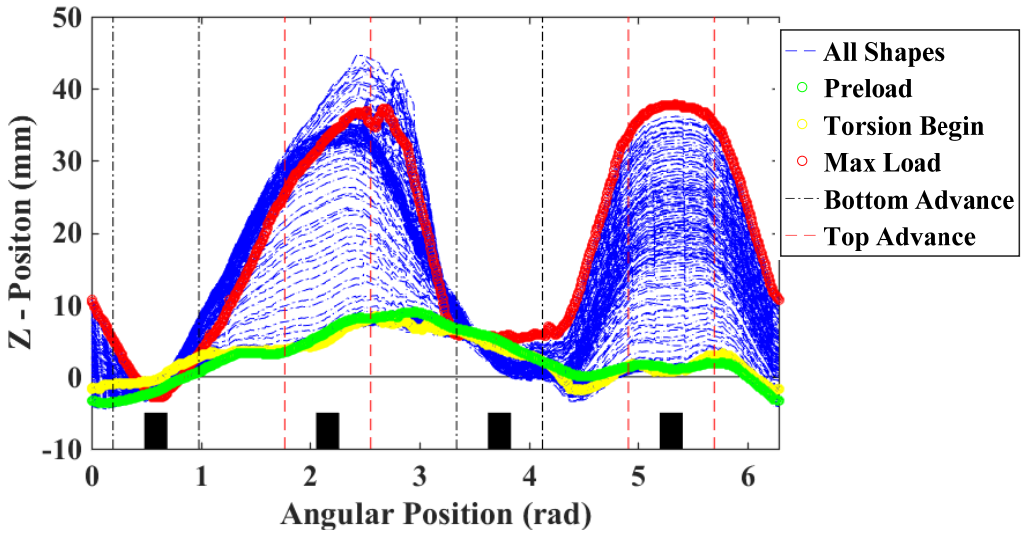

Figure 95: Vertial Deflection of T3AP-5 During Torsion

The location of the supports is shown in Figure 95 as indicated by the bars on the plot at four angular positions. The test produced large out-of-plane displacements as

shown in Figure 95, where the highest displacement were observed between the bottom advance strap pairs.

6.8. Summary of T3 Test Series

Testing of the T3 articles with varied reinforcing methods produced some interesting and useful results to better inform numerical model validation efforts as well as future torus design considerations. It is clear that the reinforcing method used can have a large impact on the performance of the article as well as the article's bending characteristics. It was found that the four-cord torus had an advantage over the other articles since the two sets of offset cords provided better bending rigidity. What was also apparent was that the ladder torus was prone to more significant bending deformations, likely due to the strap positions. Further, the article that had two different length cords did not show a loss of performance due to this intentional manufacturing defect. Overall, each of the reinforcing methods have unique strengths and weaknesses but still offer a robust load-carrying system.

Chapter 7

SUMMARY, CONCLUSIONS, AND RECOMMENDATIONS

7.1. Summary

Inflated structures are an area of very intense interest and development due to their light weight and large ratio of stowed to deployed volume. The current and potential applications for these articles are far reaching and relevant wherever packable lightweight structures are needed. Furthermore, inflatable structures have many diverse applications in space systems and terrestrial structures. The need for better understanding their performance is critical to determine the characteristics and load response of inflatable articles for these applications.

Using inflatable structures for spacecraft decelerators has been considered for quite some time, however due to the material and modeling complications they have only been recently achievable. Inflatable decelerators could help to increase payload size and improve size constraints that limit the ability to place large objects on the surface of other planetary bodies. The Hypersonic Inflatable Aerodynamic Decelerator (HIAD) is at the center of inflatable designs to further landing capacities of interplanetary payloads.

The HIAD structure is constructed using toroidal components that exhibit complex non-linear structural behavior. This presents a critical need to better understand the behavior of these articles as well as develop more robust and accurate numerical models to predict the behavior of these systems during complex and dynamic loading scenarios. The experimental procedures and results presented in this thesis attempt to examine many of the basic response characteristics of the toroidal article. Torus testing was accomplished using a sixteen actuator setup designed to allow the application of both

in-plane forces and torsion at eight locations on the torus structure. The experimental design in this work focused on producing consistent and highly reliable test data that can be used to validate structural models that are currently under development. For the purpose of creating high fidelity-data for model validation as well as achieving good control over the desired test parameters, displacement control was chosen to perform the majority of tests at UMaine. This did however limit the number of loading points that could be used for torus testing since only sixteen actuators were available, hense limiting the number of torque capable load points to eight.

Development of the control system and hardware design of the controllers was accomplished at UMaine to permit the maximum resource allocation towards torus testing. The data acquisition and control algorithms were implemented in the MATLAB environment. This computational platform enabled the test to be accomplished with a high level of control and produced data output that was consistent and highly optimized for further post processing. The unique approach used for developing the control system allowed for a significant degree of flexibility in accomplishing testing and made it possibly to fully automate the torus test execution. This automation was highly useful for inflated structures testing due to the inflation-dependent properties of the test articles. This allowed for the articles to be fully acclimated to the test pressure prior to testing as well as permit time for the torus to recover after testing. This acclimation and recovery time would be prohibitive if tests were manually executed due the high number of tests that were run on the articles.

Extensive testing was accomplished on two of the sizes used in the construction of the HIAD being the T3 and T4 articles indicated in Figure 96. Torus testing was

conducted on three T4 articles and five T3 articles. The T4 testing series included two untested pristine articles and one previously-tested article. The test run on the previously loaded T4 article (T4A-1) demonstrated load controlled test results similar to what had been previously accomplished by NASA using quasi-uniform load controlled testing. This testing series shed light on a shortcoming of load controlled testing, which is imperfect load sharing of the four cables controlled by a single actuator. These load inconsistencies could be corrected by better adjusting the setup to minimize the frictional loses, however the unstable nature of load controlled testing would still present an issue. This inherent instability also presents challenges when using the results for model validation. For these reasons subsequent tests were run using only sixteen load cables with displacement control.

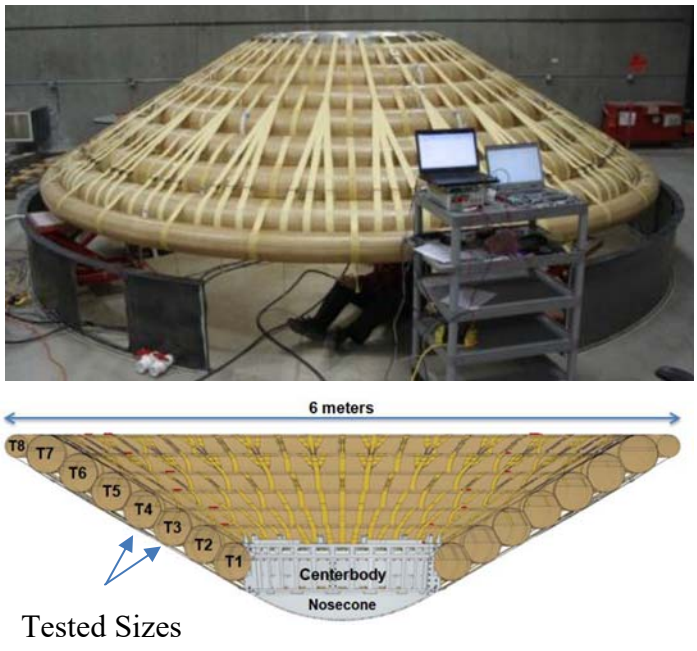

Figure 96: HIAD Construction (Swanson, 2012)

Torus testing was also performed on five T3 articles as previously mentioned. These articles were constructed using a variety of axial reinforcing schemes and were all untested pristine articles provided by NASA. Testing performed on the T3 articles consisted of small displacement, torsion and large displacement testing as well as a variety of more complex load cases. The small displacement testing was aimed at proving response repeatability and quantifying the load response characteristics of the articles when subjected to loading much less than their total capacity. Torus torsion testing was conducted to quantify the response of the articles to torsional loading and to better understand the physics behind the torsional response of the articles. Large displacement testing was conducted to determine the final load carrying capacity as well as better understand the damage and response of the articles. Selected articles were also tested with out-of-plane loading and extreme torsion in an attempt to increase the available data for numerical model comparison.

7.2. Conclusions

The torus test setup that was used provided a versatile platform that allowed for many differing loading scenarios as well as differing articles to be tested. The control system and data acquisition equipment permitted for the execution different test types to be accomplished and provided a clear pathway for testing automation. The torus testing undertaken achieved results that are valuable in understanding the performance aspects of the torus articles.

Repeatability was demonstrated in many different aspects of torus testing. For small displacement tests generally less than 38mm, it was observed that sequential

loading did not impact the performance of the torus beneath its damage threshold. This was particularly clear in the average radius measure of the torus where multiple tests were run with very repeatable results to low levels of displacement (< 38 mm). Highly repeatable results were also seen throughout all phases of torsion testing performed initially on the articles. However, the torus tests also showed that repeatability is regained even after a change in the articles response due to larger loading occurs. In other words when the torus is not loaded past a previous level, torus response is repeatable. This trend was seen for all articles tested where the response changed due to an increased load level the response of the torus settled into a consistent trend for subsequent loading.

Testing on pristine articles resulted in accumulating deformations and a loss in the stiffness as measured by the average radius. This was not seen in testing run on articles that had previously been tested indicating that there is damage that occurs to pristine tori when loaded to a high level resulting in large changes in the articles curvature. Much of the damage that occurs on to the articles is not visibly detectable and the mechanism is not clearly understood. This damage as indicated by a loss in load carrying capacity and subsequent loss of repeatability was seen in the response of all pristine articles. This damage that can only be seen in the measured response and was observed on every torus, except the four-corded article, where the load response changed without exhibiting any visible damage. During the process of running an out-of-plane loading test shear transfer was lost between the cord and the braid resulting in a rapid loss of load carrying capacity as well as clearly visible damage to the coating material. For this reason it is unlikely that this type of cord slippage is responsible for the non-visible damage to the torus during large displacement testing. It is more likely that this non-visible damage is a result of the

damage to the braid, coating and bladder and impacts on their interaction, particularly where the curvatures are most severe. `

Testing of the T3 articles with varied reinforcing schemes resulted in some interesting and useful results that can help better inform future designs of tori and HIAD devices. It is evident that the reinforcing method has a large impact on the performance and the bending characteristics of the articles. Since the four-cord torus had two offset reinforcing cords, the neutral axis is located between the two pairs of cords giving the torus a higher bending stiffness. As was seen in the data the four-corded article had larger load-carrying capacity and better load-deformation characteristics than the other tested reinforcing methods. Also apparent from testing was that the ladder torus was prone to more significant bending deformations. Furthermore, the article that had two unevenly length matched cords did not show a loss of performance due to this flaw relative to the pristine two-cord articles with equal-length cords. Overall, all the reinforcing methods proved highly robust construction during load tests and each method could be best suited for a particular application of design constraint.

7.3. Recommendations for Future Research

During the process of torus testing many questions arose that could be addressed with further. Due to the complexity of the inflatable article it is very difficult to fully measure all of the changes that occur to the torus during testing and completely determine the mechanisms upon which the load response depends. It would be highly valuable to better understand the mechanisms which cause a change in the torus load-deformation characteristics during large displacement tests. Further modeling and testing could be

undertaken in an attempt to gain a better understanding of the process and determine ways to predict and mitigate this damage. Furthermore, the testing performed on these articles resulted in very large local curvatures of the articles caused to some extent by the limited number of loading points. Valuable insight on the torus response could be gained by increasing the number of load points used. This would require more actuators and instrumentation to be added to the current system presenting a cost issue. However the control system developed as part of this thesis research could be easily adapted to handle a larger number of actuators if the hardware was available. A summary of recommendations for the future is as follows:

16 Strap Displacement Testing. In order to increase the number of load points for torus testing the existing system could be modified to use only a single actuator for loading each strap. This would remove the possibility of running torsion tests on the torus as well as not allowing for the torsion response to be measured. However, it could provide valuable insight into the response of articles previously tested with a larger number of displacement controlled loading points.

Wider Strap Tests on the Four-corded Article. It could also be informative to conduct testing on the four-cord article with wider straps to allow for the load carrying capacity of the article to be better defined. Since this article failed due to the strap plunging into the inflated cross-section the results cannot be directly compared with those of the other articles tested. This testing would allow for a better understanding of this reinforcing method to be gained and help provide data that can be more easily used for numerical model validation.

Added Reinforcement. As a result of testing performed on the torus reinforcing methods, it is suspected that a hybrid reinforcing scheme consisting of a ladder and reinforcing cords might provide improved performance. Having more than two reinforcing cords makes torus manufacturing more difficult. However, using the ladder could avoid much of this complication. If the ladder was used in conjunction with axial reinforcing cords on the inside curvature of the torus better bending characteristics would likely result. It is not clear whether this modification is valuable for the HIAD system as the interaction between tori and the HIAD shape drive much of the HIAD stiffness and strength. Nevertheless, this could be very important for a system where only one torus is used. It would be simple to conduct a test on an existing article to see if there is a benefit from having externally bonded straps on the outer curvature of the torus that share the axial load with the internal reinforcing cords. There are two methods by which this could be accomplished. The first would be to construct a ladder reinforcement scheme designed to fit an existing two-corded article. The second and perhaps more easily achievable method would be to bond a single reinforcing strap to the outside of the torus which is sized appropriately to share axial load with the internal cords. This strap could be sized and bonded after the two-corded tori was manufactured.

Coupled Tori. The test setup could be modified to test multiple articles connected as they would be in the HIAD stack. This testing would provide valuable data on the response of the entire HIAD system and could provide valuable data for model validation. This testing may require the modification of the test fixture because of the much higher load that would likely be encountered.

FE-Based Response Simulations. Simulation could provide valuable insights into the response of the articles and shed light on many questions bough up over the course of this study. Modeling of the uniform torsional study could help top determining the specific contributions of the materials in the article and help to better understand the pressure and reinforcing dependent behavior. Further FE simulations could also help to answer how to predict the load that a torus will achieve with loading after it has lost repeatability.

BIBLIOGRAPHY

Bohon, H.L., and J.W. Sawyer. 1974. *Deployment and Performance Characteristics of 1.5-Meter Supersonic Attached Inflatable Decelerators.* NASA Technical Note.

Brayley, Kevin E. 2011. *Structural Behavior of Externally Reinforced Inflated Fabric Arches and Beams.* The University of Maine.

Brayley, Kevin E., William G. Davids, and Joshua D. Clapp. 2012. ""Bending response of externally reinforced, inflated, braided fabric arches and beams"." *Construction and Building Materials* 30: 50-58.

C.G., Malm, Davids W. G, Peterson M.L., and Turner A.W. 2009. "Experimental characterization and finite element analysis of inflated fabric beams." *Construction & Building Materials* 23: 2027-2034.

Calomino, A., S. Hughes, M. Cheatwood, R. Dillman, H. Wright, and J. DelCorso. 2011. *Hypersonic Inflatable Arodynamic Decelerator (HIAD) Technology Development Overview.* NASA Langley Resarch Center.

Davids, W. 2007. "Finite-element analysis of tubular fabric beams including pressure effects and local fabric wrinkling." *Finite Elements in Analysis and Design* 44: 24-33.

Davids, W. 2009. "In-Plane Load-Deflection Behavior and Buckling of Pressurized Fabric Arches." *Struct Eng* 135(11): 1320-1329.

Davids, W., and H Zhang. 2008. "Beam finite-element for the analysis of pressurized fabric beam-columns." *Eng. Struct* 30(7): 1969-1980.

Deveikis, W.D., and J.W. Sawyer. 1970. *Static Aerodynamic Characteristics, Pressure Distributions, and Ram-Air Inflation of Attached Inflatable Decelerator Models at Mach 3.0.* NASA Technical Note.

Guo, X., Q. Li, D. Zhang, and J. Gong. 2016. "Structural Behavior of an Air-inflated Fabric Arch Frame." *Journal of Structural Engineering* 142: 04015108.

Guo, Xiao, Qingsong Li, Daxu Zhang, and Jinghai Gong. 2016. "Structural Behavior of an Air-Inflated Fabric Arch Frame." *Engineering Structures* 142: 04015108.

Hill, Jeremy Lee. 2016. *Mechanical Property Determination for Flexible Material Systems.* Daniel Guggenheim School of Aerospace Engineering.

Johnson, B.A. 1971. *Design, Fabrication, and Static Testing of First-Stage Attached Inflatable Decelerator (AID) Models.* Goodyear Aerospace Corporation Technical Report.

Kabche, Jean, Michael Peterson, and William Davids. 2010. *Effect of inflation pressure on the constitutive response of coated woven fabrics used in airbeams.* Vol. B 42. Composites.

Keville, J.F. 1967. *Semi-Rigid or Non-Rigid Structures for Re-Entry Applications, Part I: Evaluation and Design.* Air Force Materials Laboratory Technical Report.

Litton, Daniel K., David M. Bose, Stephen Hughes F. McNeil Cheatwood, Henry S. Wright, Michael C. Lindell, Stephen D. Derry, and Aaron Olds. 2011. *Inflatable Re-entry Vehicle Experiment (IRVE) - 4 Overview.* American Institute of Aeronautics and Astronautics.

Naboulsi, S. 2004. "Investigation of Geometric Imperfection in Inflatable Aerospace Structures." *AEROSPACE ENGINEERING* 98-105.

Nguyen, Q.T., J.C. Thomas, and A. Le van. 2015. "Inflation and bending of orthotropic inflatable beams." *Thin-Walled Structures* 88: 129-144.

1996. "Nonlinear Dynamics of Unidirectional, Fiber-Reinforced Tori." *Engineering Mechanics* 271-276.

Player, Charles, McNeil Cheatwood, and James Corliss. 2006. *Development of Inflatable Entry Systems Technologies.* NASA Langley Research Center.

Robinson, J.C., and A.W. Jordan. 1965. *Exploratory Experimental Aerodynamic Investigation of Tension Shell Shapes at Mach 7.* NASA Technical Note.

Ryan, J.E. 1966. *Aerodynamic Deceleration from as High as Mach 4.0 for the ALARR (Air Launched Air Recoverable Rocket) Project.* Air Force Technical Applications Center.

Smith, Brandon P., Christopher L. Tanner, Milad Mahzari, Ian G. Clark, and Robert D. Braun. 2010. *A Historical Review of Inflatable Aerodynamic Decelerator Technology Development* . Daniel Guggenheim School of Aerospace Engineering.

Swanson, G., A. Cassell, K. Johnson, S. Hughes, A. Calomino, and M. Cheatwood. n.d. *Structural Strap Tension Measurements of a 6 meter Hypersonic Inflatable Aerodynamic Decelerator under Static and Dynamic Loading.* American Institute of Aeronatics and Astronautics.

Veldman, S.L., and C.R. Vermeeren. 2001. "Inflatable Structures in Aerospace Engineering - an Overview." *Composite Materials and Structures* 93-98.

Veldman, S.L., O.K. Bergsma, A. Beukers, and K. Drechsler. 2005. "Bendin and optimisation of an inflated braided beam." *Thin-Walled Structures* 43: 1338-1354.

W.G., Davids. 2009. "In-plane load-deformation behavior and buckling of pressurized fabric arches." *Journal of Structural Engineering* 135 (11): 1320-1329.

Way, David W., Richard W. Powell, Allen Chen, Adam D. Steltzner, A. Miguel San Martin, P. Daniel Burkhart, and Gavin F. Mendeck. 2006. "Mars Science Laboratory: Entry, Descent, and Landing System Performance ." *IEEE Aerospace Conference.* Big Sky. 1467.

Weeks, George E. 1967. *Buckling of a Pressurized Toroidal Ring Under Uniform External Loading.* Langley Research Center.

APPENDIX A

SUMMARY OF MATLAB FUNCTIONS

A-1 Main Control Function

The main control function developed for this testing used a Graphical User Interface (GUI) as shown in Figure A.1. This GUI allows the user to specify the test matrix needed to set the test steps and parameters. There are also output to the GUI to allow the user to see the article pressure and the load measured by the in use load cells. It also allowed the user to record specific observations or problems that would be saved in the final test log.

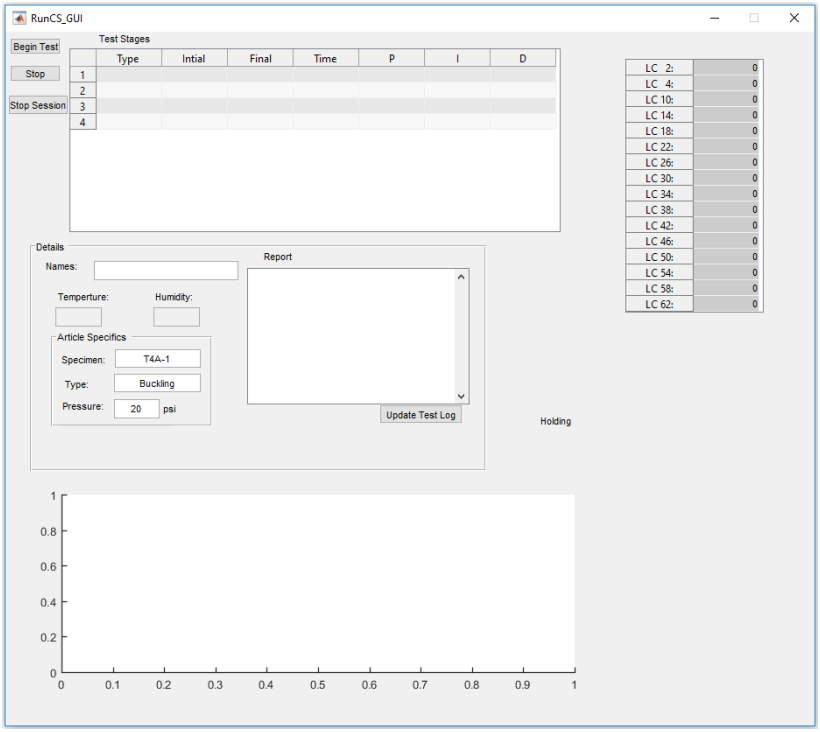

Figure A.1: Control System (GUI)

The test matrix is specified as follows:

- Control Type (1 - load or 2 - Displacement)
- Initial Load or Displacement
- Final Load or Displacement
- Time to achieve Final Load or Displacement
- Proportional control parameter
- Integral Control Parameter
- Differential control parameter

These quantities are arranged in columns respectively and the rows can be used for multiple test steps. For displacement control it is necessary to define a zero point so if the user specifies the initial quantity in a step of the test matrix the displacement is zeroed at the start of that step. Furthermore it the user required a more complex loading or displacement scheme for testing a -99 in the initial column will trigger the controller to load the TotalM.csv where the rows correspond to initial and final and the columns are each individual actuator. This can be seen in the included MATLAB controller code.

Function Inputs:

- TST_p – Test Matrix as Previously described
- PIDslopes – Slopes to use for PID
- Integr_L – Number of iterations to compute integral term of PID
- Location_strg – Location to save Test Data

```
function MainControl(TST_p,PIDslopes,Integr_L,Location_strg)
gui_hand=guihandles(RunCS_GUI);
global StopTest DAQ_session data call_time Stop_Session StopPress
itCOUNTER
global actuators_on temp_num
global  desired_center centering time_save LCdata_save SPdata_save
global SPRaw_save LCRaw_save pwm_save GEN_save curerrr
% Initializing all necessary values
if nargin <2;PIDslopes=[-1/600 1/400 1/8000] ;end
if nargin<3;Integr_L=80;end

time=0;calls=0;time(6)=0; progress=1; cur_type=TST_p(1,1);
Error_hist=zeros(Integr_L,16);PID_vals=TST_p(1,5:7);
time_Cur=0;T_hold=0;PWM_old=ones(1,16)*0.02;PWM=PWM_old;cust_count=0;
```

```
End_D=TST_p(1,3);Start_D=TST_p(1,2);lastPct=0;fill=3;
Cycle_time=0.1;LC_nums=1:64;data=zeros(10,82);call_time=zeros(1,6);
pfreq=5;itCOUNTER=1;shut_down_time=10;PID_PD_mod=20;


%% MATLAB Initialized the Hardware Interface
% If the channels have not already been initialized
if isempty(DAQ_session);Initilize_DAQ_Channels;end
% Begins the background acquisition
startBackground(DAQ_session)
[ Arduino_ID_number,Com_Port,arduino1 ] = Connect_to_Arduino;
fopen(arduino1);
% When the function end this will close the connection with the Arduino
% and extends the actuator. This will also run in case an error occurs
% and the function ends
onCleanup(@() SessionShutDown(DAQ_session,arduino1));
pause(2)


LC_Cal=csvread('Controler_Code\Load Cell Information.csv',1,0);
SP_Cal=csvread('Controler_Code\String Pot Information.csv',1,0);
SP_triang=transpose(csvread('SP_cal_ValidFrom_2016_22_16_to_Current.csv
',1,0));
TotalM=csvread('Controler_Code\TotalM.csv');% For torsion

%% Retrieve the temperature and Humidity from the Arduino
fprintf(arduino1,'-THR');THD=str2num(fscanf(arduino1));
Temperture=THD(1);Humidity=THD(2);


%% Connect to the Image Acquisition Process
freq=20;camSpeed=500;
e=actxserver('LabVIEW.Application');
vipath='C:\Users\Labview\Google Drive\Nasa\HIAD Control v4.00
Folder\SimpleCamera\Simple_2Camera_Control.vi';
vi=invoke(e,'GetVIReference',vipath);
vi.SetControlValue('Frequency',camSpeed);
vi.SetControlValue('Exposure',225);
vi.SetControlValue('Save Path',gui_hand.Save_path.String);
pause(3)


%% Sets Up Values of GUI updating
    fill_type={'Filling','Draining','Holding','Draining (w Vac)'};
    fill_color=[0 1 0;1 0 0;1 1 0;0.6 0 0];
    lfail=false;
    % Retrieving the handles to the GUI
    Pre_sp=str2double(gui_hand.Pressure.String);
    P_pres=5*Pre_sp;
    if exist('Temperture')
        gui_hand.tempeture.String=sprintf('%g',Temperture);
        gui_hand.humid.String=sprintf('%g',Humidity);
    end
```

```
    % This is the stop test command from the GUI
    StopTest=0;
    desired_center=zeros(1,16); centering=0;
%% Initializes Data Recoding Matrices
% If no actuators_on specified by user, all with be active
if isempty(actuators_on)
    actuators_on=1:16;
end
[time_switch,Tfinish]=comp_test_times(TST_p);% Computes switch times
cur_time_switch=time_switch(2);
%%
% Reallocating the data storage locations
save_pre_length=freq*time_switch(length(time_switch))+1+freq*shut_down_
time;
time_save=zeros(save_pre_length,12);
LCdata_save=zeros(save_pre_length,64);
LCRaw_save=zeros(save_pre_length,64);
SPdata_save=zeros(save_pre_length,16);
SPRaw_save=zeros(save_pre_length,16);
pwm_save=zeros(save_pre_length,16);
GEN_save=zeros(save_pre_length,10);


%% Begins Image Acquisition
tic
vi.SetControlValue('Stop','false');
pause(1)
vi.SetControlValue('Start','true');
% the loop for the primary execution of the control structure
while ~StopTest && time_Cur<Tfinish
    calls=calls+1;
    % Determine if the program just entered a different test stage
    if cur_time_switch<time_Cur
        progress=progress+1;
        cur_time_switch=time_switch(progress+1); % Determines the time
for the next stage switch
  % This step checks if this test uses load control
        if TST_p(progress,1)==1
            cur_type=1;
            if TST_p(progress,2)<0 || TST_p(progress,3)<0
                Start_D=TotalM(1+(cust_count)*2,:);
                End_D=TotalM(2+(cust_count)*2,:);
                cust_count=cust_count+1;
            else
                Start_D=TST_p(progress,2);
                End_D=TST_p(progress,3);
            end
  % This step checks if this test uses displacement control
        elseif TST_p(progress,1)==2
            if  TST_p(progress,2)==0|| (TST_p(progress,2)==-
…99&&TotalM(1+(cust_count)*2,1)==0)
                zeroSP=SPdata; % sets the zero for the string pots
            end
            f_call=calls;
```

```
            cur_type=2;
            pam=TST_p(progress,5);
            if TST_p(progress,2)==-99 || TST_p(progress,3)==-99
                Start_D=TotalM(1+(cust_count)*2,:);
                End_D=TotalM(2+(cust_count)*2,:);
                cust_count=cust_count+1;
            else
                Start_D=TST_p(progress,2);
                End_D=TST_p(progress,3);
            end

        end
        Error_hist=zeros(Integr_L,16);
        PID_vals=TST_p(progress,5:7);
    end


    %% Read Data from Hardware


[time,LCdata,SPdata,Pressure,SPRaw,LCRaw,PWM1_Read,fail]=DAQ_read(time(
6),SP_...Cal,LC_Cal,SP_triang,gui_hand);% The time in seconds is passed
back to prevent receiving the same values



    %% Evaluates the error
    if cur_type==1 % Load Control
        desired_load=(End_D-Start_D)*(time_Cur-
…time_switch(progress))/(cur_time_switch-
time_switch(progress))+Start_D;
        desired=desired_load;
        [ LCave] = LCAvergOne( LCdata );
        Error_hist=[LCave-desired_load;Error_hist(1:Integr_L-1,:)];
    elseif cur_type==2 % Displacment Control
        desired_position=(End_D-Start_D)*(time_Cur-
…time_switch(progress))/(cur_time_switch-
time_switch(progress))+Start_D;
        desired=desired_position;
        curerrr(calls,:)=-SPdata+zeroSP-desired_position;
        Error_hist=[(-SPdata+zeroSP-
desired_position);Error_hist(1:Integr_L-…1,:)];
        % Gives the P value a large bost for the beginning of the test
        PID_vals(1)=pam+pam*PID_PD_mod/(calls-f_call+1);
    end

    %%
    % For the section below the logic
    if length(desired)>9
        desired_T=desired(9);desired_B=desired(1);
    else
        desired_T=desired(1);desired_B=desired(1);
    end
```

```
%% Set the Actuators to the desired Voltage
    if ~fail
        [ PWM_hold,PID_use  ] = PID(
PID_vals,Error_hist,1/freq,LCdata,PIDslopes,PWM,PWM_old,actuators_on);%
if the program is lagging a lot this could be an issue since del_T is
fixed
    else
        PWM=PWM_old;
    end
    PWM_old=PWM;
    PWM_2_Write=PWM_hold.*(PWM_hold~=PWM_old);
    PWM=PWM_hold;


    PWM_OUT_write(vi,[PWM_2_Write  PID_vals camSpeed 1],arduino1,fill);
    %% Error Check
    % CHaeck if any cables break or disconnect
    if calls>2
        LC_CK=LCdata_save(calls-1,:)-LCdata>10;
        if any(LC_CK)
            StopTest=1;
            Stop_Session=1;
            fprintf('Load Cell %g Disconnected',max(LC_nums(LC_CK)))
        end
    end


 %% Data Saved to Variables
    time_save(calls,:)=time;
    LCdata_save(calls,:)=LCdata;
    LCRaw_save(calls,:)=LCRaw;
    SPdata_save(calls,:)=SPdata;
    SPRaw_save(calls,:)=SPRaw;
    pwm_save(calls,:)=PWM;
    GEN_save(calls,:)=[PID_use' desired_T desired_B Pressure cur_type
fill   …camSpeed PWM1_Read];%Needs to be modified for position control


    %% Pressure Control
    lastPct=lastPct+1;
    Psum=Psum+Pressure;
    % On the first iteration of the control system, this loop needs to
check
    % the current pressure and compare it to the desired pressure and
if it is
    % outside of 2psi error abort the test
    if (abs(Pressure-Pre_sp)>2&&Pressure==0)&&(calls==1||calls==2)
        StopTest=1;
    elseif lastPct>freq/pfreq
        Cycle_time=floor(P_pres*(abs(Psum/lastPct-Pre_sp)-
(Psum/lastPct-…Pre_sp))/.5);
        Psum=0;lastPct=0;
```

```
    end

    gui_hand.user_text.String=sprintf('Pressure %6.3f psi',Pressure);
    gui_hand.LC_Table.Data=LCdata(2:4:64)';
    %% Data is updated to GUI
    if  toc-calls/freq<1/freq % Only Updates if not lagging
        gui_hand.LC_Table.Data=LCdata(2:4:64)';
        gui_hand.Fill_Condition.BackgroundColor=fill_color(fill,:);
        gui_hand.Fill_Condition.String=fill_type{fill};
    end



    %%
    % Pause to check if a stop command has been issued
    pause(0.00000000001)% also allows MATLAB to clear queue
    %%
    % Synchronization of execution to achieve desired frequency

    while toc-calls/freq<1/freq
    end
    time_Cur=toc-T_hold;


end
%%
%_____________________________________________________________________
___%
%% The Test had been Completed or Aborted
% The following section shuts down the system and saves the recorded
% data and puts the actuators at full extend
PWM_OUT_write(vi,[zeros(1,16)+0.02  PID_vals camSpeed 1],arduino1,3)


%% Ramp down test (Unloading for 10 seconds)
sd_time=time_Cur;
for p=1:shut_down_time*freq
    calls=calls+1;

    %% Read Data from LV

[time,LCdata,SPdata,Pressure,SPRaw,LCRaw,PWM1_Read,fail]=DAQ_read(time(
…6),SP_Cal,LC_Cal,SP_triang,gui_hand);

    % save Data
    time_save(calls,:)=time;
    LCdata_save(calls,:)=LCdata;
    LCRaw_save(calls,:)=LCRaw;
    SPdata_save(calls,:)=SPdata;
    SPRaw_save(calls,:)=SPRaw;
    pwm_save(calls,:)=PWM;
    GEN_save(calls,:)=[0 0 0 0 0 Pressure cur_type fill camSpeed
…PWM1_Read];
```

```
    % Update GUI
    gui_hand.LC_Table.Data=LCdata(2:4:64)';
    gui_hand.Fill_Condition.BackgroundColor=fill_color(fill,:);
    gui_hand.Fill_Condition.String=fill_type{fill};

    %% Stops Image Acquisition
    if p==(shut_down_time-2)*freq
        PWM_OUT_write(vi,[zeros(1,16)+0.5  PID_vals 0
…1],arduino1,fill);
        vi.SetControlValue('Stop','true');
        vi.SetControlValue('Start','false');
    end
    % Synchronization of execution to achieve desired frequency
    while toc-calls/freq<0.05
    end

    time_Cur=toc-T_hold ;
    gui_hand.user_text.String=sprintf('Shuting down...\nTime: %0.1fs',-
…(time_Cur-sd_time)+shut_down_time);
    pause(0.00000000001)
end

try
    csvwrite('C:\Users\Labview\Google
Drive\Nasa\CurrentData.csv',[time(1:6) GEN_save(calls,4)
GEN_save(calls,5) GEN_save(calls,7) LCdata SPdata GEN_save(calls,6) PWM
GEN_save(calls,1:3) PIDslopes Integr_L fill 0 1 1]);
end

gui_hand.Fill_Condition.BackgroundColor=[0.94 0.94 0.94];
gui_hand.Fill_Condition.String=fill_type{3};
handles=guihandles(RunCS_GUI);

%% Save Data to Disk
if nargin <5
    loc=strrep(handles.Save_path.String,'.csv','_Mat.txt');
else
    loc=strrep(Location_strg,'.csv','_Mat.txt');
end


temp_num=write_temp_files('Controler_Code\temp',time_save,LCdata_save,L
CRaw_s…ave,SPdata_save,SPRaw_save,pwm_save,GEN_save );

WriteTestLog(handles,temp_num)

if cust_count>0

write_temp_test_log('Controler_Code\temp',handles,Integr_L,PIDslopes,TS
T_p,lo…c,actuators_on,TotalM)
else
```

```
write_temp_test_log('Controler_Code\temp',handles,Integr_L,PIDslopes,TS
T_p,lo…c,actuators_on)
end
WriteDataFile(loc,time_save,LCdata_save,SPdata_save,pwm_save,GEN_save,P
IDslop…es,Integr_L)
```

A-2 Initialize Data Acquisition Channels

```
function Initilize_DAQ_Channels

global DAQ_session DAQ_listener

DAQ_session = daq.createSession('ni');

for i=2:9
    disp(sprintf('Adding PXI2Slot%g -- Load Cell Card LC: %g - %g'
,i,i*8-15,i*8-8))

addAnalogInputChannel(DAQ_session,sprintf('PXI2Slot%g',i),0:7,'Bridge')
;
end

for i=5:6
    disp(sprintf('Adding PXI1Slot%g -- String Pot Card SP: %g -
%g',i,i*8-7-8*4,i*8-8*4))

addAnalogInputChannel(DAQ_session,sprintf('PXI1Slot%g',i),0:7,'Bridge')
;

end
disp(sprintf('Adding PXI1Slot%g -- Pressure Transducer',7))
addAnalogInputChannel(DAQ_session,'PXI1Slot7',0:1,'Voltage');
warning ('off','all');

for j=1:64
    DAQ_session.Channels(1,j).ExcitationVoltage=10;
    DAQ_session.Channels(1,j).NominalBridgeResistance=350;
    DAQ_session.Channels(1,j).BridgeMode='Full';
end
for j=65:80
    DAQ_session.Channels(1,j).ExcitationVoltage=10;
    DAQ_session.Channels(1,j).NominalBridgeResistance=350;
    DAQ_session.Channels(1,j).BridgeMode='Full';
    DAQ_session.Channels(1,j).Range=[-.25 .25];
end
warning ('on','all');

DAQ_session.IsContinuous=1;
```

```
DAQ_session.Rate=25600;
DAQ_session.NotifyWhenDataAvailableExceeds=25600/20;

%% PWM Inishilization
disp(sprintf('Adding PXI1Slot%g   PWM channels CH: 1 - 8',2))
addCounterOutputChannel(DAQ_session,'PXI1Slot2',0:7,'PulseGeneration');
disp(sprintf('Adding PXI1Slot%g   PWM channels CH: 9 - 16',4))
addCounterOutputChannel(DAQ_session,'PXI1Slot4',0:7,'PulseGeneration');

for i=83:98
    DAQ_session.Channels(1,i).DutyCycle=0.02;
    DAQ_session.Channels(1,i).Frequency=20000;
end
disp('All Channels Added successfully!')

DAQ_listener = addlistener(DAQ_session,'DataAvailable', @SaveData);
```

A-3 Serial Connection to Arduino

```
function [ Arduino_ID_number,Com_Port,arduino1 ] = Connect_to_Arduino(
exclude_com_ports )
%% Connect_to_Arduino
%  This function connects to any serial objects connected to the
computer if an irduino with the control system code is found it will
output the
%  ID of the specific unit.
if nargiin<1
    exclude_com_ports=[];
end
dis=1;
channel=4;
while dis && channel<20 && ~ismember(channel,exclude_com_ports)
    try
    arduino1=serial(sprintf('COM%g',channel),'BAUD', 115200);
    fopen(arduino1);
    dis=0;

    catch
        delete(arduino1)
        channel=channel+1;
    end
end
if ~dis
Com_Port=Channel;
fopen(arduino1);
pause(0.5)
fprintf(arduino1,'-ID_R');
text_response=fscanf(arduino1);
fclose(arduino1);
if strfind(text_response,'ID:')
   Arduino_ID_number=str2double(strrep(text_response,'ID:',''));
else
    Arduino_ID_number=0; % No valid ID response
```

```
end


    fprintf('Connected to arduino: %g on COM
…%g',Arduino_ID_number,channel);
else
    disp('Failed to arduino');
    Com_Port=0;
    arduino1=0;
    Arduino_ID_number=0;
end
```

A-4 Read Values from Data Acquisition

```
function
[time,LCdata,SPdata,Pres,SPRaw,LCRaw,PWM1_Read,fail]=DAQ_read(Last_seco
nds,SP_Cal,LC_Cal,SP_triang,handles)
     global StopTest  call_time data Stop_Session
SP_min=SP_triang(1,:);
SP_max=SP_triang(2,:);
cur=Last_seconds;
max_load=800;
fail=false;

att=1;

it=1;
    last=cur;
    cur=call_time(1,6);
    while cur==last && it<50
        it=it+1;
        pause(0.000001)
        last=cur;
        cur=call_time(1,6);
    end
% % % % % %
%

time_save=call_time; %
LCRaw=mean(data(:,1:64),1);
LCRaw(:,17)=0;
SPRaw=mean(data(:,65:80),1);
Pressure_raw=mean(data(:,81),1);
LCdata=LCRaw.*(LC_Cal(:,5))'+(LC_Cal(:,6))';
SPdata_unscaled=SPRaw.*(SP_Cal(:,5))'+(SP_Cal(:,6)');
Pres=Pressure_raw*9.8172-1.3606;
PWM1_Read=mean(data(:,82),1);

 % This logic checks if the string pots are about to extend past the
max, to prevent damage to the string pots the test will be ended (if
the SP were past 99% of their maximum values.
if sum(SPdata_unscaled>SP_max*0.99)>0
```

```
    %StopTest=1;
    [m_v,ind]=max(SPdata_unscaled>SP_max*0.98);
   display(sprintf('SP %g Has hit Maximum Extension',ind));
    errorMessage(handles,sprintf(' SP %g Has hit Maximum Extension
',ind))
    StopTest=1;
    Stop_Session=1;
elseif sum(SPdata_unscaled<SP_min*0.99)>0
        [m_v,ind]=max(SPdata_unscaled<SP_min*0.98);
   display(sprintf('SP %g Has Bottomed Out',ind));
    errorMessage(handles,sprintf(' SP %g Has Bottomed Out ',ind))
    StopTest=1;
    Stop_Session=1;
elseif max(LCdata)>max_load
    [m_v,ind]=max(LCdata);
    StopTest=1;
    Stop_Session=1;
    display(sprintf('LC %g Has Exceded %glbf',ind,max_load));
    errorMessage(handles,sprintf('LC %g Has Exceded
%glbf',ind,max_load))
end

time=[time_save clock];

%% Calculating the Actual displacement for the SP
offset=0.375;
h_0=SP_triang(3,:);
ex=SP_triang(4,:);
length_cab=SPdata_unscaled+ex;
drop=(length_cab*0.27)./LCdata(1,2:4:64);
h=h_0+drop;
SPdata=sqrt((length_cab).^2-h.^2-offset^2);
```

A-5 Set Pulse Width Modulated Output

```
function  PWM_OUT_write(vi,data,arduino1,fill)
global DAQ_session Last_pwm_Com
Last_pwm_Com=clock;
vec=83:98;
for j=vec(data(1:16)~=0)
    DAQ_session.Channels(1,j).DutyCycle=data(1,j-82);
End

fprintf(ardiuno1,sprintf('001,001,001,001,001,001,001,001,%g',fill));
```

APPENDIX B

SUMMARY ARDUINO CODE

```
int ID_NUMBER = 1027; //Arduino Identification Number

String command;
unsigned long timeD = 0;
// PWM Pins
int PWM1_pin = 2;
int PWM2_pin = 3;
int PWM3_pin = 4;
int PWM4_pin = 5;
int PWM5_pin = 6;
int PWM6_pin = 7;
int PWM7_pin = 8;
int PWM8_pin = 9;


int fillpin = 11;
int plugpin = 12;
int vacpin = 13;

void setup() {
  // put your setup code here, to run once:
  pinMode(PWM1_pin, OUTPUT);
  pinMode(PWM2_pin, OUTPUT);
  pinMode(PWM3_pin, OUTPUT);
  pinMode(PWM4_pin, OUTPUT);
  pinMode(PWM5_pin, OUTPUT);
  pinMode(PWM6_pin, OUTPUT);
  pinMode(PWM7_pin, OUTPUT);
  pinMode(PWM8_pin, OUTPUT);
  pinMode(fillpin, OUTPUT);
  pinMode(plugpin, OUTPUT);
  pinMode(vacpin, OUTPUT);
  digitalWrite(fillpin, LOW);
  digitalWrite(plugpin, LOW);
  digitalWrite(vacpin, HIGH);
  Serial.begin(115200);
}

void loop() {

  // put your main code here, to run repeatedly:
  if (Serial.available())
  {
    char c = Serial.read();
    if (c == '\n')
    {
      parseCommand(command);
      command = "";
      timeD = millis() + 2000;
```

```
    //Serial.print("Processing");
   }
   else
   {
    command += c;

   }
  }
  if ( millis() > timeD && command == "") //THis means the ardino needs to regulate the pressure
  { digitalWrite(fillpin, LOW);
   digitalWrite(plugpin, LOW);
   digitalWrite(vacpin, HIGH);
   analogWrite(PWM1_pin, 0);
   analogWrite(PWM2_pin, 0);
   analogWrite(PWM3_pin, 0);
   analogWrite(PWM4_pin, 0);
   analogWrite(PWM5_pin, 0);
   analogWrite(PWM6_pin, 0);
   analogWrite(PWM7_pin, 0);
   analogWrite(PWM8_pin, 0);

  }
}

void parseCommand(String com)
{
 String PWM1;
 String PWM2;
 String PWM3;
 String PWM4;
 String PWM5;
 String PWM6;
 String PWM7;
 String PWM8;
 String Fill;
 int FillLog = 0;

//================================================================================
========================
  // If values are sent for PWM control
  if (com.length() > 32) {
   PWM1 = com.substring(0, 3);
   PWM2 = com.substring(4, 7);
   PWM3 = com.substring(8, 11);
   PWM4 = com.substring(12, 15);
   PWM5 = com.substring(16, 19);
   PWM6 = com.substring(20, 23);
   PWM7 = com.substring(24, 27);
   PWM8 = com.substring(28, 31);
   Fill = com.substring(32, 33);

   int APWM1 = PWM1.toInt();
   int APWM2 = PWM2.toInt();
   int APWM3 = PWM3.toInt();
```

```
  int APWM4 = PWM4.toInt();
  int APWM5 = PWM5.toInt();
  int APWM6 = PWM6.toInt();
  int APWM7 = PWM7.toInt();
  int APWM8 = PWM8.toInt();
  int FillLog = Fill.toInt();

  analogWrite(PWM1_pin, APWM2);
  analogWrite(PWM2_pin, APWM2);
  analogWrite(PWM3_pin, APWM3);
  analogWrite(PWM4_pin, APWM4);
  analogWrite(PWM5_pin, APWM5);
  analogWrite(PWM6_pin, APWM6);
  analogWrite(PWM7_pin, APWM7);
  analogWrite(PWM8_pin, APWM8);
 }
 if ((com.substring(0, 1) == "1" && com.length() < 3) || (1 == Fill.toInt())) //Fill
 {
  digitalWrite(fillpin, HIGH);
  digitalWrite(plugpin, LOW);
  digitalWrite(vacpin, HIGH);
 }
 else if ((com.substring(0, 1) == "2" && com.length() < 3) || (2 == Fill.toInt())) //Drain
 {
  digitalWrite(fillpin, HIGH);
  digitalWrite(plugpin, HIGH);
  digitalWrite(vacpin, HIGH);
 }
 else if ((com.substring(0, 1) == "3" && com.length() < 3 ) || (3 == Fill.toInt())) //Hold
 {
  digitalWrite(fillpin, LOW);
  digitalWrite(plugpin, LOW);
  digitalWrite(vacpin, HIGH);
 }
 else if ((com.substring(0, 1) == "4" && com.length() < 3) || (4 == Fill.toInt()))//Drain With Vac
 {
  digitalWrite(fillpin, HIGH);
  digitalWrite(plugpin, HIGH);
  digitalWrite(vacpin, LOW);
 }
 else if ((com.substring(0, 5) = "-ID_R") && (com.length() > 3)) {
  Serial.print("ID:");
  Serial.print(ID_NUMBER);
  Serial.print("\n");
  Serial.print(com);
 }
}
```

BIOGRAPHY OF THE AUTHOR

Daniel Whitney was born in Tarrytown, New York on February, 17 1991 to Michael and Narelle Whitney. He was raised in Topsham, Maine and graduated from Chop Point High School, Woolwich, Maine, in 2009. He attended the University of Maine and graduated in 2013 with a Bachelor of Science degree in Engineering Physics with a Mechanical Engineering concentration. He began working towards his Master of Science degree in Mechanical Engineering in January of 2015.

Daniel likes to spend his free time outdoors in the state of Maine. He especially enjoys camping and fishing. He also enjoys working on cars and prototyping with hobbyist circuit equipment such as Arduinos.

After receiving his degree, Daniel will begin working as Materials and Structures Engineer at Pratt and Whitney in North Berwick Maine. He is a candidate for the Master of Science degree in Mechanical Engineering from the University of Maine in December 2016.